POLITECNICO DI TORINO

Master of science degree in
Automotive engineering

Master’s degree thesis

Design of an electromechanical rotative damper prototype for automotive applications

Supervisors:
prof. Andrea Tonoli
prof. Nicola Amati
Co-supervisors:
Renato Galluzzi
Sanjarbek Ruzimov

Candidate:
Severino Corsini

December 2018

Academic Year 2017 – 2018

A mio padre, mia madre e mia sorella

Agli amici che mi hanno supportato in questi anni

Abstract

The main objective of this thesis project is to design an electromechanical rotative damper for automotive applications: in particular the work is focused on the design of the gear transmission stage and then on the development of the damper actuator assembly to realize a prototype for bench testing. A preliminary analysis of the state of the art of rotative dampers gives some hints on possible solutions concerning the assembly, the gearbox and the leverages. The first design phase is concerning the gearbox: on the base of a previous study, the configuration selected is a double stage planetary gear set. The dimensioning of the planetary stage is performed with KISSsoft software: the target of the optimization is to minimize the size of the gears while keeping acceptable values of safety factors. In these calculations, different loading conditions are considered: besides the constant input, a more realistic load spectrum is defined by simulating road profile irregularities. Once the macro-geometry of the gear set is defined, the work is going on with the design of the damper actuator assembly: it includes the gearbox stage, the electric machine and the leverage system. The 3D model of the damper assembly is built in SOLIDWORKS: starting from the KISSsoft model, the design is focused mainly on the shafts and the planetary housing. The study of the gear shafts is integrated with the analysis of the gears (KISSsoft) in order to minimize stresses and deformations and to evaluate their reciprocal effects on the gears life. The external housing of the actuator is designed to be fitted on a customized test bench: this allows to experimentally evaluate the performances in a future phase of the project. Nonetheless, in the design phase the evaluation of performances is performed thanks to simulations and software computations, taking into account three main parameters: efficiency, mass and inertia, noise level. The gearbox efficiency is computed on the KISSsoft model. The equivalent inertia added to the suspension motion is computed starting from the rotational inertia of the damper and then transformed into linear equivalent mass. The evaluation of noise level includes different steps: first some numerical acoustic simulations are performed in COMSOL; second, a noise level map is obtained by the KISSsoft gear calculation; finally, a more refined analysis is carried out trying to integrate the evaluation of generated noise with the more realistic road profile load. Finally, even if this thesis work is oriented to the prototype phase, anyway a preliminary analysis of the issues concerning the real suspension architecture is carried out. In particular, the feasibility of the proposed leverage solutions is investigated, a first model of input arm is defined and then a possible positioning of the damper device inside the suspension architecture is analyzed.

Contents

List of figures

List of tables

List of symbols

a	gears centers distance
α	gear pressure angle
b	gear tooth facewidth
B	bearing width
C_0	bearing basic static load rating
c'	singular tooth stiffness
d	diameter
D	bearing external diameter
dt	planet pin axis misalignment
ε	gear transverse contact ratio
F	force
f	frequency (acoustic analysis)
h	gear tooth height
i	gearbox transmission ratio
J	rotational moment of inertia
k	total transmission ratio from suspension stroke to electric motor rotation
K_a	application factor (gear tooth stress calculation)
$K_{H\alpha}$	transverse load factor (gear tooth stress calculation)
$K_{H\beta}$	face load factor (gear tooth stress calculation)
K_γ	load distribution coefficient (gear tooth stress calculation)
K_v	dynamic factor (gear tooth stress calculation)
l	length
L_{nh}	bearing service life
m	mass
m_n	gear normal module
ω	angular speed
P_0	bearing equivalent static load
P_v	gearbox power loss

s_0	bearing static safety factor
SF	safety factor for tooth bending stress
SH	safety factor for tooth contact stress
S_{yield}	static safety factor for yield limit
S_{lim}	static safety factor for ultimate strength
SPL	sound pressure level
σ	stress
σ_y	yield stress of material
σ_{max}	ultimate tensile strength of material
σ_{root}	tooth maximum tensile stress due to bending
σ_{flank}	tooth maximum contact stress on tooth face
t	gear rim thickness
T	torque
τ	leverage transmission ratio
v	linear speed
x^*	gear profile shift coefficient
Y_m	alternating bending factor (gear tooth stress calculation)
z	gear number of teeth
ζ	next tooth engagement position in mesh cycle (COMSOL model)

1 Introduction

The suspension of a vehicle is a subsystem of the chassis that is the link between the wheel and the car body (sprung mass), and for this reason it contributes in a relevant way both to the comfort and to the vehicle dynamics (handling).

In particular, in all the different types of suspensions, several elements can be identified according to their function [1]:

- *Structural elements:* are the components of the suspension that define the kinematics of the wheel moving relatively to the body and that allow the transmission of forces from the ground to the sprung mass. They have to properly constrain the degrees of freedom of the wheel in order to ideally allow only its vertical motion; by the way the real motion and attitude of the wheel are strongly depending on the type of suspension itself. Typical elements that supply this task are: connecting rods, A-arms and prismatic guides.
- *Elastic elements:* these components have the main function of controlling the motion of the wheel (its single degree of freedom) and so they can filter out the vibrations and the excitations coming from the wheel-ground interface. Helical springs are the most used, but this function can be performed also by torsion bars or air springs (this latter type are typically used for industrial vehicles, but nowadays is applied also on high segment cars); moreover, we need to remember also the contribution of the elastic bushings in the joints between structural elements.
- *Damping elements:* are the ones that dissipates the elastic energy stored and released by the elastic elements due to the wheel motion. They are also called shock absorbers, since they are also effective in reducing the amplitude of such motions. The dissipation of energy is typically obtained by viscous friction of a fluid (hydraulic shock absorbers), but in the past also solutions with dry friction were used.

In the following section we will focus on the evolution of the automotive shock absorbers, since the damper element will be the object of this thesis.

1.1 Review on automotive shock absorbers: historical outline

From an historical point of view [2], the passengers comfort was an issue already known in the fifteenth century; the horse coaches were basically composed of a body that was suspended on the rigid frame through some leaf springs. The origin of the motor car is strictly related to these horse coaches: simply putting, the animal traction was substituted by an on board power source.

So the first car models were keeping this characteristic configuration of having the body separable from the chassis: the joining between these two elements was flexible enough to avoid to transmit the frame deformations to the body.

The function of the suspension system in the early models were mainly related to the filtering of road irregularities and to define the vehicle trim (four wheeled vehicle are hyperstatic structures); at beginning there was no need to introduce also a damping element because, due to the low speeds, the friction acting among the mechanical components (for example between the elements of a leaf spring) was big enough.

With the development of cars going on, the separable chassis solution was not satisfying any more the increasing performances requirements in terms of dynamics and comfort. Starting from the 1920s, there have been the first examples of integrated bodies: being the body not separable from the chassis, the so called “unibody” was the optimal solution for the trade off between the weight and the structural strength. Examples are the Lancia Lambda of 1922 and the Citröen in 1934.

With increasing performances, also the development of suspensions was going on: the first shock absorber dates back to the 1910s, but introduced only as after-market additional feature. These first devices were exploiting mechanical friction; some examples are shown in ***Figure 1.1***: on the left the friction is among the leafs that are sliding in the circular case, while in the rotary shock absorber on the right the friction is among the metal disks.

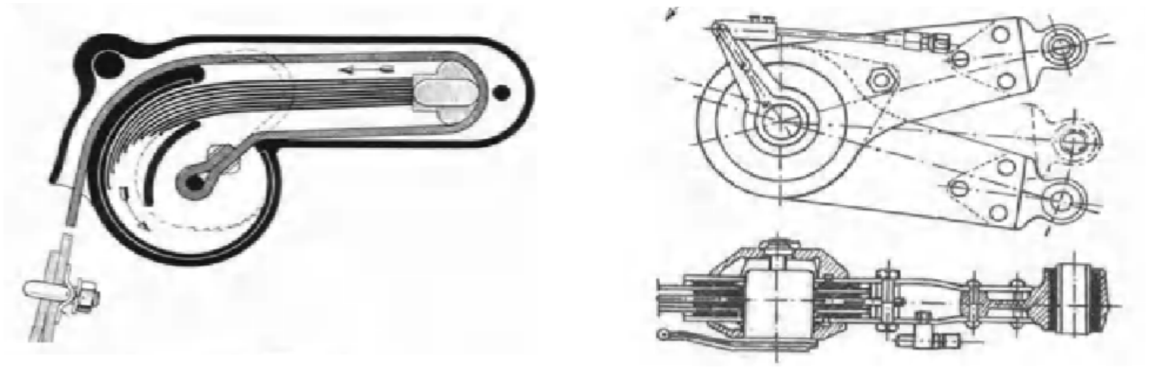

Figure 1.1*: two examples of the first shock absorber models [2] exploiting dry friction for damping*

The first linear hydraulic shock absorber was the Télesco shock absorber presented in 1912 (***Figure 1.2***): actually the telescopic tube was including both an helical spring and also oil and a valve providing the damping action [24]. Lancia Lambda in 1922 was fitting a telescopic slider that integrated the structural, the springing and the damping functions: this was also one of the first applications of independent suspension. A similar solution was developed by Dubonnet and applied by Fiat in 1935 (***Figure 1.3***).

The Man Whose Car
Is Equipped With

Le Télesco
Shock Absorbers

knows a comfort in riding such as he never before enjoyed. This is not mere rhetoric, but a statement founded on the actual experiences of many prominent owners and makers in Europe who have put on **Le Telesco** after trying other leading makes.

This super-efficiency is due to a combination of spring and hydraulic action—springs removing the jars and hydraulic slackened reaction taking care of the rebound.

Motorists looking for the most practical and efficient shock absorber should investigate **Le Telesco.**

Dealers catering to the best class of trade should carry **Le Telesco,** for it gives greater satisfaction than any other.

Write us for descriptions and prices

Le Télesco Company
Franklin Building Baltimore, Md.

Figure 1.2*: magazine advertisement of the Télesco shock absorber*

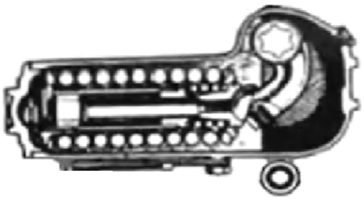

Figure 1.3*: Dubonnet shock absorber used by Fiat from 1935 [2]*

The independent suspension configuration started to be used in 1930s, since at beginning it did not give any practical advantage due to the higher complexity respect to the solid axle: its use gave much more freedom also for the vehicle architecture.

The very famous McPherson suspension was first introduced by Ford in France in 1947 (***Figure 1.4***): the real advantage of this solution is the fact that the hydraulic tube shock absorber is providing also the structural function, much simplifying the suspension architecture; clearly, on the other hand, the freedom in designing the kinematics is lower compared to other solutions.

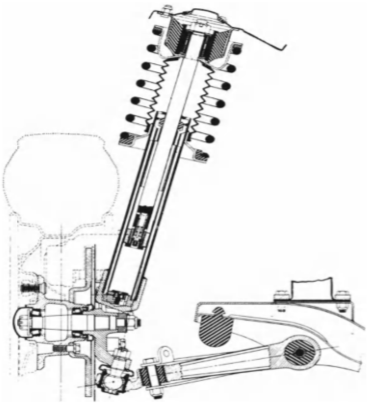

***Figure 1.4**: McPherson suspension used by Ford in 1947 [2]*

At this point we can describe the basic working principle of a conventional hydraulic shock absorber [1]: in ***Figure 1.5*** we can see a simplified representation of a double tube shock absorber that is useful to understand how the fluid is dissipating energy.

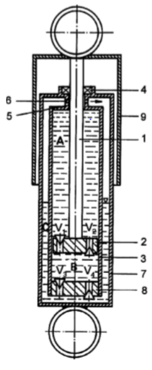

***Figure 1.5**: schematic representation of a double tube shock absorber [1]*

At the two ends, the damper is connected to the sprung and unsprung mass, so their relative motion determines the motion of the piston: this forces the oil to pass through the valves on the piston and on the tube. The oil viscosity and the consequent pressure drop on the valves gives as final result the dissipation of the kinetic energy into heat. In particular, the damping is determined by the valve on the tube during compression and by the one on the piston during extension.

By the way, by definition this energy is lost; as known, the total fuel efficiency of a passenger car is rarely reaching 30 % in optimal conditions: the remaining 70 % (and more) of energy is wasted due to losses in the engine, in the drivetrain, as aerodynamic and rolling resistances.

Many solutions have been adopted to increase the fuel efficiency in order to reduce the overall environmental impact: improved engine design and new control strategies; regenerative braking systems; optimized aerodynamics and reduced rolling resistance of tyres. With the increasing requirements on the fuel consumption issues, clearly additional solutions must be explored in order to exploit other “sources” of wasted energy.

In the last years, several studies focused their attention on the energy dissipated by the shock absorbers: different system capable to recover this kinetic energy were proposed, ranging from linear electromagnetic actuators to electro-hydraulic systems. As an example, the solution proposed by Zuo [3] is a magnetic sliding tube: it can recover up to 400 W on normal road conditions at 96 km/h, reaching peaks of 1600 W on more rough roads.

In the following section, we will analyze some solutions of non conventional shock absorbers, that could be coupled with a regenerative energy system; in particular the analysis is focused on the rotative damper configuration, that is the solution adopted in our project.

1.2 Rotative dampers: state of the art

The first examples of rotary dampers applications for vehicle suspensions and their related patents date back in 1980s. The aim of these new shock absorbers solutions is to optimize the suspension design by eliminating the conventional tube damper: this allows to have a better space efficiency, and also possibility of weight reduction (as claimed by different patents).

In the following sections, some rotative dampers will be analyzed more in detail in order to have a general overview of the possible technical solutions to be adopted in the development of our damper design.

1.2.1 *"Vehicle suspension using a rotary dampen" (Honda 1991)*

This solution was patented by Honda Motor Co. Ltd in 1991 [4]: the rotative damper used in this suspension is an hydraulic, single vane damper. It is positioned in the pivot point of one of the suspension arms, so it can be easily used for different types of suspension.

To describe its working principle, we will refer to ***Figure 1.6***, where it is applied to a double wishbone suspension. In this configuration, the rotary damper is connected to the upper arm: the external vane casing is moving with the arm, the internal vane is fixed to the body and so the suspension motion determines the relative motion of the vane inside the case. The damping force is obtained thanks to the valve mounted on the vane that controls the fluid flow from one chamber to the other one. On the other hand, the springing function is provided by a torsion bar placed in the pivot point of the lower arm: this element and the rotative damper completely control the wheel motion.

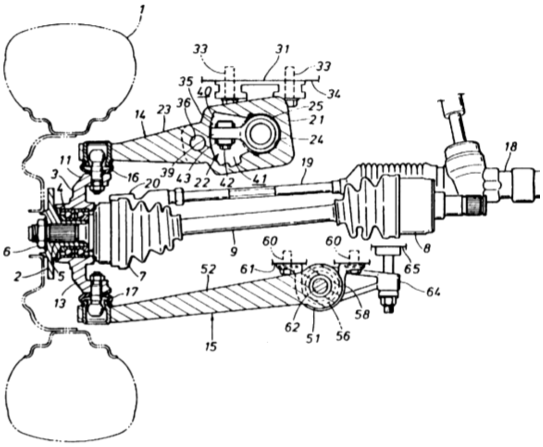

Figure 1.6: suspension with rotative damper proposed by Honda in 1991 [4]

This solution is the preferred one because of the positioning of the rotary damper: since it has been placed on the shorter arm, the larger rotation allows to obtain a bigger damping force. By the way, this damper can be easily used in different types of suspensions.

In McPherson strut suspension, the damper and the torsion bar are both integrated in the pivot point of the lower arm, consequently the strut assembly is much simplified. In another double wishbone suspension, the rotary damper and the torsion bar are both placed in the lower arm. Finally, also in a trailing arm suspension, the damper and torsion bar assembly can be integrated in the hinge point of the arm on the vehicle body.

As claimed, the advantage of this rotative damper solution is to have a better space efficiency for the whole suspension assembly due to the elimination of the tubular damper: the structure is simplified, with reduced size and weight, thus allowing more freedom in vehicle body design.

1.2.2 *Rotary dampers: solutions proposed by Audi*

In recent years, Audi is the most active car manufacturer in publishing patents on alternative solutions to the conventional hydraulic damper; in particular, it is focusing on rotative electromechanical damper systems, and in this section some of them will be analyzed to highlight the different leverage arrangements and the gear transmissions used.

Even if a wide variety of solutions can be found, we can take as reference the “Electric shock absorber for a motor vehicle” first described in 2010 [5]; it is an electric damper applied to a vehicle suspension. A schematic drawing of the system is represented on the left in ***Figure 1.7***. On the right, the different functional elements can be identified: the leverage system (6) transforms the wheel stroke into rotational movement, the gear transmission stage (13) increases the rotational speed and finally this input torque is provided to the damping stage (8) that generally features an electric motor used as generator.

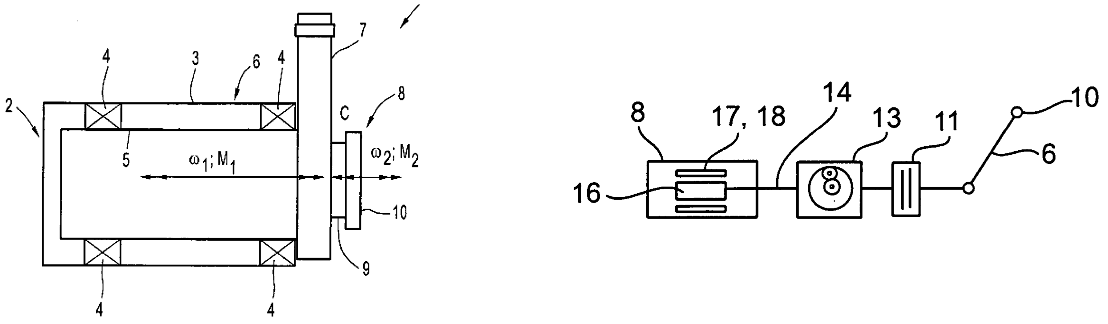

Figure 1.7: simplified scheme of the rotary damper proposed by Audi in 2011 [6]; on the right, the functional scheme [11]

One of the fundamental element of those systems is the leverage that connects the wheel and the vehicle body (since we want to damp their relative motion): such leverage transmits the suspension motion to the damping device. Two solutions are presented in ***Figure 1.8***: on the left (2010 patent [5]) there is a simple arm (9, 11) connecting the suspension and the rotative damper, that is fixed on the body in point D; on the right (2014 patent [7]) the arms arrangement is similar, with the damper on the axis A, but in this case the damper is moving with the lower suspension arm, not as a sprung mass.

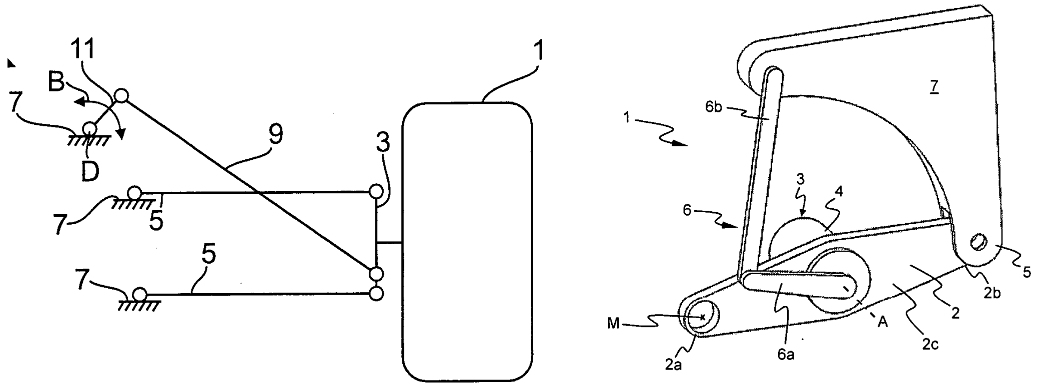

Figure 1.8: two suspensions with rotative dampers proposed by Audi: schematic drawings of the leverages ([5] and [7])

Directly connected to the leverage, there is the input arm: with the leverages, it transforms the wheel vertical motion into rotation, also trying to maximize the angular speed despite the small vertical stroke of the wheel. In the proposed solutions, this element is very simple: two examples are shown in ***Figure 1.9***. The solution described in [6] (on the left in the figure) is featuring a triangular shape that favours the integration of the input arm, the planetary gearbox stage and the electric machine housing (for example having the input on the planetary ring gear). A much simpler solution, a straight input arm (on the right in the figure), was published in 2017 [8].

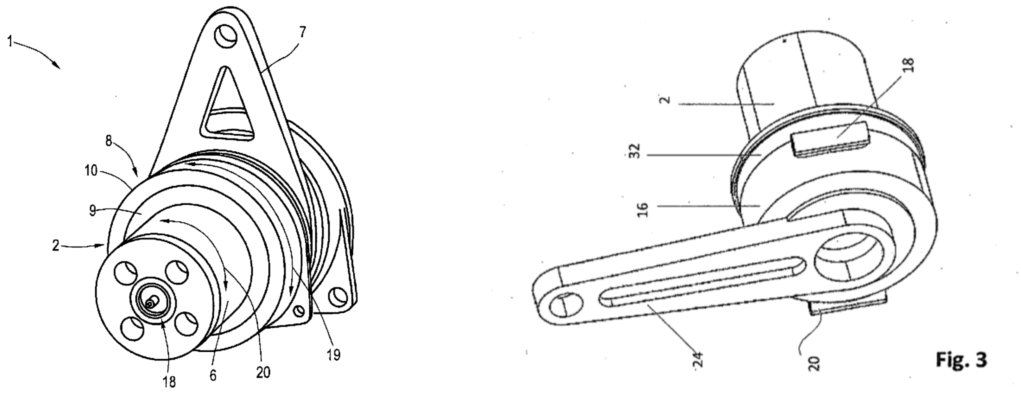

***Figure 1.9**: two examples of input arms for the rotative dampers proposed by Audi (*[6] and [8])

A particular system is described in [9], and represented in ***Figure 1.10***: despite the simplicity of the straight input arm, the peculiarity is represented by two rubber end stops (elements n° 7) that provide the major control on the wheel end strokes by direct contact on the damper input arm.

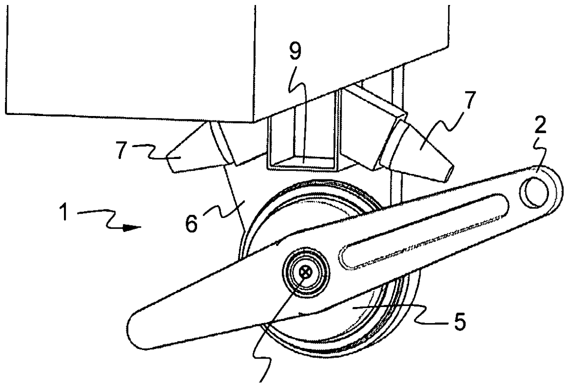

***Figure 1.10**: rotative damper with input arm and rubber end stops (Audi 2017 [9])*

By the way, in general the leverage system is not enough to provide the proper input rotational speed to the damper stage: a gearbox transmission stage is required to amplify the leverage motion, and consequently to assure a relevant induced voltage in the electric machine and an increased damping force.

One of the more detailed examples is represented in ***Figure 1.11***: in this case, the gearbox is a planetary stage. The overall assembly from the input arm to the output to the electric machine is designed to minimize the dimensions of the device, so for example the input arm driving the ring gear is integrated in the stator body. As claimed, the gearbox configuration can be varied and adapted according to how the connections to the leverage and to the motor are obtained, with he combination of input and output shafts that gives the most compact solution: for example the input torque can be provided to the ring gear or to the planetary carrier, the output to the planetary carrier or to the sun gear.

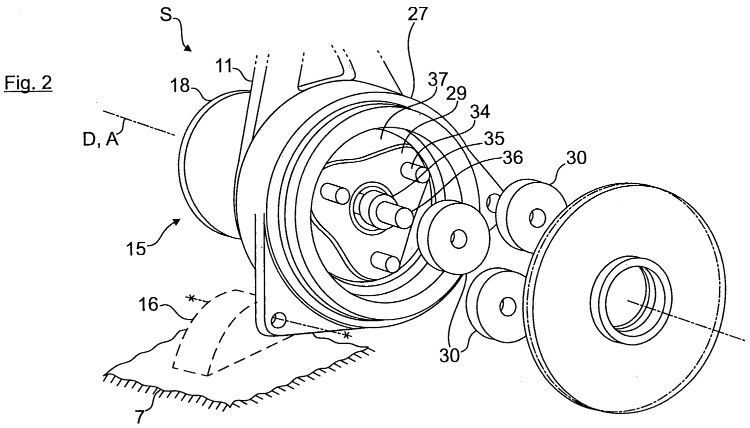

Figure 1.11: rotary damper with the planetary gearbox, Audi patent 2010 [5]

The design for compactness is clearly visible in ***Figure 1.12***, solution published in 2014 [10]: the input is provided to the ring gears (30, 32), the planetary carriers are fixed and the output rotation of the sun gears is provided to the rotor (central element n° 22); the stator body is integrated with the external assembly of arm and ring gears. The use of two symmetric planetary stages is necessary to compensate the axial forces that arise from the helical gears.

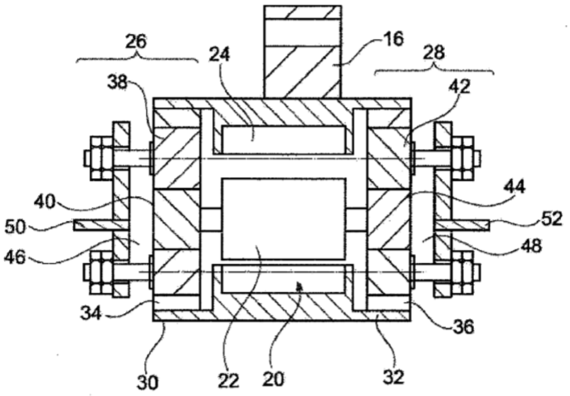

Figure 1.12: example of planetary gearbox stage, Audi patent 2014 [10]

Even if the planetary gearbox is the most proposed solution, among the different patents there is not a preferred choice for the transmission type: as claimed in [6] the transmission can be a planetary stage or a wave gear transmission, with spur or helical gears; in [8] the damper is directly designed with a strain wave gear transmission.

Finally, a short description of the damping stage is necessary to have a general understanding of such systems. In all these electromechanical rotative dampers, the damping force is obtained by an electric machine: the input torque is generating an induced voltage and so the motor is working as a generator. This allows to recover the kinetic energy coming from the suspension motion and to convert it into electric energy that can be fed to the electric system of the vehicle. Moreover, if the motor is electronically controlled, the system can be designed to provide an active control of the damping force.

By the way, the damping action is not entirely supplied by the electric motor: it is specified that additional damping is needed to improve the performances of the machine. For example, as described in [5], an hydraulic damper stage is required to filter out the high frequency oscillations so to avoid fast variations of the induced voltage; in [6] additional elastomeric damping bodies are included between the relative moving bodies; in [11] the input from the leverage is filtered by a slip clutch, to avoid excessive peaks of input torque.

All the previous described solutions show the active interest of Audi in finding new alternatives to the conventional hydraulic damper, even if up to now the advertised project, namely “eRot” [12] [18], is still in a prototype phase (***Figure 1.13***); in fact it is designed to work only on vehicles provided with a 48 V electrical circuit. In line with the fuel saving issues, with this electromechanical rotative damper, Audi declares to recover up to 600 W on country roads, and at the same time improving the comfort and the handling thanks to the possibility of an active damping system control. By the way, the amount of energy that can be recovered is smaller compared to the one generated by the car alternator (more than 1 KWh), so the system will be only effective in reducing the load on the alternator itself. Moreover, we need to account also for the energy required to control the active damping system, but further data are required to understand the real balance between the used and recovered energy.

In conclusion, the prototype is more focused on the active control feature, with its advantages that are mostly related to the compactness and to the faster and more precise response (compared to hydraulic or pneumatic active systems).

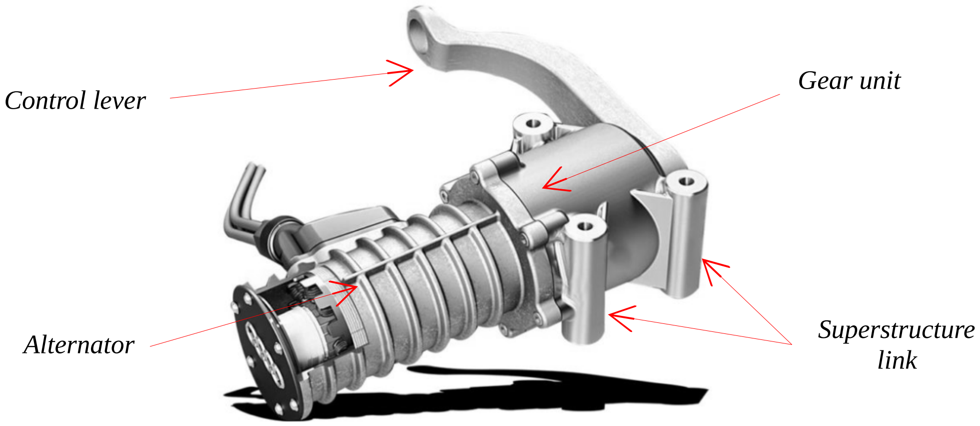

***Figure 1.13**: "eRot", the electromechanical rotary damper prototype presented by Audi [18]*

1.2.3 "Rotary damper for a vehicle" (ZF 2014)

Also ZF proposed an alternative to the conventional vehicle damper in order to obtain a more compact solution: it is a rotative damper [13], similar from a functional point of view to the devices analyzed before. It features a gear transmission stage and an electric machine: the working principle is based on the conversion of the wheel motion into rotation, obtaining the braking damper force thanks to an additional dynamic brake. In this case, since the dynamic brake based on eddy currents requires high speed to provide a proper braking force, the gearbox is of paramount importance to amplify the input rotation: among the several solutions proposed, in ***Figure 1.14*** it is interesting to have a look to some of the multistage planetary gearbox configurations. By the way, the overall assembly design can vary depending on the relative arrangement among the planetary stages, the electric machine rotor and stator, and the dynamic brake that can be placed in series or in parallel with the electric machine.

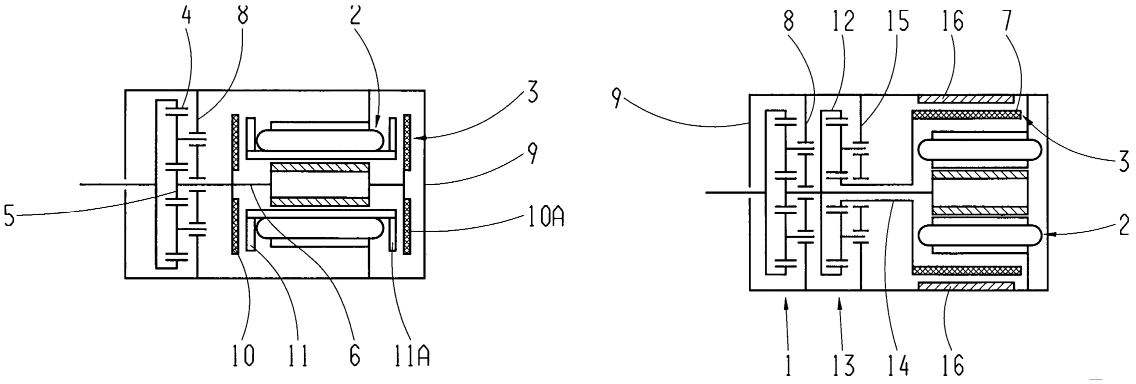

***Figure 1.14**: two examples of multistage planetary gear transmissions (the input is on the left), proposed for the ZF rotary damper [13]*

1.3 Objective of the thesis

The project related to this thesis work is concerning the design and development of an electromechanical rotative damper device to substitute the conventional hydraulic damper in vehicle applications. In particular, the main aim of this thesis is to design the gear transmission stage that will be coupled to the electric machine, and then to develop the CAD model of the damper assembly. This model is finalized to the realization of a prototype to be tested on bench.

The activity is not starting from zero: an electro-hydraulic solution was already presented, but then the idea was to develop a mechanical configuration in order to compare the performances in terms of masses and efficiency.

The preliminary study for the new electromechanical type is carried out in [15]: that work was focused on the analysis of possible leverages architectures for the installation of the damper in a vehicle suspension, and then a first comparison between different types of gear transmissions was performed. Combined together, the leverage and the gearbox must satisfy the transmission ratio required for the proper working of the electric machine.

On the base of these first results, the following thesis work is starting with the refined design of the gear transmission stage: in particular we will develop a double stage planetary gearbox, with the aim to minimize its dimensions according to the requirements of loads applied and strength.

Once defined the details of the planetary gearbox, we start with the design of the 3D CAD model of the main body of the damper actuator. As said, the final objective will be to have a first prototype model to be able to perform in the future some bench tests to experimentally evaluate noise, efficiency and potential of energy recovery of such rotary damper.

1.4 Thesis structure and organization

In the first part of this introductory chapter, after a short description of the automotive damper, an historical outline on the development of such component was presented. Following such evolution, then we analyzed the state of the art of rotative dampers solutions, focusing on some devices that are more similar to our electromechanical device.

The second chapter is describing the dimensioning process of the planetary gearbox: starting from the preliminary design of the previous project, the different steps leading to the optimization of the gears are presented. Here we perform the sizing with the aid of KISSsoft software (setting up more realistic calculation parameters), but we need to take into account that the final version is also the result of a parallel and integrated analysis on the 3D CAD model.

Once defined the gearbox main dimensions, the third chapter is dedicated to the description of the development of the 3D model: the main components (gears, shafts, bearings and overall housing assembly) are analyzed one by one to highlight the major issues and the specific solutions adopted are described. As said, those design choices are strictly related also to the results coming from the gear design process. In the last part of the chapter, the prototype model with the customized test bench is presented and shortly analyzed.

The fourth chapter is dedicated to the analysis of performances of the damper through simulations and software computations. Here we summarize the results concerning three main aspects of the performances: the gearbox efficiency (evaluated in the range of nominal operating conditions), the mass and inertia properties (that are important parameters also affecting the suspension operation) and the evaluation of the noise level produced during the damper operation (performing the acoustic analysis with different approaches, both with numerical simulations and analytical methods).

In the last chapter we mainly focus on the possible future development of the project, that is the installation of the device on a real vehicle suspension. Even if the design phase is oriented to the definition of the prototype, anyway we analyzed some issues concerning the assembly on a real suspension architecture. Taking into account the preliminary analysis on leverage solutions (carried out in the previous thesis work), here we analyze possible critical points of those leverage configurations while proposing an alternative positioning inside the suspension. Finally, there is also an overview of the modifications to be adopted on the model for fitting it on the suspension.

2 Planetary gearbox

The rotative damper that is the object of this thesis project is similar from a functional point of view to the patented models presented in the previous chapter; in particular, it is an electromechanical rotary damper that is featuring a gearbox stage (that amplifies the rotational input from the suspension leverage motion) and an electric motor (that is providing the damping force with its inertia). A functional scheme representing the main stages of the device is represented in ***Figure 2.1***. As said, the design is focused on the gearbox, since the electric machine will be re-used from a previous work (an electro-hydraulic damper).

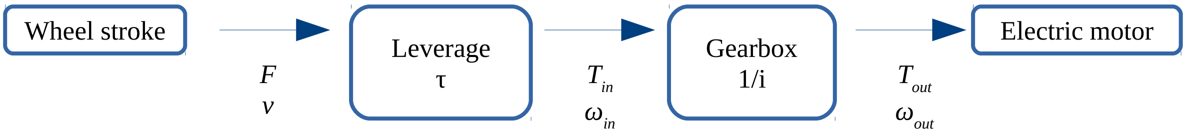

Figure 2.1*: functional scheme of the electromechanical rotative damper*

In this chapter, the design process of the planetary gearbox will be described step by step, starting from the first rough model to the last refined version, analyzing at the same time the main factors influencing the gear design.

2.1 Brief introduction on KISSsoft

Nowadays, any engineering work is widely supported by the computer: it speeds up the design process and allows to perform lots of simulations, and this can help the engineers in the optimization of any project.

In our case, the software used for the gears design is the *KISSsoft* package [14] (version release 2017): a software for mechanical engineering applications, a “high-quality tool for sizing machine elements, reviewing calculations, determining component strength, and documenting safety factors and product life parameters”. In particular, it performs sizing calculations of mechanical transmissions elements, including not only gears but also bearings and shafts.

The gearbox model is managed from the main window (***Figure 2.2***): the 3D view is in the middle, on the left there is the model tree that is showing the components of the model, while on the right there is the functional diagram that is showing the power flow and the relative connections among the constitutive elements.

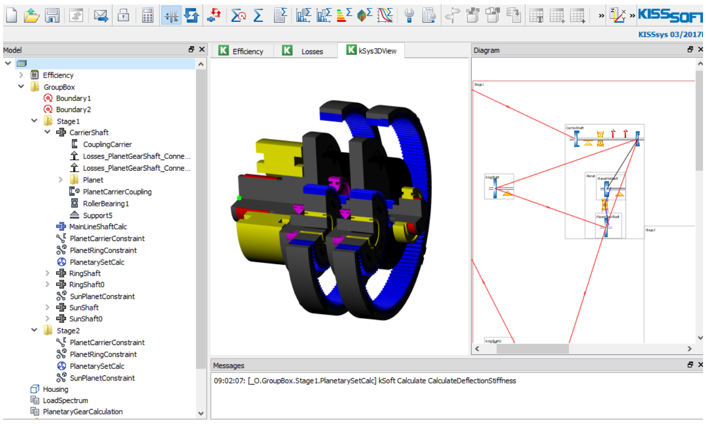

```
09:02:07: [_O.GroupBox.Stage1.PlanetarySetCalc] kSoft Calculate CalculateDeflectionStiffness
```

***Figure 2.2**: KISSsoft: user interface main window for the management of the gearbox model*

The gears calculation module is organized in a three step process:

- *Rough sizing*: from very few basic input (nominal transmission ratio, number of teeth), the calculation is providing some gears configurations that are satisfying those constraints within a certain range.
- *Fine sizing*: starting from the selected rough solution, the fine sizing calculation allows to refine the design by taking into account more detailed parameters as gear module, profile shift, diameter constraints and other conditions. The output of the computation is showing a list of many variants of the gears configuration, among which the optimal solution can be selected by comparing different parameters such as contact ratios, weight, efficiency, noise level or safety factors (also thanks to a graphical comparison of the results).
- *Modifications sizing*: ideally this is the last step of the gear design process. After having defined the complete gear macro geometry, an advanced analysis of the gears can be performed: tooth profile modifications can be introduced and their effect on the working performances of gears can be analyzed (for example to reduce the wear or to optimize the noise level). Clearly the choice of the proper modifications requires a deeper experience and knowledge of the gear design, and in this case we will not consider such modifications.

2.2 Original planetary gearbox model

As said, the main features of this project have already been set up in a previous thesis work [15]; in particular it was focused on two points: the analysis and selection of the most appropriate leverage solution (considering the constraints of the suspension architecture and of the transmission ratio required for the proper working of the electric machine) and a preliminary gearbox design.

Since on a vehicle the constraint of space and weight are nowadays very demanding, the comparison among the different possible gearbox architectures has been evaluated taking into account the overall dimensions and the gearbox weight, but also efficiency and noise level are important factors to be considered.

The two examined solutions are represented in ***Figure 2.3***:

- *fixed axis* configuration (on the left): the gearbox is featuring 3 stages with spur gears, with power split on the first and second stage;
- *planetary* configuration (on the right): it is a 2 stage gearbox with three planets for each stage; the input is provided to the planetary carrier, the external ring gear is fixed on the case assembly while the output is on the sun gear. For sake of simplicity, the two stages are equal.

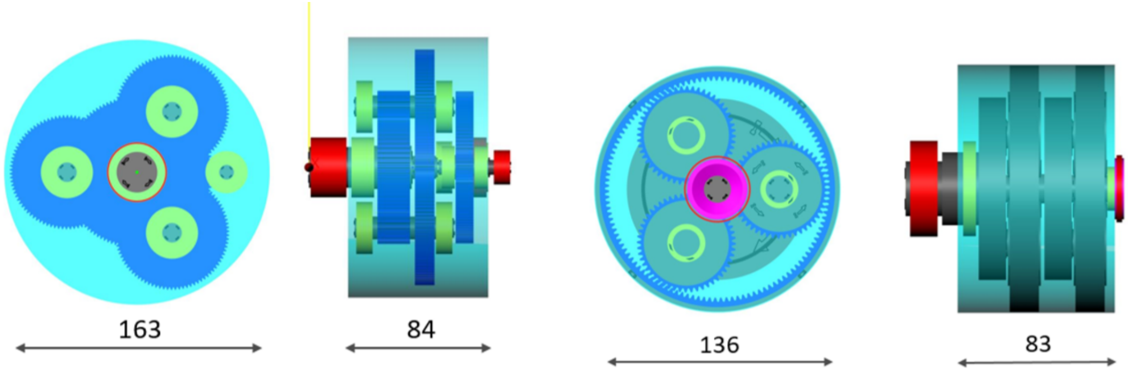

(a) *Overall dimension parallel Axes* (b) *Overall dimension planetary Axes*

***Figure 2.3**: preliminary gearbox design: the two proposed configurations [15]*

From the analysis of the two models, there is not a dominant solution in terms of overall performances; the fixed axis configuration results to have a slightly lower noise level, a slightly higher efficiency (even if the difference between the two is negligible since the major contribution is given by the electric machine), while the planetary configuration keeps a smaller external diameter.

Clearly this preliminary analysis is not enough to state what is the optimal solution; by the way, in our work we decided to focus on a single configuration and to try to optimize it. Since at first approach the overall dimensions are a relevant characteristic in the design of the whole system (also for the coupling with the electric motor), the solution selected is the two stage planetary gearbox. As can be seen in the previous figure, the planetary model has a smaller diameter (about 27 mm less): at equal dimensions, a planetary stage is capable to perform a higher transmission ratio, so this potential is important if we want to obtain a more compact solution.

Before giving further details on the planetary gear set, is necessary to list what are the starting points considered for the gearbox design. Taking in mind the functional scheme of the rotative damper assembly in ***Figure 2.1***, we can better understand the transmission ratios of the different stages. The electric machine is capable to supply a torque $T = 1{,}1$ Nm @ ω_{out} = 10.000 rpm and in order to obtain the required damping force on the wheel stroke, the system (leverage and gearbox) must guarantee a total transmission ratio k = 1,5 mm/rad (that is the ratio between the input vertical wheel speed and the output rotational speed of the gearbox). The considered leverage configuration assures a transmission ratio τ = 115 mm/rad, so the required ratio for the gearbox is i = 76. By the way, to have a conservative dimensioning, the target ratio was set equal to 88.

The data about the required transmission ratio are referred to the leverage configuration represented by solution 4 in ***Figure 5.2***; more details about the leverage and its requirements will be provided in *Chapter 5*, when introducing the suspension model.

$$\begin{aligned} &\textit{overall transmission ratio} && k = \frac{v}{\omega_{out}} = \tau \cdot \left(\frac{1}{i} \right) = 1{,}5\, mm/rad \\ &\textit{nominal leverage transmission ratio} && \tau = \frac{v}{\omega_{in}} = 115\, mm/rad \\ &\textit{required gearbox transmission ratio} && i = \frac{\omega_{out}}{\omega_{in}} = 76 \end{aligned} \qquad \textbf{Eq. 2.1}$$

It is important to notice that in this case the gearbox must work as a multiplier, in order to increase the output rotational speed respect to the input provided by the leverage.

From the characteristic of the hydraulic damper it is possible to obtain the values of the required force. The nominal load that was considered for this first sizing of the gears is an input torque to the gearbox T_{in} = 115 Nm @ ω_{in} = 113 rpm: by the mentioned ratios it corresponds to force at the wheel F = 1000 N @ v = 1,36 m/s, that is representing an operating point around the middle of the minimum damping characteristic (***Figure 2.5***).

On the base of this, a rough and a fine sizing were performed in KISSsoft: in order to have a reference starting point, and to compare this model to the last improved versions of the planetary gear set, some geometrical data are summarized in ***Table 2.1***.

Planetary spur gears		
m_n	1	mm
α	20	°
i *(single stage)*	9,3	-
z_{sun} / z_{planet} / z_{ring}	15 / 52 / -123	
b *(equal stages)*	15,5	mm

Table 2.1*: main geometrical dimensions of the original planetary gearbox [15]*

In ***Table 2.2***, also the results concerning the stresses and the safety factors evaluation are summarized: they are referred to the first stage, since it is the most critical from loading point of view (highest input torque, that is reduced in the second stage). The material considered for the gears is the steel alloy 18CrNiMo7-6, with yield limit σ_y = 850 MPa and ultimate strength σ_{max} = 1200 MPa.

	Sun gear	*Planet gear*	*Ring gear*
σ_{root} **[MPa]**	229	293	253
σ_{flank} **[MPa]**	1185	1323	1313
SF	2,18	1,80	2,96
SH	1,04	1,21	2,31

Table 2.2*: stresses and safety factors related to the first planetary stage [15]*

Finally, not only the weight but also the resulting equivalent inertia is fundamental for the dynamics of suspension motion. The rotating inertia is converted into linear equivalent inertia by considering the leverage transmission ratios.

Gearbox mass	m_{tot}	3,9	kg
Equivalent rotational inertia	J_{eq}	0,528	kg*m^2
Equivalent mass	m_{eq}	40	kg
Total equivalent mass *(gearbox + motor + leverage)*	$m_{eq\ tot}$	55	kg

Table 2.3*: masses and inertia of the preliminary planetary gearbox solution [15]*

These are only the main characteristics of the planetary configuration: starting from this first model, the design process is carried out in order to refine the dimensioning of the gearbox.

2.3 Planetary gearbox: design steps

After having checked the main performances of the original planetary model described in the previous chapter (in particular focusing on the safety coefficients), the refinement of the gear stage is starting with a first fine sizing calculation in KISSsoft. It is important to notice that the gears considered (here and in the following planetary models) are always spur gears with straight teeth: we will not consider variations of the pressure angle that is fixed $\alpha = 20°$, and so it will be often not specified to avoid repetitions. Even if helical gears provide better performances in terms of noise and wear, while spur gears give an higher efficiency, in our case we will not consider the use of helical gears to avoid to introduce axial forces and so to simplify the design of the supports of the gear shafts.

2.3.1 *First planetary gearbox fine sizing*

As first trial, we consider to apply an input torque T_{in} = 115 Nm @ ω_{in} = 166 rpm, that is corresponding to a vertical force on the wheel F = 1000 N @ v = 2 m/s: actually these values are not corresponding precisely to a working point in the damper characteristic, but simply it is the mean force value considered at the maximum speed.

$$nominal\ input\ load\ for\ first\ sizing \qquad T_{in} = 115\,Nm\ \ @\ \ \omega_{in} = 166\,rpm$$

These data are the input on the first planetary stage: we will focus on the first stage since it is subjected to the highest torque, and all the following results are referred to the first stage, unless specified in another way.

The selected gear material is the steel 18CrNiMo7-6, case hardened, generally proposed for high strained gears and shafts; it has a yield limit σ_y = 850 MPa and ultimate strength σ_{max} = 1200 MPa.

$$gears\ first\ material\ selection: \boldsymbol{steel\ \ 18\,CrNiMo\,7-6}$$
$$strength \qquad \sigma_y = 850\,MPa \qquad \sigma_{max} = 1200\,MPa$$
$$surface\ \ hardness = 61\,HRC \qquad core\,hardness = 325\,HBW$$

Clearly, the aim of the fine sizing is to select an optimal solution with reduced dimensions but that keeps acceptable values of safety factors. The main characteristics of this first configuration are summarized in ***Table 2.4***: as we can see, in order to keep the required transmission ratio, the diameter is reduced by reducing the gear module (the overall external diameter accounts also for the housing defined in the KISSsoft model). By the way, we need to check what is the effect on the teeth stress, and consequently on the safety coefficients.

Planetary gears		
m_n	0,8	mm
i *(single stage)*	9,34	-
z_{sun} / z_{planet} / z_{ring}	16 / 58 / -134	
b_{sun} / b_{planet} / b_{ring}	13,5 / 13 / 13,5	mm
d *(external)*	120	mm

Table 2.4*: planetary first fine sizing: main characteristics*

The calculation module is performed according to the ISO 6336:2006 method B, that evaluates the fatigue life of gears: the rating loads must be defined.

- Constant input, “nominal” load T_{in} = 115 Nm @ ω_{in} = 166 rpm: it is clearly not the normal continuous operating condition of the rotative damper, but it gives a first indication on the margin of size reduction that can be obtained with a further planetary optimization;
- First rough definition of a more realistic loading condition: the input is not considered constant, but divided into “load bins”, since the gearbox is subjected to the maximum input force only for a minimum amount of time. So this load spectrum is defined in such a way: for 10 % of time we apply the “nominal” load, while for 90 % of time we consider to reduce the input values to 1/8 T_{in} and 1/4 ω_{in}. By the way, it is important to remark that for each load bin, the input torque and speed are anyway constant, so it is not properly a realistic condition.

In the following table, the results are compared for the two cases. *SF* is the safety factor concerning the tooth bending root stress, while *SH* is the tooth flank safety coefficient due to Hertzian contact stress; the reference gear life is set to 20.000 h.

		Sun gear	Planet gear	Ring gear
Constant input nominal load	**SF**	1,98	1,25	2,37
	SH	0,85	1,00	2,52
Load bins 10% - 90%	**SF**	2,02	1,76	3,34
	SH	1,07	1,26	3,11

Table 2.5: first fine sizing: safety results comparison

As can be seen, the critical points are concerning the flank safety, also due to the high requirement on the gear life: as suggested also by the KISSsoft manual, it is recommended to have a flank safety higher than 1.

So at this point, the straight choice is to modify the gears material in order to obtain a stronger flank resistance: from the KISSsoft database, the new selected material is the grade 3 steel AGMA 2001-C95 (case carburized, with σ_y = 887 MPa and σ_{max} = 1035 MPa). Compared to the 18CrNiMo7-6 steel, it has the same surface hardness, but a higher endurance limit flank.

$$\begin{gathered} gears\ new\ material\ selection: \boldsymbol{steel\ grade\,3\ AGMA\,2001-C\,95} \\ strength \qquad \sigma_y = 887\,MPa \qquad \sigma_{max} = 1035\,MPa \\ surface\ hardness = 60\,HRC \qquad core\,hardness = 300\,HBW \end{gathered}$$

The improvement obtained are shown in the following table, considering the constant torque input.

		Sun gear	Planet gear	Ring gear
Constant input	**SF**	2,40	1,52	2,88
	SH	1,07	1,25	3,16

Table 2.6: safety values with the new gear material selected

At this point, in order to refine the gear dimensioning, it is not enough to consider simply the constant input load, but we need to define a more realistic loading condition that can be used in the computation. In the following section the method to obtain such realistic load spectrum is described.

2.3.2 *Definition of the load spectra used in the calculations*

Having a constant input is not clearly the actual load acting on the vehicle suspension; the real excitations coming from the road profile should be analyzed and processed in such a way to be inserted as input for the gear set calculations.

So the starting point is to obtain a time history sample of the force and speed arising from the wheel moving on the road irregularities; an experimental data collection is not feasible, so a faster and more practical way is to perform some computer simulations with a virtual car model.

The considered quarter car model has two degrees of freedom (a basic description of the vehicle dynamics can be found in [2]) and it is implemented in Simulink® (Matlab MathWorks). Its functional scheme is represented in ***Figure 2.4***: the road profile *h* (represented by a random signal) is given as input to the quarter car dynamic model, while the resulting force is taken by the damper characteristic (once obtained the wheel vertical speed by the dynamics of the model).

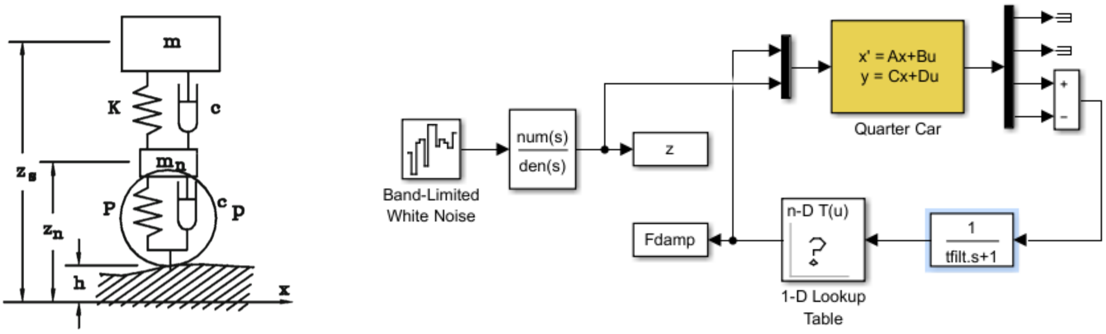

Figure 2.4*: two degrees of freedom quarter car model implemented in Simulink (block scheme on the right) to perform road profile simulations*

The first thing to define is the damping characteristic that we want to reproduce: it is simply represented as a look up table defined by few force *F* - speed *v* points. Since in a more large perspective there could be the possibility to introduce active damping control, we will consider the two extreme characteristic curves, with minimum and maximum damping; they are represented in ***Figure 2.5***:

- the minimum damping curve (blue) is a straight line, that is starting from zero and it is arriving to the maximum *F* = 1500 N @ *v* = 2 m/s;
- the maximum damping curve (orange) is an ideal bilinear regressive characteristic, with the knee at *F* = 1000 N @ *v* = 0,05 m/s and reaching its limit load at *F* = 2000 N @ *v* = 2 m/s.

The maximum force value will be the load used for the static strength verification (worst case for mechanical integrity).

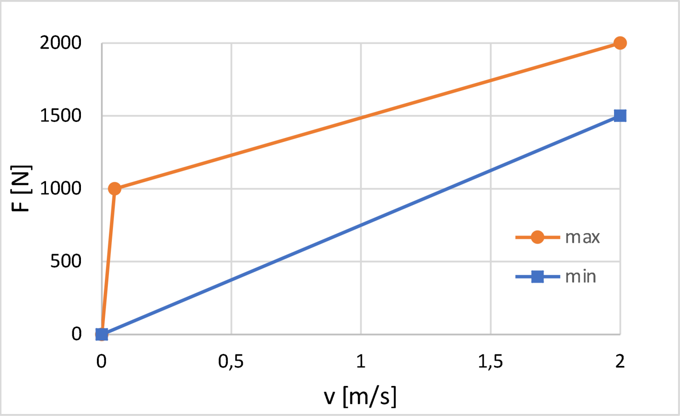

***Figure 2.5**: damper characteristics: maximum and minimum damping*

The other important input to be defined is the signal representing the road profile; obviously such road irregularities can be only described in a statistical way, so we will refer to the ISO 8608 standard road classification: there are five road quality classes, from class A (very good road) to class H (unpaved, very poor quality road), each of them characterized by a certain power spectral density of the vertical road displacement.

Once defined such input parameters, the simulation is performed: an example of the results obtained is the damping force as function of time, represented in the following plot.

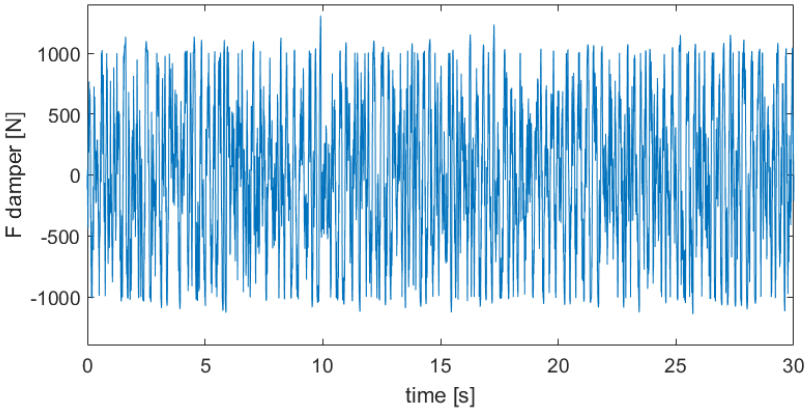

***Figure 2.6**: example of damping force time history obtained by quarter car model simulations (only 30 s of simulation are shown)*

Now the problem is how to translate the force and speed signals into suitable input for the KISSsoft calculation; obviously, first of all they are converted into torque and rotational speed considering the transmission ratio τ.

KISSsoft allows computations with not constant load, but this “varying” load is actually defined by a load spectrum: the load spectrum is subdivided into load bins, each of them representing a fraction of the total gear operating time, but anyway in each load bin the torque and the speed are defined by constant values.

On the base of this, if we would ideally reproduce the random torque input, we would have defined a load spectrum constituted by an “infinite” number of load bins representing the instantaneous variations of the input values; being this solution not practically applicable, the only way is to discretize the load history. This is acceptable from the point of view of fatigue evaluation: considering that the fatigue is a cumulative phenomenon, in case of a variable stress we evaluate the damages accumulated for each stress level and then simply obtain the total damage by adding the different contributions. This is the concept applied in the load spectrum calculation: we “count” for how long the gears are exposed to a certain value of stress.

It is important to not confuse the external torque input that is varying in time with the normal fatigue loading to which each tooth is subjected due to the gear rotation (even with constant speed): so any approach that is considering the torque in terms of mean value or amplitude of oscillations (for example the rainflow approach) will be not properly correct.

In practice, we define some torque (and speed) intervals (10 Nm is a reasonable trade off between the number of bins and the accuracy of the discretization) and by analyzing the load time history we evaluate for how long the torque value remains within each interval (obviously automatically performed in the Matlab script); in this way we define the load spectrum. The negative values of torque and speed represent rotations in the opposite direction.

These load spectra used in KISSsoft are defined by: the fraction of time, the torque value and the rotational speed. In the following plots, each load bin is represented by a point, the connecting lines have only an aesthetic function. Here are listed the different operating conditions considered, all referred to the input on the first planetary stage: these load spectra are obtained with different road profiles, in order to be used in the further dimensioning of the gears.

- **ISO C @ 100 km/h** road profile (***Figure 2.7***): in the two plots the simulations with both damping characteristic are represented. As can be seen, in case of maximum damping characteristic (orange curve) the highest frequency load is about the force value of the knee point (F = 1000 N corresponding to T_{in} = 115 Nm).

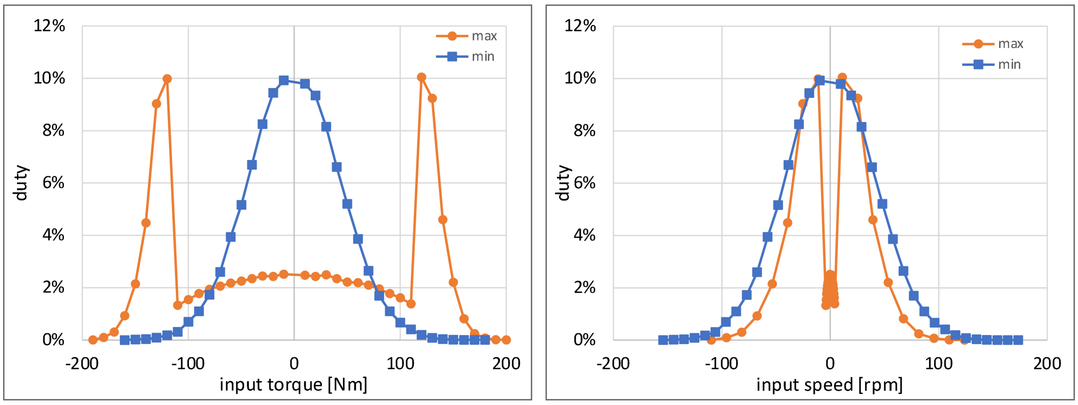

***Figure 2.7**: load spectrum obtained with ISO C road profile @ 100 km/h, with maximum and minimum damping*

- **ISO B @ 70 km/h** road profile (***Figure 2.8***): it will be considered the average city road used as reference for dimensioning. The detailed data table of this load spectrum (bin frequency, input power, speed and torque) is included in the KISSsoft calculation report, presented in *Appendix A.*

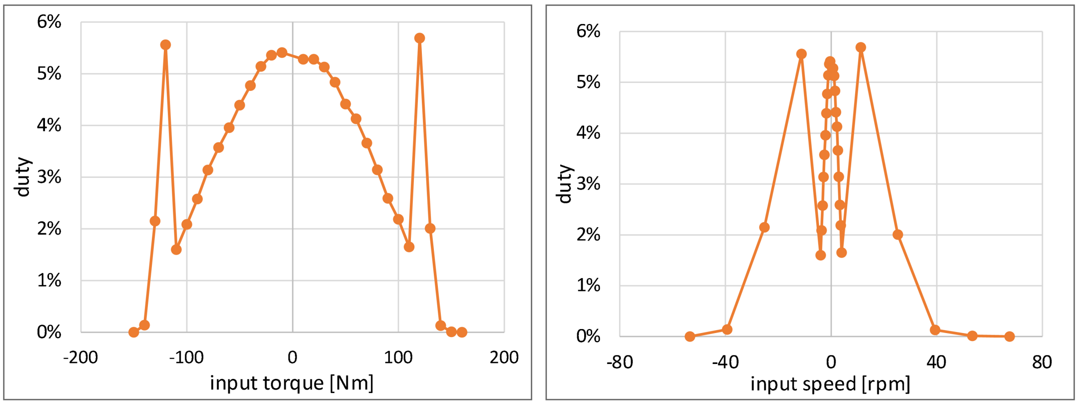

***Figure 2.8**: load spectrum obtained with ISO B road profile @ 70 km/h*

- **ISO A @ 120 km/h** road profile (***Figure 2.9***): very well paved road, it represents the driving conditions on highways. Clearly, due to the smaller road irregularity, the most of loading conditions are concentrated about smaller values of torque.

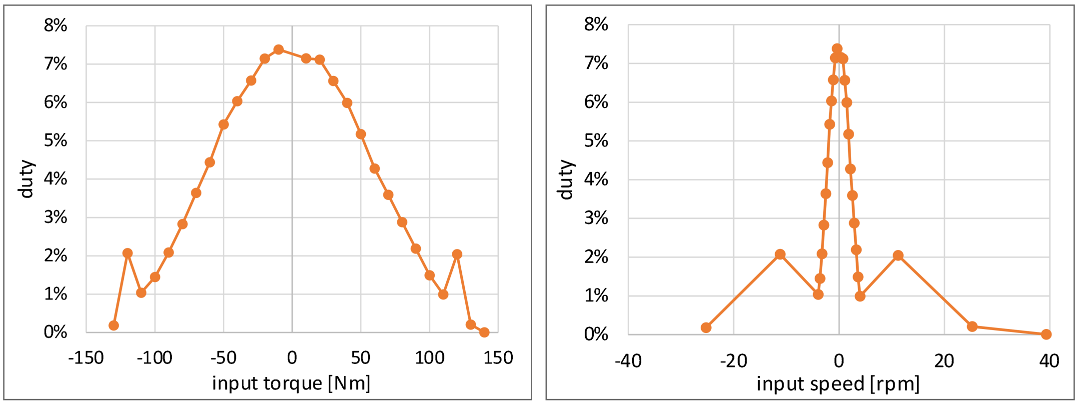

***Figure 2.9**: load spectrum obtained with ISO A road profile @ 120 km/h*

On the base of these considerations, we can evaluate the new safety values considering the loading conditions given by the ISO C road profile: as can be seen in ***Table 2.7***, the safety factors are higher than the previous results because there is a relevant percentage of loads that are lower than the maximum force considered before, even if running on an ISO C road at 100 km/h is a quite demanding operating mission for a passenger car.

		Sun gear	*Planet gear*	*Ring gear*
ISO C @ 100 km/h	***SF***	1,32	1,74	2,60
	SH	1,23	1,52	3,74

***Table 2.7**: safety factors considering the ISO C load spectrum input*

After these first gears dimensionings, a first modification of the shafts and carriers dimensions is required in order to adapt them to the new gears size; in particular, the planetary carrier thickness is reduced to 12 mm (so reducing the axial length), its diameter is reduced to 90 mm and the planet pin shaft diameter is reduced to 12 mm.

By the way, these modifications have little effect on the gears sizing because they are concerning only the KISSsoft model: in the gear computation no inertial effect is considered and, for the moment, no shaft misalignments or deformations are taken into account. As we will see in the following chapter, a more detailed analysis of the carrier will be performed when developing the 3D model: in that case, the geometry definition will be strongly affected by the stresses and deformations caused by the loading conditions, so a certain optimization of the shape will be carried out.

The only relevant thing that we can notice is concerning the efficiency of the gearbox: by reducing the planet shaft diameter, the planet bearings are smaller and the overall efficiency of the system is higher because the losses due to planet pin bearings are lower.

As can be seen by the previous results, considering a more realistic load there is still a margin of improvement, if we want to reduce the dimensions by keeping reasonable safety values (since the minimum safety factor was 1,23). For this reason, another sizing computation is performed and, among the proposed configurations, a new solution is selected. In particular, the main geometrical dimensions are listed in the following table: the external diameter is reduced thanks to a lower module.

Planetary spur gears		
m_n	0,6	mm
i *(single stage)*	9,26	-
z_{sun} / z_{planet} / z_{ring}	21 / 76 / -174	
b_{sun} / b_{planet} / b_{ring}	13,5 / 13 / 13,5	mm
d *(external)*	115	mm

Table 2.8*: planetary configuration with 0,6 mm module*

Up to now, the gears sizing has been performed simply considering the basic gear geometry: we defined the module, the transmission ratio, the centers distance and the number of teeth, consequently the diameters are known. By the way, the simple involute profile of the tooth often is not enough to guarantee the proper working of the gears in particular operating conditions (for example to vary the center distance by keeping the same number of teeth). In such cases, the proper selection of the profile shift and profile modifications is required in order to avoid interferences in meshing or the excessive and abnormal wear of the gears teeth.

Obviously, a strong experience is required to set the proper parameters, anyway an analysis is performed to understand what could be the influence of such modifications on the gearbox performances. Moreover, we need to take into account a possible future prototype phase, so the feasibility of such modified profiles will be only possible with customized gears, not by using gears from catalogues.

So starting from the previous gearbox configuration with the module equal to 0,6 mm, different modifications are considered to try to optimize the gear meshing and to improve the efficiency.

The first configuration described in ***Table 2.8*** has the profile shift coefficient x^* suggested by default by the software: it is set to optimize the specific sliding between the teeth faces.

The first introduced change is related to the profile shift only: the new values are set to obtain an higher efficiency. Finally, in the last model also additional profile modifications are introduced:

- profile shift coefficient to optimize the specific sliding and so to reduce the losses due to gear meshing;
- tip and root relief (deviation from the ideal involute profile) for smooth meshing;
- rounding of tooth tip edges to improve the meshing and reduce the wear.

The effect on gear meshing can be easily seen in ***Figure 2.10***, just to show an example of contact analysis: it represents the evaluation of tooth flank wear of the sun gear, where we can appreciate the modifications on the profile (on the right) and consequently the smaller amount of removed material due to wear (blue lines).

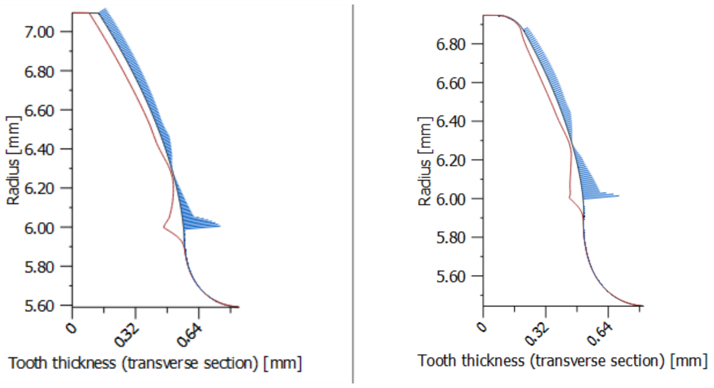

***Figure 2.10**: tooth flank wear comparison: basic model and tooth with profile modifications*

The improvement given by the modifications can be described in a quantitative way by evaluating the gearbox efficiency (a more detailed description of the efficiency calculation will be provided in *Chapter 4*). In this case we will focus only on gear meshing losses, since the churning losses are negligible, the losses due to sealing are not taken into account and the bearings losses remain unchanged in the three models.

As can be seen in ***Table 2.9***, starting from the basic planetary configuration with module 0,6 mm, there is an improvement of efficiency of more than 1 %, showing that the modifications on the tooth profile are effective. By the way, we need to take this results only as rough comparison, since the efficiency is computed with constant input load (T_{in} = 115 Nm @ ω_{in} = 166 rpm) and the calculation parameters are still not adjusted to represent more realistic loading conditions.

	"basic" model module 0,6 mm	*Model with optimized profile shift*	*Model with profile modifications*
Gear meshing efficiency	95,67 %	96,07 %	96,82 %

***Table 2.9**: efficiency calculation: influence of profile modifications*

Moreover, it is interesting to have a look also to the safety values just to have a more complete comparison. In ***Table 2.10*** the results related only to the sun gear of the first stage are shown, which is the smallest gear and so subjected to the biggest stress. It can be noticed that there is not a direct correlation with the improvement of the efficiency: even if the modifications give an overall better meshing, the tooth profile is modified and consequently both the tooth thickness and the face contact are affected, so influencing the stress values in a different way.

	"basic" model module 0,6 mm	*Model with optimized profile shift*	*Model with profile modifications*
Root safety SF	1,33	1,06	1,10
Flank safety SH	1,17	1,10	1,11

Table 2.10*: safety factors of sun gear computed with the ISO C road profile load spectrum*

2.3.3 *Planetary sizing: considerations on the gear life*

The required gears life was set equal to 20.000 h in the previous dimensionings: actually if we take as reference the vehicle running at 100 km/h on the ISO C road profile, this results in having a rotative damper life of 2 millions of kilometres, a lifecycle comparable to the one of a truck. Obviously, this required gear life determines an over-dimensioning of the system, since the minimum safety values must be assured for such operating time.

For this reason, the required life must be set to a reasonable value for the calculation: considering that the average useful life of a car is assumed to be 250.000 km, at 100 km/h this corresponds to an operative lifetime of 2.500 h. This value is the new planetary gearbox required life, since it is a suspension basic component and should not be subjected to any repair or substitution.

Moreover, this new sizing has been performed with directly input the load spectrum as loading conditions, so the solutions proposed by the software will be already more refined.

The results of the first sizing with these new calculation parameters are summarized in ***Table 2.11***: it has a diameter 10 mm smaller compared to the previous solution.

Planetary spur gears		
m_n	0,5	mm
i (single stage)	9,26	-
z_{sun} / z_{planet} / z_{ring}	23 / 82 / -190	
b (equal stages)	13,5	mm
d (external)	105	mm

***Table 2.11**: main characteristics of planetary model with 2.500 h gear life required*

By the way, to have an idea of the operating conditions, we need to check the safety values. In the following table we can see that the critical point of this model is the root bending stress *SF*, due to the excessive reduction of the tooth thickness (in fact the module is 0,5 mm). In addition to this, we need to take into account the actual planetary operation: the real torque is oscillating, giving an additional fatigue contribution to the normal tooth fatigue stress, and the three planets could be not loaded in the same way (these issues will be analyzed later).

		Sun gear	Planet gear	Ring gear
ISO C @ 100 km/h maximum damping	**SF**	1,03	1,11	1,45
	SH	1,25	1,52	3,61

***Table 2.12**: safety factors of planetary model with 2.500 h gear life required*

Since these safety values are quite low, a different planetary configuration is selected: a minimum root safety higher than 1,1 is assured by choosing gears with bigger diameters. The main features are shown in ***Table 2.13***.

Planetary spur gears		
m_n	0,5	mm
i (single stage)	9,345	-
z_{sun} / z_{planet} / z_{ring}	24 / 88 / -201	
b (equal stages)	13,5	mm
d (external)	110	mm

***Table 2.13**: second sizing with 2.500 h gear life required*

Since this solution is acceptable for what concern the fatigue safety, we must also check the strength with a static load.

- **Maximum load** for static strength verification: input T_{in} = 230 Nm @ ω_{in} = 166 rpm, corresponding to a force F = 2000 N @ v = 2 m/s. This load is the maximum limit force provided by the damping characteristic, and even if it is not a nominal operating point, we want to assure the mechanical integrity also in this exceptional case.

The results of safety computations with these different loading conditions are summarized in the following ***Table 2.14***.

		Sun gear	Planet gear	Ring gear
ISO C @ 100 km/h maximum damping	**SF**	1,14	1,15	1,60
	SH	1,28	1,61	4,05
ISO C @ 100 km/h minimum damping	**SF**	1,46	1,46	2,04
	SH	1,54	1,91	4,61
Maximum load static strength	**S_{yield}**	2,86	2,91	4,30
	S_{lim}	3,34	3,40	5,02

Table 2.14: *safety factors evaluation (second sizing with 2.500 h required life)*

It is interesting to point out that in both cases we tried also to introduce some profile modifications, but due to the safety factors that are already small, there has not been an effective improvement of the efficiency without further reducing the margin of safety.

At this point it is reasonable to introduce more refined hypothesis on the loads considered. With a variable damping control system, actually the maximum damping characteristic is not used for 100 % of the time: so there is still margin in reducing the planetary dimensions if we consider the previous sizing with the ISO C road profile. Just to have a first idea, a planetary configuration was dimensioned with the ISO C load spectrum with minimum damping characteristic: the diameter is reduced to 103 mm, but clearly also the safety values are smaller, as can be seen in the following table.

		Sun gear	Planet gear	Ring gear
ISO C @ 100 km/h maximum damping	**SF**	1,02	1,08	1,42
	SH	1,26	1,53	3,23

Table 2.15: *safety factors of planetary model dimensioned with the minimum damping characteristic*

2.3.4 *Planetary sizing: considerations on the reference loading conditions*

As seen before, the ISO C road profile @ 100 km/h is a quite several running condition for a vehicle: for simulation purposes it is important to have a good correlation between the mathematical models and the real road profiles in order to obtain significant and not misleading results, as in case of energy recovery potential.

An interesting study on this topic is *“Simulated Road Profiles According to ISO 8608 in Vibration Analysis”* [16]: it points out that the ISO 8608 road classification is based on experimental data collected in the 1960s and 1970s, so it is clear that these road classes are not updated; in fact it is said that class B and C profiles can be used to simulate nowadays low quality paved roads. Moreover, taking into account the limitations on the comfort levels, the maximum suggested speed on a class C road is between 30 km/h and 60 km/h.

On the base of these considerations, obviously the load spectrum obtained by the ISO C road profile @ 100 km/h is determining a certain over-dimensioning of the rotative damper. So we need to define new reference loading conditions that will be used in the new steps of planetary size refinement (the load spectrum definition was already presented in section *2.3.2*).

- **ISO B @ 70 km/h** road profile with maximum damping characteristic: it represents the average city road, used as reference for fatigue dimensioning. Obviously the different vehicle speed also changes the required service life of gears: it is set equal to 3.600 h (since 3.571 h are corresponding to 250.000 km for a vehicle running at 70 km/h).
- **ISO A @ 120 km/h** road profile, for fatigue life evaluation: it represents highway driving conditions, it will be used only as comparison.
- **Bump** of 20 mm @ 70 km/h, for static strength: it determines a peak input torque T_{in} = 151,4 Nm @ ω_{in} = 55,4 rpm (corresponding to a maximum force at wheel equal to F = 316,5 N @ v = 0,67 m/s).
- **Maximum limit load**, worst case for static strength: the maximum value of the damping force characteristic F = 2000 N @ v = 2 m/s gives an input torque T_{in} = 230 Nm @ ω_{in} = 165,4 rpm.

The first new sizing using as input the ISO B road profile load spectrum gives a planetary gearbox with an overall diameter of 93 mm (keeping 0,6 mm module and 13,5 mm facewidth), that is a great improvement compared to the previous 110 mm. Anyway, the relevant difference between the class C and class B load spectra is still evident in the safety values: as can be seen in the following table, the higher safety margins allows to further reduce the gearbox dimensions.

		Sun gear	*Planet gear*	*Ring gear*
ISO B @ 70 km/h	***SF***	1,45	1,58	2,21
	SH	1,27	1,64	4,22

Table 2.16*: safety values of the first planetary dimensioned with the ISO B road profile*

The first possibility is to reduce the tooth facewidth to 10 mm; with a second sizing we also obtain that the eternal diameter is 90 mm: this planetary gearbox configuration is the one that is used to start to develop the first 3D CAD model, and its features are summarized in ***Table 2.17***.

Planetary spur gears			
Normal module	m_n	0,6	mm
Pressure angle	α	20	°
Center distance	a	22,5	mm
Transmission ratio (single stage)	i	9,346	-
Number of teeth	$z_{sun} / z_{planet} / z_{ring}$	16 / 58 / -134	
Tooth facewidth (equal stages)	b	10	mm
Profile shift coefficient *sun ; planet ; ring gears*	x^*	0,459 ; 0,065 ; 0,409	-
Overall external diameter	d	90	mm

Table 2.17*: gears properties of the final sizing with the ISO B @ 70 km/h load spectrum*

This planetary configuration is also optimized from the point of view of shafts dimensions: as said the facewidth is 10 mm, while the thickness of the two planetary carriers is 6 mm (this is a result of a first attempt to optimize the carrier shape according to a FEM stress analysis, as it will be described in the dedicated chapter). The resulting total axial dimension is then reduced to 82,5 mm (***Figure 2.11***).

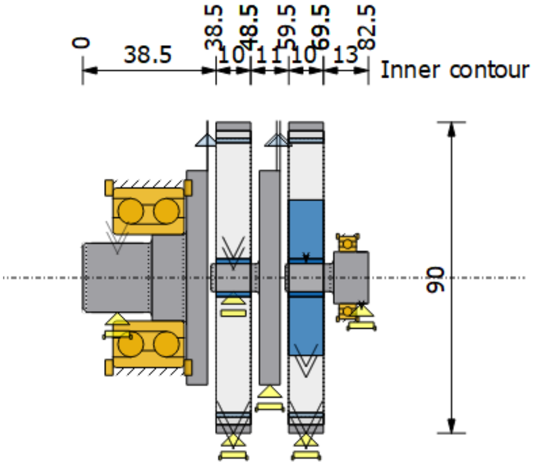

***Figure 2.11**: shaft configuration of the last planetary model dimensioned with ISO B load spectrum*

To have the complete view of the performances of this model, clearly also the safety factors have been evaluated, both for the fatigue life and static strength. The results are presented in ***Table 2.18***: we can see that the fatigue life has reached a minimum but still acceptable limit in the case of sun gear (about 1,1), while we have no issues in the verification of the static loads.

		Sun gear	*Planet gear*	*Ring gear*
ISO B @ 70 km/h	***SF***	1,12	1,22	1,79
	SH	1,09	1,42	3,55
Bump @ 70 km/h	S_{yield}	3,14	2,72	4,41
	S_{lim}	3,67	3,17	5,15

	Sun gear	*Planet gear*	*Ring gear*
ISO A @ 120 km/h	1,32	1,57	2,33
	1,32	1,71	4,18
Maximum limit load	2,07	1,79	2,90
	2,41	2,09	3,39

***Table 2.18**: summary of the safety calculations of the model with 90 mm diameter*

With this planetary model, actually further reduction of the dimensions are not possible, since we have different constraints in the design of the gear set.

First of all, we need to guarantee a certain minimum safety factor, and 1,1 is already to the limit since actually we have not introduced yet some parameters in the calculation that account for more realistic loading conditions. Second, we have a target transmission ratio, that is related to the number of teeth and consequently the main limitation is the minimum number of teeth of the smallest gear: with such gears parameters (without considering any profile shift or modification), the minimum number of teeth to avoid interference in tooth meshing is z_{sun} = 16.

$$sun\ gear\ minimum\ number\ of\ teeth$$

$$transmission\ ratio\ sun-planet \qquad i=\frac{z_{planet}}{z_{sun}}=\frac{58}{16}=3{,}625$$

$$z_{sun\,MIN}=\frac{2\,/\,i}{-1+\sqrt{\frac{(\sin\alpha)^2}{i}\cdot\left(2+\frac{1}{i}\right)+1}}=15{,}3 \ \rightarrow \ 16$$

Eq. 2.2

Finally, we need to take into account also the manufacturing of the gears and the related stress on the shaft: assuming that it is possible to manufacture the sun gear of the first stage directly on the carrier of the second stage, the resulting shaft diameter is 8 mm. Considering the input load given by the road bump, a torque T = 16,2 Nm (reduced by the first stage transmission ratio) will be applied on the sun gear, with a resulting equivalent stress of 279 MPa on the shaft, as it shown in the diagram in ***Figure 2.12***.

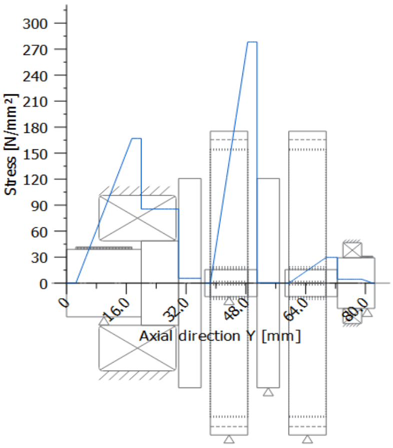

Figure 2.12: *Von Mises equivalent stress (blue line) on shafts (bump input load)*

2.3.5 Considerations on the calculation parameters and final version of the planetary gearbox

From the previous dimensioning of the planetary gearbox, the model with an overall diameter of 90 mm is a good starting point to define a first version of the 3D CAD model of the whole rotative damper assembly, since its dimensions are compatible with the diameter of the existing electric machine (that has a flange diameter of 88 mm).

By the way the development and the modifications introduced in the 3D model are not freezing the analysis of the gear set: actually their relative dimensioning requires an integration of the gears calculation performed in KISSsoft and the FEM analysis of stresses and deformations that could occur when the system is subjected to real loads.

For this reason, after a process of optimization of the different components (as we will see in detail in the following chapter), the final dimensioning of the planetary gear set tries to take into account also the results of the FEM analysis.

In the previous calculations, actually we considered an ideal planetary stage: perfect torque split among the three planets, ideal rigid supports and ideal shafts without no deformations, so assuring an ideal meshing between the gear teeth. Clearly these are not the normal operating conditions, so we need to introduce some parameters that allow to consider a more realistic loading. In the following list we will describe the new parameters updated in the calculations setup (the detailed values of such factors can be found in *Appendix A*); these calculation factors are described in the KISSsoft manual, but they are general coefficients for tooth stress evaluation, that are simply "correcting" the nominal stress value (***Eq. 2.1***).

- *Load spectrum input*: since in the spectrum there are bins with negative values that represent the rotation in the opposite direction, this is affecting the flank safety because actually the loads are acting on both faces of the tooth (instead of having all the load on a tooth face as in a single direction of rotation). So the resulting flank safety factor will be related only to one direction of rotation (the worst one) and it will be slightly higher than considering a single direction of rotation.
- *Application factor K_a*: in general it takes into account the regularity and any uncertainty on the load. Obviously, the load coming from road irregularity is not uniform at all and it can presents also relevant shocks (as a road bump), so K_a should be bigger than 1; by the way since the calculation is performed with the load spectrum (that already represents a variable load), this factor is set equal to 1 as required by the software.
- *Dynamic factor K_v*: it takes into account additional forces caused by natural frequencies (resonance) in the tooth meshing. It is directly computed according to the selected calculation method, and in particular it ranges from 2 to 2,5 among the different load bins.
- *Transverse load factor $K_{H\alpha}$*: it accounts for the non-uniform load distribution along the line of contact during tooth meshing, which is due to the deviations from the ideal tooth profile. Also this factor is automatically computed according to the calculation method.
- *Load distribution coefficient K_γ*: takes into consideration the uneven load distribution across multiple planet gears, but actually in the calculation the input load is multiplied by this coefficient, so in our computation it remains set to 1, otherwise it will determine a fictitious increase of load on all the planets. Moreover, this is the suggested value in the manual in case of 3 planets stage. The effects of uneven torque split will be analyzed from the point of view of the resulting stresses and deformations on the carrier.

- *Alternating bending factor Y_m*: in a single revolution, the teeth of planet gears are subjected to an alternating bending load due to the meshing with the ring and sun gears: they are driven by the ring gear and they are driving the sun gear. So we set $Y_m = 0{,}7$ only for the planet gears.
- *Face load factor $K_{H\beta}$*: it takes into consideration the uneven load distribution along the facewidth that is influencing the contact stress. It is computed by the software, and it results bigger than 1. This factor is strongly influenced by the supports and the shaft configuration, and in particular by the resulting shaft deformations: so at this point it is fundamental to define the axis alignment and to take into consideration the related analysis performed in the 3D model, in particular focused on the carrier of the first stage.

  We will compare two results just to have an idea of the process; the input load is the road bump, and the resulting force is equally distributed on the planets (2243 N on each planet pin): the two analyzed carriers are shown in ***Figure 2.13***. On the left there is the first model considered, with pins supported only on one side: the resulting deflection of the pin axis was 23,4 μm, clearly too much for the proper operation of the gears; on the right the latest optimized version is represented: in this case the axis misalignment is only 1,9 μm.

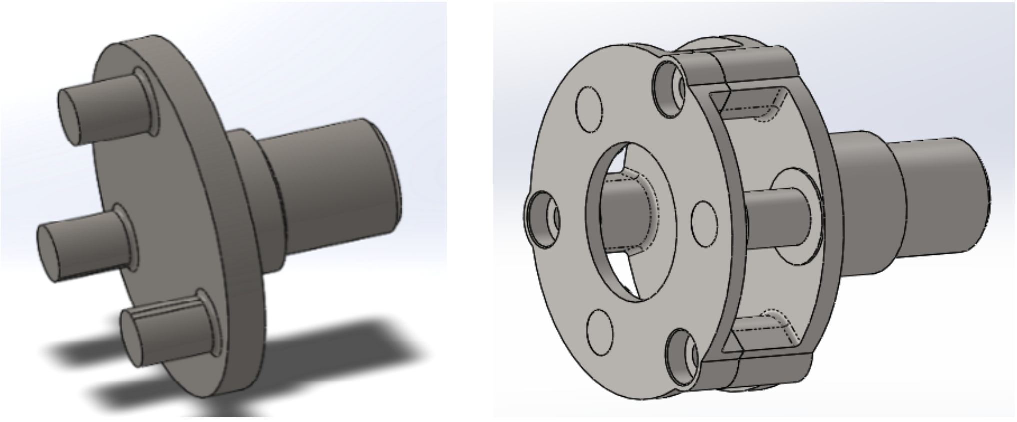

Figure 2.13: *carrier optimization process: example of the design improvement*

Even if the deflection is reduced, actually our target is to reach values lower than 1 μm. By the way, this deflection is given by a load that is not constantly applied to the gearbox (being a road bump), so in other operating conditions the resulting deflection will be lower. On the base of these considerations, the input value for the tilting of planet axis is set as a constant value *dt* = 1 μm in the KISSsoft calculation module: it is lower than the computed one, but it is anyway conservative because it is constant and independent from the load. The detail of the planet pin axis misalignment is represented by the scheme in ***Figure 2.14***.

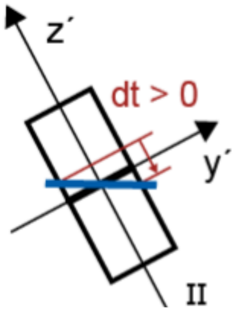

Figure 2.14*: scheme of the axis deflection of the planet gear pin shaft (KISSsoft)*

To conclude the description of these parameters, in order to have a better understanding of them it is important to underline how they are affecting the evaluation of the gear stress. They are defined according to the ISO 6336 standard calculation method: on the base of this, the nominal tooth root stress σ_{F0} (the one determined by the tangential force applied on the tooth as a cantilever beam) is actually modified by such stress correction factors to account for different uncertainties in load application.

$$\text{tooth root stress} \qquad \sigma_F = \sigma_{F0} \cdot K_A \cdot K_V \cdot K_\gamma \cdot K_{H\alpha} \cdot K_{H\beta} \qquad \textbf{Eq. 2.3}$$

The reference planetary configuration is always the one described in ***Table 2.17***: we will perform a new safety calculation to evaluate the effects of such more realistic conditions. The results concerning the fatigue with ISO B load spectrum are shown in the following table.

	Stage 1			*Stage 2*		
	Sun gear	*Planet gear*	*Ring gear*	*Sun gear*	*Planet gear*	*Ring gear*
SF	0,95	0,97	1,65	6,72	5,45	5,56
SH	1,00	1,31	4,24	2,12	2,69	7,27

Table 2.19*: safety values of planetary stages with the modified calculation parameters*

Up to now we have considered the two stages to be equal, and as we can see the second stage is clearly over-dimensioned since the input torque is reduced by the transmission ratio; on the other hand, the safety values of the first stage are reduced to critical values smaller than 1.

At this point, the straightforward modification is to differentiate the two stages: we will keep the same gears features but we will “redistribute” the tooth facewidth: the one of the first stage is increased to 15 mm and the facewidth of the second stage is reduced to 5 mm. In this way the axial dimensions are not changed, and the total inertia is reduced because the planets of the second stage, which are rotating at higher speed, have a smaller size.

In the following tables we will summarize the main characteristics of the final dimensioning of the planetary gear set, and the results concerning the safety evaluation: even if the safety factors are improved, they are still quite low (slightly bigger than 1 for the first stage). The main dimensions are already presented in ***Table 2.17***. Just for sake of completeness, we include the whole KISSsoft report of the first planetary stage in *Appendix A*: here the detailed results of the gear calculation are listed, as for example loads applied, tooth strength and safety coefficients, tooth profile and geometry, gear meshing characteristics.

	Stage 1			*Stage 2*		
	Sun gear	*Planet gear*	*Ring gear*	*Sun gear*	*Planet gear*	*Ring gear*
SF	1,03	1,04	2,21	4,88	4,00	3,76
SH	1,03	1,35	4,91	1,94	2,46	5,95

Table 2.20: *safety calculation for the final model of the planetary gear set (input: ISO B load spectrum)*

	Road bump			*Maximum limit load*		
	Sun gear	*Planet gear*	*Ring gear*	*Sun gear*	*Planet gear*	*Ring gear*
S_{yield}	5,63	4,76	6,93	3,71	3,13	4,56
S_{lim}	4,83	4,08	5,94	3,18	2,69	3,91

Table 2.21: *static strength evaluation on the first stage of the final planetary model*

In the following ***Figure 2.15*** we can see the 3D KISSsoft model of the final planetary gear set configuration: the input shaft (carrier of the first stage) is on the left, the gears are represented in blue, while the yellow elements are the bearings. The carrier is shown as a single flange configuration because a double flanged carrier shaft is not directly implemented in the KISSsoft model; anyway we can consider that the planet pins are supported on both sides simply in the computation parameters set up. Obviously the definitive shape of the carrier will be finalized in the 3D CAD model.

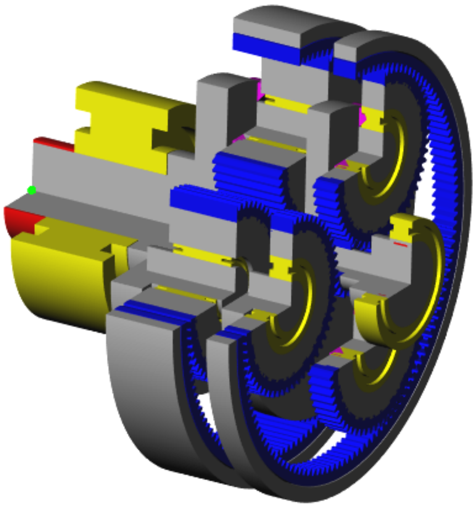

Figure 2.15*: 3D KISSsoft model of the final planetary configuration (its main characteristics are summarized in Table 2.17): it features different tooth face widths for the two stages*

3 Rotary damper actuator

In this chapter we will describe the process of design of the 3D model of the electromechanical damper, including the planetary gearbox, its housing, and the electric machine. In particular, the different components will be presented separately, to highlight the main issues that have been faced and the solutions adopted. The final aim of this phase is to define a model of the rotative damper that will be used on a test bench equipment, so in the last part of the chapter also the final prototype version will be presented and analyzed.

The 3D model is developed in SOLIDWORKS®, and all the related FEM analysis are performed with the included SOLIDWORKS Simulation tool.

3.1 Gears

After the first trials in dimensioning the planetary gearbox, only when reasonable dimensions and acceptable safety values were reached, the design of the gears was frozen for what concern the macro geometry in order to start to define the 3D model. The reference planetary gearbox configuration is the one presented in ***Table 2.17*** (a single stage is represented on the left of ***Figure 3.1***), but as we have seen, a further optimization process has followed. In fact, since from the beginning, the two gear stages were considered identical, but when we arrived to the limit in the optimization of their size, clearly we needed to differentiate their facewidth according to the load applied on each of them (final planetary gears on the right in ***Figure 3.1***).

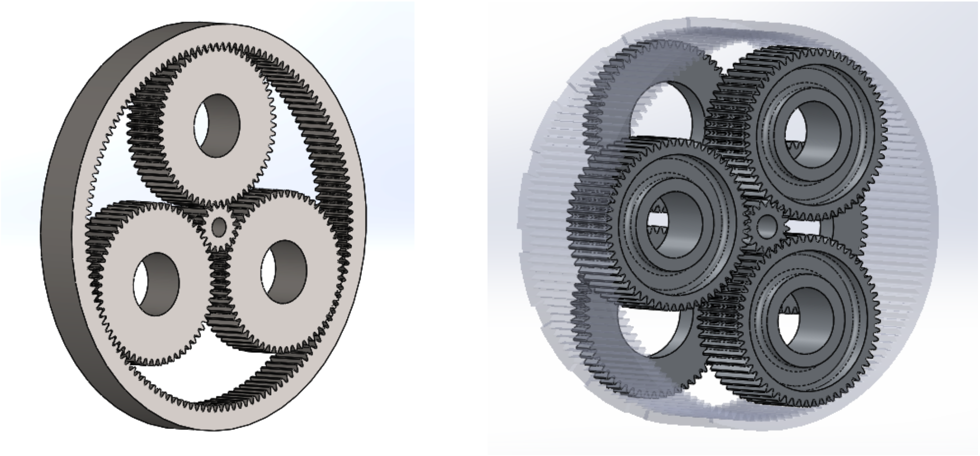

Figure 3.1: evolution of the planetary gear set model in the design optimization process

3.1.1 *Sun gears*

These are the smallest gears of the gearbox, and due to their reduced diameter, the main issues are related to the number of teeth and their manufacturing.

Since from the first planetary configurations, the root diameter was already very small, lower than 10 mm: even if from the point of view of tooth fatigue and strength this was acceptable, we need to consider that the sun gear transmits the torque on the shaft of the carrier of the second stage. Obviously, the only possibility to obtain this gear is to directly manufacture it as part of the carrier shaft, otherwise an interference fit (a separate hollow gear mounted on the shaft) would require a shaft diameter d = 4 mm, excessively small to transmit the required torque. A first result concerning the stress on the carrier shaft was presented in ***Figure 2.12***: it was related to the peak load due to a road bump, and it was below the yield limit of the first material selected for shafts (steel C45).

With the optimization of the carrier shape, also the shaft material was changed, selecting the steel 18CrNiMo7-6. With this new material, we verify the strength with the maximum limit load as input (T_{in} = 230 Nm): the peak stress on the second stage carrier is 411 MPa (***Figure 3.2***), below the yield limit σ_y = 640 MPa.

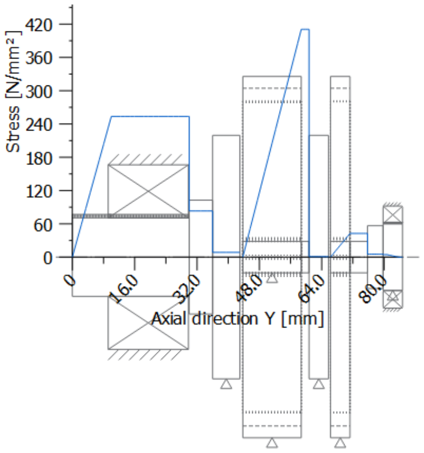

***Figure 3.2**: Von Mises equivalent stress on shaft with maximum limit load applied*

Moreover, as computed in the previous ***Eq. 2.2***, the minimum number of teeth to avoid tooth meshing interference is $z_{sun\ min} = 16$, so if we want to keep the transmission ratio there is no possibility to further reduce the diameter of the sun gear.

In the following figure the final models of the sun gears of the two stages are represented, and we can appreciate their different facewidth; the sun of the first stage is machined on the planet carrier of the second stage, the sun of the second stage is manufactured on the rotor shaft of the electric motor.

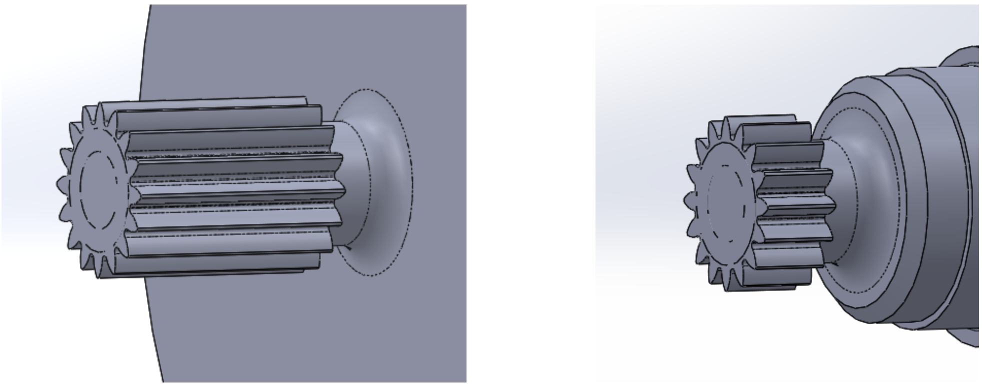

***Figure 3.3**: final version of the sun gears of first (on the left) and second (on the right) stages*

3.1.2 *Planet gears*

The main modification concerning the planet gears is the variation of the facewidth: even if this was introduced mainly to improve the safety coefficients, it has also a beneficial effect on the total equivalent inertia. In fact, we have reduced the facewidth of the second stage whose planets are rotating at an higher speed.

To further reduce the mass, we also introduced a groove only on the planet gear sides of the first stage since they are wider.

The inner diameter is defined by the size of the planet pin shaft and consequently by the size of the bearings.

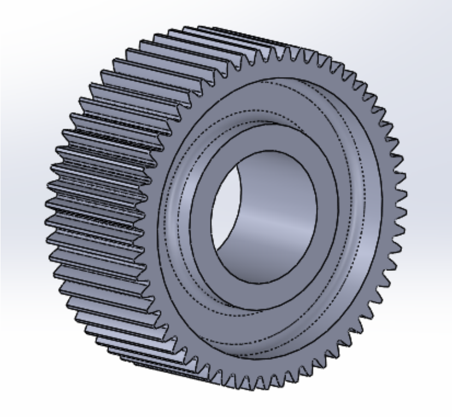

Mass $\boldsymbol{m_{p1}}$	67	g
Moment of inertia $\boldsymbol{J_{p1}}$	12359	g*mm^2

***Figure 3.4**: planet gear of the first stage, and its mass properties*

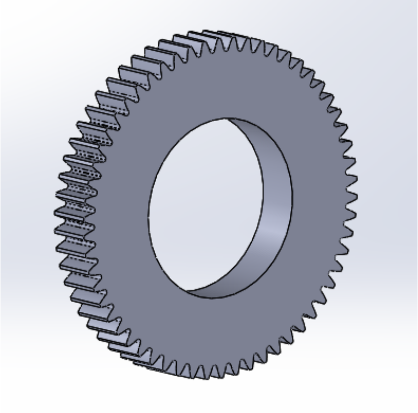

Mass $\boldsymbol{m_{p2}}$	26	g
Moment of inertia $\boldsymbol{J_{p2}}$	5063	g*mm^2

***Figure 3.5**: planet gear of the second stage, and its mass properties*

3.1.3 *Ring gear*

The ring gear is the internal spur gear that in our configuration is fixed (since the input/output are on the planet carriers and on the sun gears). By the way, sometimes we will refer to it as the external ring gear, that only indicates its bigger diameter. The first version of the model features a ring gear for each stage, as directly derived from the KISSsoft model.

Actually this solution is not practical, because it is increasing the number of components required (two rings and a spacer to keep them in place, as it is represented in ***Figure 3.6***), and consequently this is introducing more difficulties in the assembly.

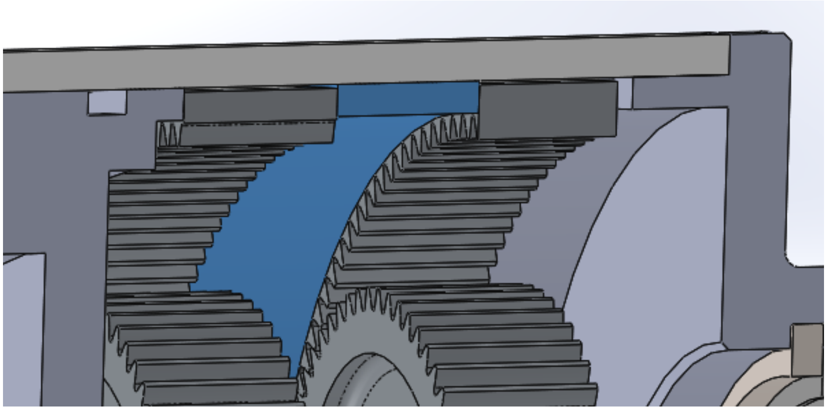

Figure 3.6: *first models with two separated ring gears, one for each stage*

For this reason, the adopted solution is to have a single ring gear in common for both stages: clearly this is possible thanks to the equal module and number of teeth of the two gear stages.

Since the ring gear is the most external one, its diameter has a direct influence on the overall diameter of the housing: having the target of reducing to a minimum the dimensions of the device, the ring gear poses the major constraint on the external dimensions. In fact, once selected the module and the number of teeth, the pitch diameter is defined, so the only possibility of modification is related to the gear rim thickness and consequently to its external diameter. The limitation is represented by the minimum rim thickness (the amount of material below the gear teeth) required. This minimum value is also depending on the capability of the manufacturing process, but as general suggestion its minimum value must be at least big 1,2 times the tooth height.

$$\text{minimum rim thickness} \qquad t = 1{,}2 \cdot h_{tooth} = 1{,}2 \cdot 2{,}25 \cdot m_n = 1{,}62\ mm \qquad \textbf{Eq. 3.1}$$

On the base of these observations, the ring gear is then designed to have a rim thickness of 1,92 mm, with a resulting external diameter of 85,5 mm.

From the point of view of gearbox operation, the ring gear rotation must be fixed to provide the reaction torque to the planets carrier. By the way, in order to optimize the gear meshing and to have a better stress distribution, a certain radial clearance and flexibility is required: thus the interference fit of the ring gear directly inside the housing is not the best solution. The internal diameter of the planetary housing is 86 mm, so the resulting radial gap between the ring gear and the housing is 0,25 mm.

At this point, the issue is related to the actual constraint of the ring rotation: since its fixing cannot be obtained radially due to the reduced rim thickness (for example with some radial pins on the external diameter), the adopted solution features a teeth pattern on the side surface of the gear (***Figure 3.7***). This “toothing” is characterized by 16 grooves, 1,5 mm deep and 5 mm wide, and it is engaging a specular pattern on the motor housing.

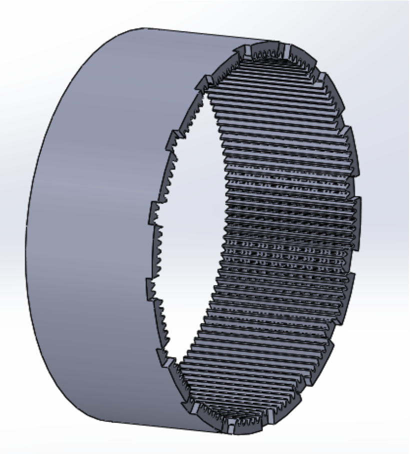

***Figure 3.7**: final version of the ring gear, with the toothing pattern on the side surface*

To verify the resistance of the toothing, we consider the worst case (maximum limit load of 2000 N, T_{in} = 230 Nm): all the input torque has a reaction applied by the ring gear. The results of the static strength simulation are represented in ***Figure 3.8***: we can see that the maximum stress is about 620 MPa, below the yield limit of 887 MPa.

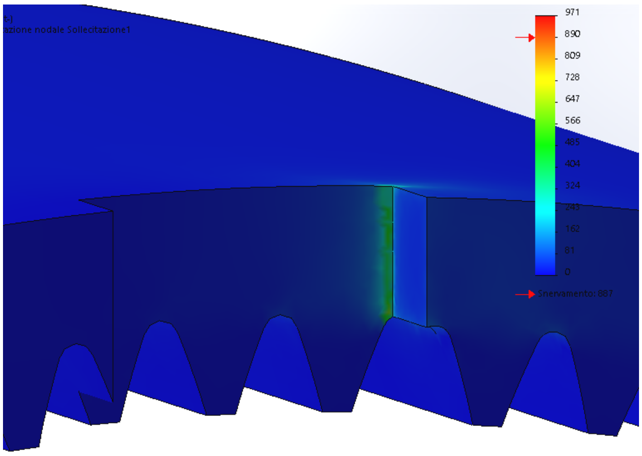

***Figure 3.8**: stress evaluation on the toothing of the ring gear (with 230 Nm input torque)*

3.2 Planets carrier of the first stage

The planet carrier is the input shaft and so its main functions are to guarantee the transmission of the input torque and to properly constraint the planet gears for optimal operation.

The starting point is the KISSsoft model described in the section *2.2*: as result of the preliminary design, the carrier shape was clearly not optimized, with a diameter d = 95 mm, a flange thickness l = 15 mm and a pin diameter d_p = 15 mm, and a relevant rotational moment of inertia J_{c1} = 10,2 kg*cm^2 (***Figure 3.9***).

The material used in these first models is the one proposed by default by the software: it is a C45 through hardened steel.

$$\begin{gathered} \textit{shaft first material selection}: \quad \boldsymbol{\textit{steel C 45 through hardened}} \\ \textit{strength} \qquad \sigma_y = 370\,MPa \qquad \sigma_{max} = 630\,MPa \\ \textit{surface hardness} = 186\,HBW \qquad \textit{core hardness} = 186\,HBW \end{gathered}$$

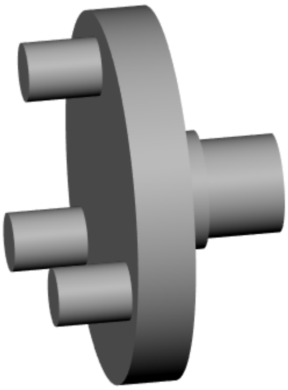

Figure 3.9*: planetary carrier of first stage, KISSsoft preliminary design [15]*

Starting with the first planetary dimensioning, even if the 3D CAD model of the whole system was not yet defined, a first study on the carrier is performed in order to have some hints on the possible optimization. In this case we will consider an input torque on the shaft T = 115 Nm, while the tip of the pins is constrained. In ***Figure 3.10*** we can see two examples of carrier shapes: the basic circular shape and a “star” configuration with three arms, other simulations are performed varying the thickness or the diameter. Due to the relevant thickness, in all the analyzed cases the resulting maximum equivalent stress is slightly bigger than 100 MPa, but well below the yield limit, also because the load is not the limit one.

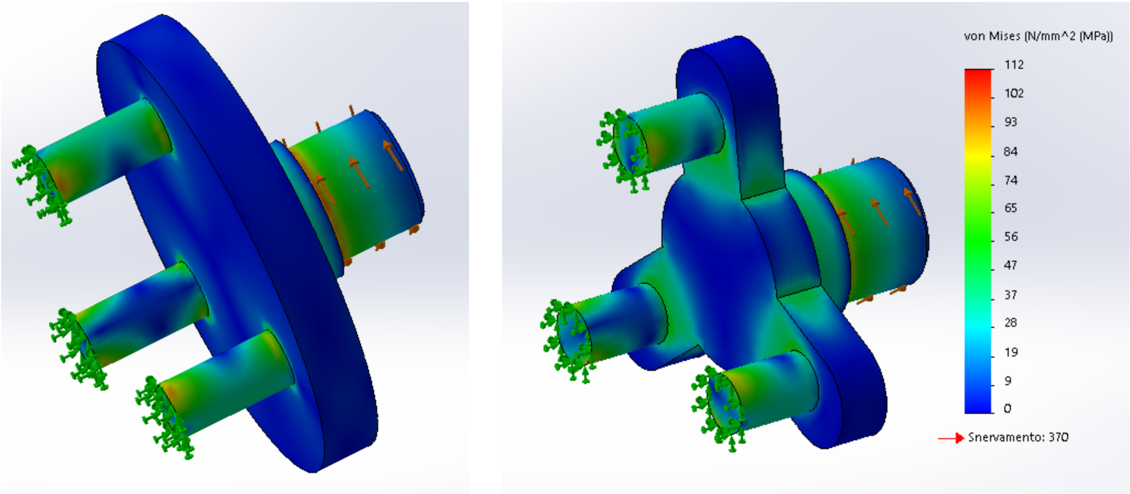

***Figure 3.10**: equivalent stress results obtained by first simulations on carrier shaft*

With the new planetary sizing (the reference configuration given in ***Table 2.17*** that fixed the main diameters of the gears), we started the development of the complete 3D CAD model of the whole system: thanks to the previous results, and also considering that the planetary overall diameter was reduced to 90 mm, the new considered carrier model is for sure smaller (d = 65 mm, l = 8 and d_p = 8 mm, J_{c1} = 1,28 kg*cm^2).

To perform these new simulations, we consider different load applications to simulate the actual working condition of the carrier and of the planet pins. In particular, the load applied was T = 151 Nm or the corresponding total radial force acting on the three planet pins F = 6729 N (the force is computed dividing the torque by the center distance between gears): we used the torque or force input depending on how the boundary conditions and the simulation constraints were set. In nominal conditions, the total force is equally split among the three pins, by the way we also checked the stress in case that the whole force is supplied by a single pin: the maximum stress at the pin base is higher than 1000 MPa. By the way, having a single planet gear engaged is clearly not possible in normal operation, so we will not take into account any more this extreme condition.

Also in this case, different shapes were analyzed to find the best trade off between strength and inertia (***Figure 3.11***).

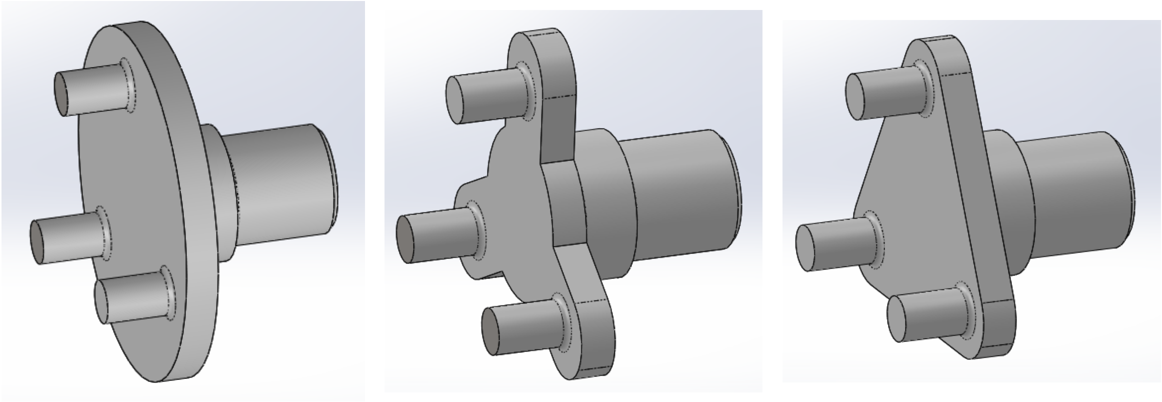

Figure 3.11: other examples of carrier shapes, with reduced thickness and diameter

For the moment, the preferred choice is to have a triangular shape: with the target of reducing the mass while keeping acceptable stress and deformations it is important to remove the right amount of material. With the aid of the simulations, in ***Figure 3.12*** we can actually see what is the effective volume of material that is subjected to the most of the stress: this is clearly suggesting a triangular configuration or with arms.

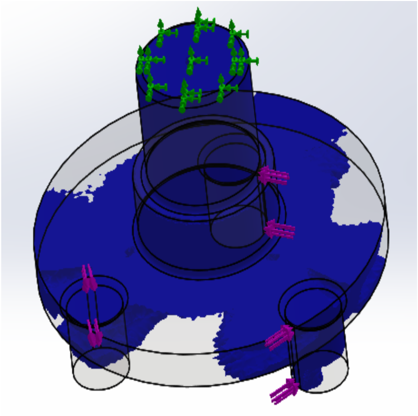

Figure 3.12: simulation on carrier showing the volume of material that is subjected to the major stress

Among the different loading conditions, the most realistic one is represented by the input force equally distributed among pins, applied on the side of pin as the corresponding radial reaction from the planets (F = 2243 N on each pin). In this case, the maximum stress is exceeding the yield limit (440 MPa), and it is localized at the base of the pin since they are subjected to bending (with a pin axis deflection of 30 μm).

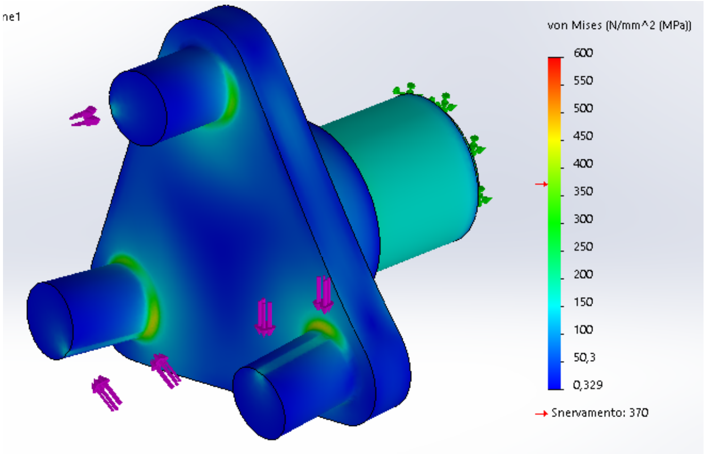

Figure 3.13: *resulting stress with load equally split among planets (F = 2243 N on each pin)*

To solve the issue of the stress, clearly the solution is to change material: we select a high strength steel 18CrNiMo7-6, typically used for shafts but also for gears (properties from SOLIDWORKS database).

$$\begin{array}{lll} \textit{shaft final material selection}: & \boldsymbol{steel\ 18\,CrNiMo\,7-6} & \\ \textit{strength} & \sigma_y = 785\,MPa & \sigma_{max} = 1100\,MPa \end{array}$$

By the way, even if this model appears to be a good solution (d = 62 mm, l = 6 and J_{c1} = 0,46 kg*cm^2), it presents further issues. First of all it requires a non conventional constraint of the planet gears with washers and Seeger rings, as can be seen in the figure below, and moreover the deformations are still excessive for such precision gearbox.

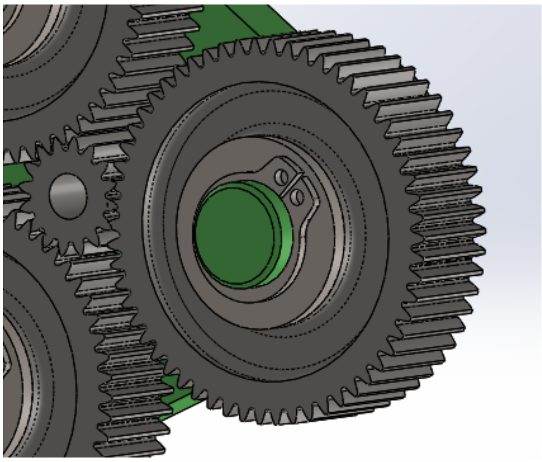

Figure 3.14: *detail of the fixing of the planet gear: the carrier with a single flange is supporting the pin shafts only on one side*

All these issues can be addressed by adopting a new configuration: the carrier will be composed by two flanges, as in most of the commercial planetary gearboxes (***Figure 3.15***). This guarantees to have the planet pins supported on both sides, with beneficial effects on deformations, stress distribution and consequently on gear meshing.

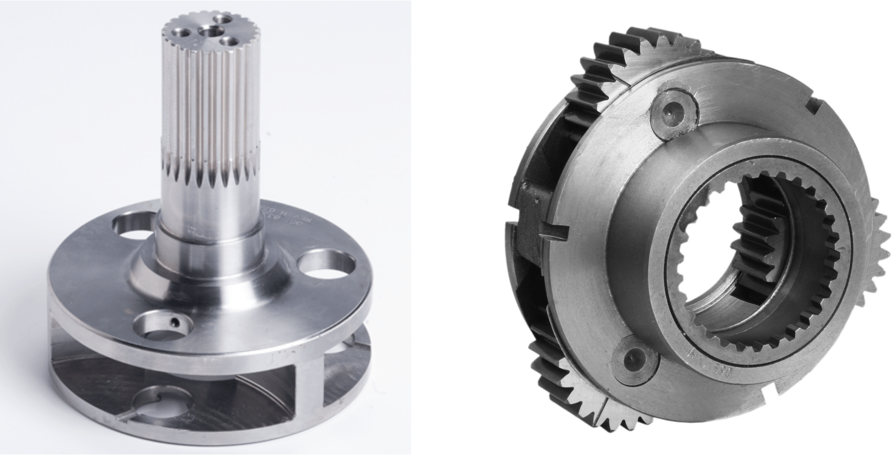

Figure 3.15*: two examples of commercial planetary carriers featuring a double flange configuration [Ontario Drive & Gear; Millat Equipment Limited]*

In the following ***Figure 3.16*** we can see the first version of the double flanged carrier: it has an external diameter d = 62 mm, the thickness of the two flanges l = (3 + 2) mm, a moment of inertia J_{c1} = 0,54 kg*cm^2. In particular the planet pins are integral on the shaft piece, and the second flange is fixed with three simple screws.

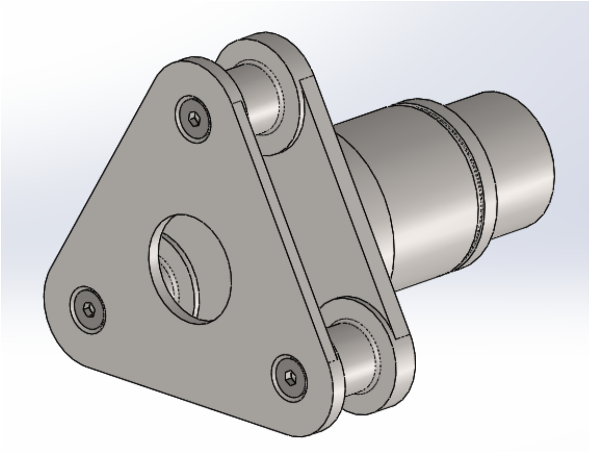

Figure 3.16*: first carrier model with a double flange configuration*

Actually, this carrier configuration still presents some problems. First of all, since the needle cage roller bearings must revolve on the planet pins surface, the pin must be manufactured with an higher quality surface finishing and tolerance: so it is not possible to have the planet pins directly machined as integral parts of the carrier shaft. Second, since the planet pins are not fixing any more the two flanges together, there is the need to introduce some supports between the two plates (as can be seen also in ***Figure 3.15***).

All these considerations led to a further step toward the final model: we need to come back to a disc shape in order to accommodate the supports between the planet gears; the pin shafts are machined separately as simpler cylindrical parts, so the two flanges are connected with screws on the supports. In ***Figure 3.17*** we can see this new model, and the relative simulation where we considered an equal distribution of the force on the three pins: compared to the previous double flanged triangular carrier (***Figure 3.16***), the diameter and the flange thickness are not changed, but clearly the moment of inertia is increased $J_{c1} = 0{,}97\ \text{kg*cm}^2$.

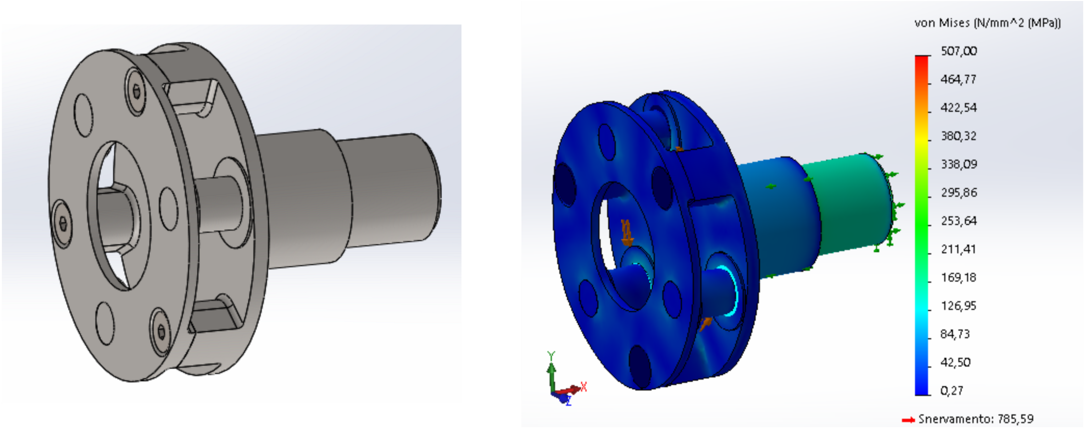

Figure 3.17*: carrier with calibrated separable pin shafts and supports between flanges; stress analysis with equal force distribution (on the right)*

Actually, even if the stress values are not critical, the pin axis deflection is about 9 μm, still too big: it seems a small value, but we need to consider the gear meshing and the negative effect that any misalignment can produce on the fatigue resistance of gears. By the way, on the other hand in these FEM simulations we cannot take into account the fact that the tooth meshing between gears is actually constraining the pins and the carrier deformation. So at this point we need to integrate the gears dimensioning performed in KISSsoft and the simulations for the optimization of the carrier model. As suggested target, the axis deflection must be smaller than 1 μm in nominal operating conditions.

The first modification aimed at reducing such deformation is the use of a calibrated screw (ISO 7379) for assembling the two flanges: a detail of the assembly is shown in ***Figure 3.18***. Thanks to its calibrated body, compared to a simple screw, it reduces to a minimum the

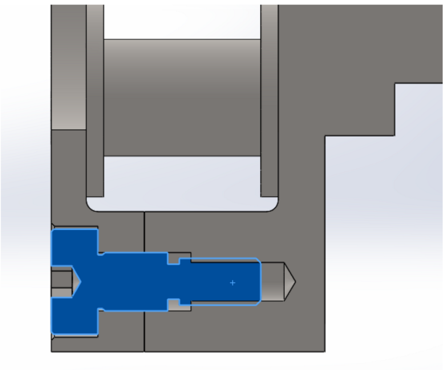

Figure 3.18: section detail of carrier flanges assembly with calibrated screw

possible sliding that can occur between the two plates.

By the way, this is not enough to reduce the misalignment to acceptable values, also because meanwhile the first stage facewidth is increased and consequently also the planet pins are longer: we finally perform some simulations with a gradual increasing of the thickness of the two flanges. The bigger thickness reduces the bending of the two plates due to the input torsion and so it allows to better control the pin deflection. For what concern the loading, as said in the previous chapter, we should consider more realistic conditions, as for example an uneven torque split, but we still keep the input torque T = 151 Nm equally distributed. This choice is also related to the KISSsoft analysis: in fact, also in gears sizing, the torque is equally distributed among planets.

In so doing, we check what is the level of misalignment in ideal conditions but with a load that is not nominal (peak torque given by the road bump). As result of the simulations, the final carrier model is modified with an increased thickness of the two flanges l = (4 + 3) mm: the resulting pin axis deflection with such load is 1,9 μm. Even if it is bigger than the target value, actually we have kept a conservative margin in the KISSsoft calculation: we set as input a constant axis deflection equal to 1 μm, lower than the one computed in critical conditions, but surely higher than the misalignment with lower normal loading conditions.

Before to show this final model of the carrier, its development is completed by some considerations on the design of the input shaft.

3.2.1 *Input shaft design*

At the beginning, the input side of the carrier was a simple plain shaft, with the seat for the bearing; as we will see, the dimension of this diameter is depending on the selection of the bearing itself.

Now we will focus on the coupling between the shaft and the external leverages: it must be designed in order to transmit the input torque to the planetary stage. Some first trials have been made in order to design a proper input arm that is intended to be fit in the suspension assembly (we will see some figures in the dedicated chapter), but then we decided to focus on a general coupling that could be also used on bench test equipments.

The reference load to be transmitted is the maximum limit torque T_{in} = 230 Nm. If we consider the maximum shear stress admissible by the material strength (Von Mises equivalent stress), we can evaluate what is the minimum required diameter.

$$\text{safety factor } SF = 2 \qquad \sigma_{adm} = \frac{\sigma_y}{SF} \qquad \tau_{adm} = \frac{\sigma_{adm}}{\sqrt{3}}$$

$$\text{minimum shaft diameter} \qquad d_{min} = \sqrt[3]{\frac{16 \cdot T_{max}}{\pi \cdot \tau_{adm}}} = 17{,}3\,mm \qquad \textbf{Eq. 3.2}$$

The starting shaft diameter is 20 mm: even if it is not a problem for what concern the equivalent stress, actually the conventional mechanical couplings require some grooves or notches that intensify the stress concentration, so using a key coupling is not possible.

The other solution could be to use a straight key spline shaft (ISO 14:1982); in this case we refer to characteristic tables that gives the admissible torque values depending on the spline size [19]: having a shaft diameter of 20 mm, and assuming an effective bearing length of 20 mm, the transmissible torque is lower than 230 Nm. Moreover we need to consider the real manufacturing process, and so the effective spline length will be shorter or it will determine an excessive axial dimensions if we want to transmit such torque.

To avoid splines on a small diameter, another possibility could be to use a tapered lock bush coupling [19], that exploit the friction force between the two conical surfaces. After performing some computations, actually this system requires a relevant axial preload when tightening the hub on the shaft: in addition to the tapered surface then we will have an additional length of the locknut up to 18 mm (nut size required to guarantee such axial preload).

Clearly, due to the difficulties encountered on such small diameter, the only solution is to increase this value: the shaft external diameter is now set to d = 23 mm. Also the bearing size is finally changed to account for this modification.

Whit this diameter, and considering again the straight key spline with an effective length of 20 mm, now the transmittable torque is higher than 300 Nm, more than the limit input torque. This final configuration is represented in ***Figure 3.19***: it features the splined shaft, the locknut (small since it has not to provide any axial preload) and the washer, with a total axial dimension of 32 mm starting from the bearing.

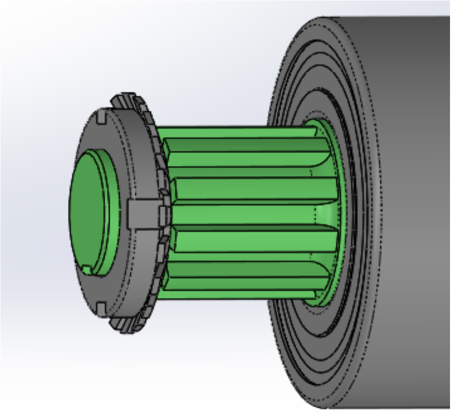

***Figure 3.19**: design of the coupling on the input shaft with a straight key spline*

Actually, starting with the definition of the prototype for bench testing, this input shaft design is slightly modified in order to be adapted to the transmission system: the shaft will be coupled to the pulley of the belt drive with an involute spline (DIN 5480:1991), that generally allows higher torque transmission capabilities compared to the straight spline. The evaluation of strength and geometry is performed in KISSsoft; the defined spline has z = 17 teeth, α = 30°, a normal module m_n = 1,25 mm, an effective bearing length of 20 mm, with a resulting minimum safety factor of 1,7. Obviously, also in this case, the effective total length will depend on the manufacturing process and to the fixing with the pulley.

Finally, in ***Figure 3.20*** we can present the final version of the planetary carrier model of the first stage: external diameter d = 66 mm (slightly bigger than before due to the holes for calibrated screws), flanges thickness l = (4 + 3) mm and pin diameter d_p = 10 mm. The central hole on the shaft has the only function to slightly reduce the mass, the counterbore accommodates a PTFE washer that is needed constrain the axial movement of the second stage carrier.

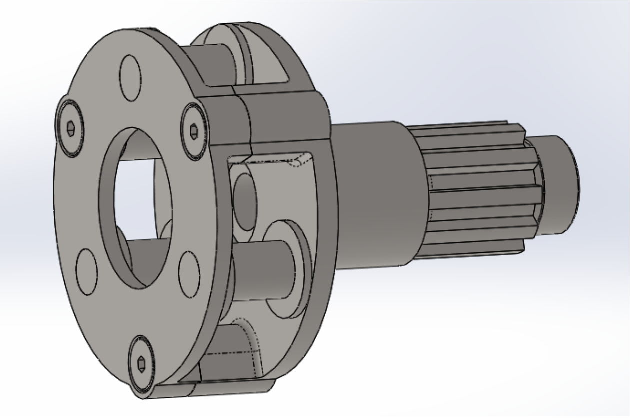

Mass $\mathbf{m}_{c1}$	410	g
Moment of inertia $\mathbf{J}_{c1}$	1,50	kg*cm^2

***Figure 3.20**: final model of the planet carrier of the first stage, and its mass properties*

3.3 Planets carrier of the second stage

The design of the carrier of the second stage is following in parallel the modifications made for the carrier of the first stage, because at beginning, for sake of simplicity, the two stages were considered to be equal. On the other hand, anyway, we need to remember that the input torque on the second stage is lower, and so we have less demanding requirements in terms of strength.

In performing the first analysis, we consider the input load determined by the road bump, and for the worst case we set that all the equivalent force (720 N) is entirely applied on a single pin.

$$\textit{input torque stage } 1 \qquad T_{i\,n\,1} = 151{,}4\,Nm$$

$$\textit{transmission ratio} \qquad i = 9{,}346$$

$$\textit{input torque stage } 2 \qquad T_{i\,n\,2} = \frac{T_{i\,n\,1}}{i} = 16{,}2\,Nm$$

The results of this first simulation are represented in ***Figure 3.21***: the carrier has a triangular shape, with a thickness of 6 mm. The resulting maximum stress at the base of the loaded pin is 147 MPa, and the deflection of the pin axis is about 20 µm. An higher stress is occurring on the sun shaft, but anyway it is below the limit of the material (as we have already seen when describing the sun gear).

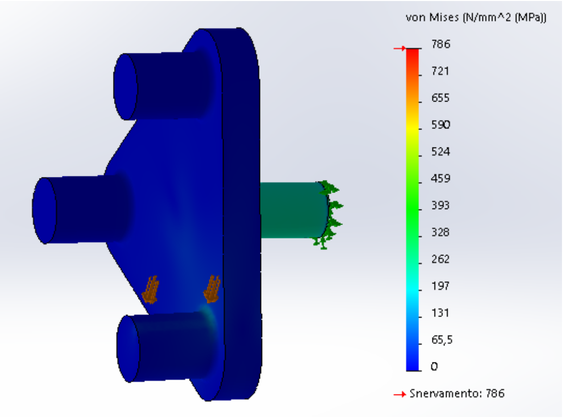

Figure 3.21*: stress evaluation on the carrier of second stage, whole force on a single pin*

Actually, we checked only this worst case condition: the carrier has a single plate (so the planets are supported only on one side) and the peak force is totally applied on a single pin. By the way, following the improvements of the first stage, we will obtain a much lower axis deflection.

The first change introduces a two plate configuration (still with a triangular shape) to have the possibility to manufacture separately the pin shafts for the needle roller bearings. The requirement of having separated planets shafts forces to use the disc shape to accommodate also the supports (***Figure** 3.22*). The thickness in both cases is *l* = (3 + 2) mm.

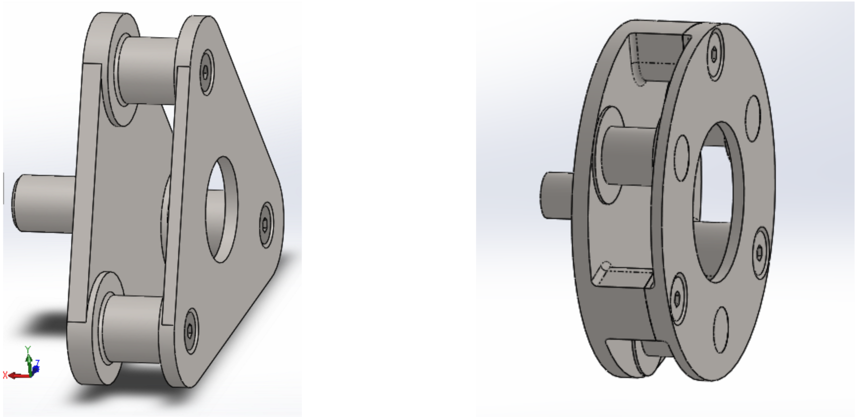

***Figure 3.22**: modifications on the carrier of second stage: configurations with two flanges*

At this point, the important improvement that led to definitive model of the carrier is the differentiation of the width of the two stages: this final carrier model is represented in ***Figure 3.23***. The plate thickness is smaller than the first stage (*l* = (3 + 2) mm), while the stage has a tooth facewidth of 5 mm: with the consequent reduction of the pin length, it is not possible to use a needle roller bearing, so we need to select a normal ball bearing. Even if the ball bearing does not require such a precise shaft surface finishing as for the needle roller bearing, anyway we keep separated pin shafts as for the first stage to assure a better assembly of the two plates (which in this case are fixed with three simple screws).

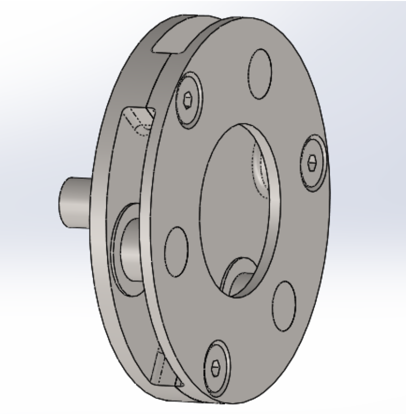

Mass m_{c2}	142	g
Moment of inertia J_{c2}	0,72	kg*cm^2

***Figure 3.23**: final model of the planet carrier of the second stage, and its mass properties*

To finally conclude the description of the carrier of the second stage, it is important to analyze more in detail its working conditions. Being a planetary stage, the carrier is constrained by the meshing contacts of the sun gears and of the three planets: in order to avoid to introduce further unnecessary constraints, the planet carrier is required to be free in the axial direction. Obviously, this means that we need to introduce a certain minimum axial gap but small enough to avoid the contact between the two carriers.

To better understand this issue, in the following ***Figure 3.24*** the complete assembly of the two planetary stages is presented. Here the red circles are highlighting the clearances (1,25 mm in total) on the axial motion of the carrier of the second stage; the related axial constraints are the contacts with a PTFE washer on the left and the rotor shaft on the right.

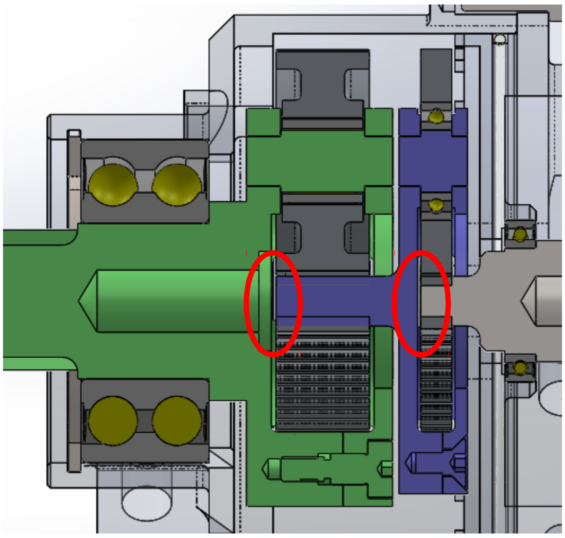

Figure 3.24*: detail of the axial clearances in the assembly of the two planetary stages*

3.4 Bearings selection

Bearings are important elements in the assembly because they provide the support to all the rotating elements as shafts and gears: in the following ***Figure 3.25***, the section view of the final model is represented in order to evidence these main support points. As we can see, the carrier of the second stage is not supported by bearings but it is simply constrained by the meshing of the gear pairs.

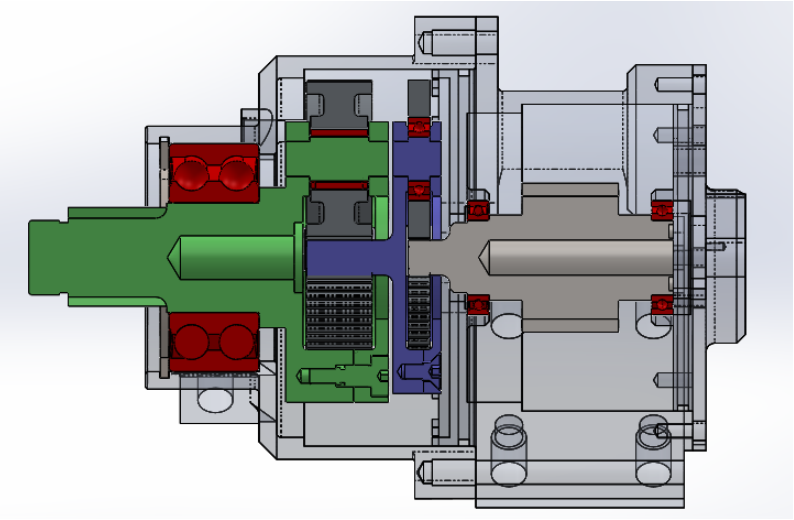

Figure 3.25: assembly section in which the positions of the support bearings (red elements) are highlighted

Now we will analyze more in detail the selection of the bearings one by one: the reference for their dimensioning is the SKF catalogue [20], but we will perform also some verifications on the KISSsoft shaft model that includes also the bearing calculations module.

3.4.1 *Input shaft bearing*

In the original preliminary planetary model, the bearing selected to support the input shaft was a simple ball bearing. By the way, if we take into account the real working conditions of the carrier inside the assembly, we see that it is supported only on one side while on the other there are the reaction forces provided by the gears.

Ideally, if the input load was a pure torsional load, the ball bearing would be enough to guarantee the proper gear meshing, but the input rotation is actually provided by a leverage system: the force acting on the input arm will then determine both a radial load on the bearing but also a bending action on the shaft. The scheme of the load application is shown in ***Figure 3.27***: we assume an input arm length of about 70 mm, taken from the reference leverage configuration. Even if the design of the input arm is strictly related to the suspension architecture, anyway we performed a preliminary study on it: its particular shape has the aim of reducing the bending action on the shaft by aligning the force axis with the bearing mid-plane.

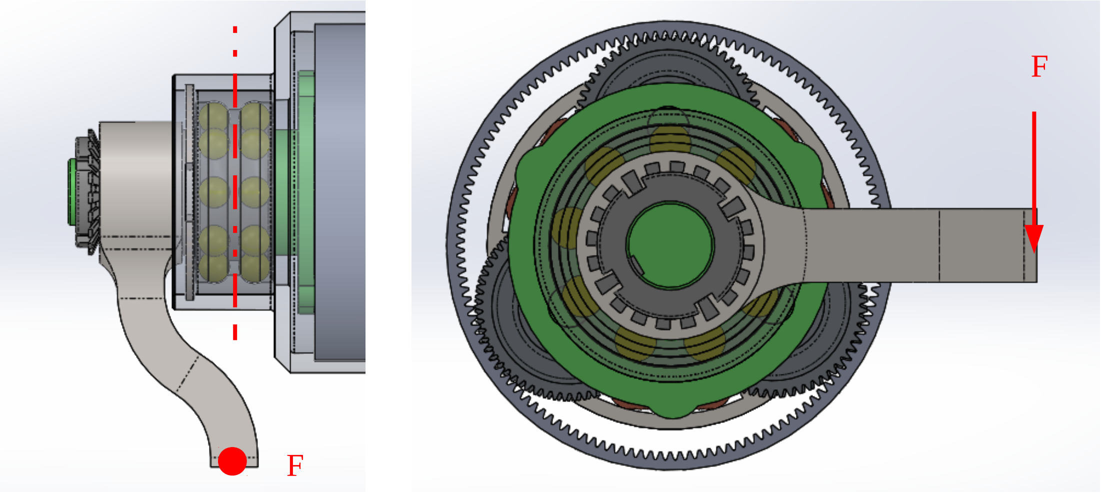

Figure 3.26: schematic representation of the external input force application, with a preliminary design of the input arm

For this reason, the bearing must be able to supply also a reaction to the tilting action: the best solution is to use two angular contact ball bearings arranged in “O” configuration in order to have a certain force arm between the bearings reaction forces. The scheme of this bearings arrangement is represented in ***Figure 3.27***, and on the right there is the solution adopted by the “Squadra Corse” team (Politecnico di Torino) for the transmission of the Formula SAE car [21].

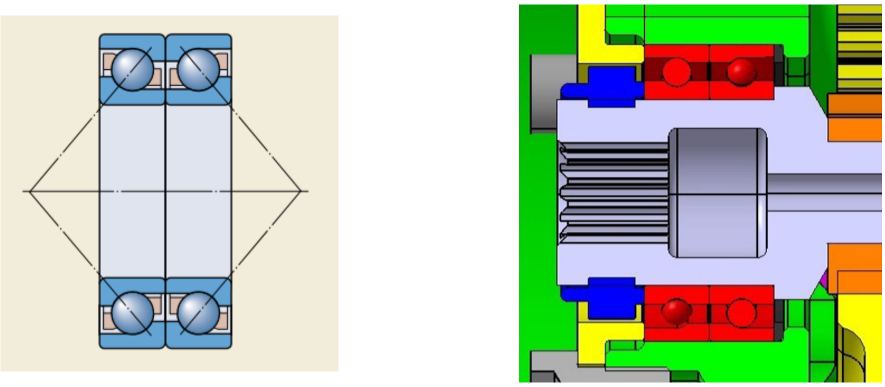

Figure 3.27: support on input shaft with two angular contact ball bearings in "O" configuration [20], and on the right the solution implemented on the Formula SAE “SCdiciassette” car [21]

By the way, in our case this solution was not adopted for two reasons:

- First, the bearing on the input shaft must provide the sealing against the leakages of the lubricant oil contained in the planetary housing: unfortunately, the angular contact ball bearings do not feature an integral contact seal since they can be disassembled. A double row angular contact ball bearing with a two piece inner ring is an equivalent alternative, but it has the same problem.

- Second, the assembly of the two bearings side by side requires a precise mounting with specific axial preloads, and this will introduce some complications in the design of the input shaft and the housing.

After all these considerations, finally we decided to use a double row angular contact ball bearing with a single piece inner ring: being pre-assembled, the correct internal clearances and preloads have been set during the manufacturing process. Moreover, there is the possibility to have an integral contact seal that prevents oil leakages.

At this point, we need only to define the bearing dimensions. Depending on the operation of the whole damper device, this bearing is subjected to an oscillating rotation due to the limited stroke of the suspension (the input shaft will never complete an entire revolution): then its sizing will be based on a static dimensioning. The reference load will be the one determined by the limit input torque: with T_{in} = 230 Nm, the corresponding input force applied on the arm (assuming an arm length of 72 mm) is F_r = 3194 N, that is also the resulting radial load applied on the bearing.

The final bearing is a SKF 3205 A-2RS1 (d = 25 mm, D = 52 mm and width B = 20,6 mm), mounted on the shaft with a diameter of 25 mm: from its specifications we can verify its static strength.

$$\begin{gathered} \text{input shaft bearing}: \text{static verification} \\ \begin{array}{ll} \text{equivalent static load} & P_0 = F_r = 3194\,N \\ \text{bearing basic static load rating} & C_0 = 14{,}3\,KN \end{array} \\ \text{static safety factor} \quad s_0 = \frac{C_0}{P_0} = 4{,}5 \end{gathered} \qquad \textbf{Eq. 3.3}$$

As we can see, the static load is not a problem for the bearing: actually, its over-dimensioning is constrained by the design of the splined shaft diameter, so we are forced to keep this bearing with a bigger size.

Finally, to conclude this analysis, we can have a look to the prototype development: in the set up of the experimental test bench, the input is provided by a belt pulley, so the actual input load will be a pure torque, while the radial load will be for sure smaller and only determined by the belt tension in mounting required for power transmission.

3.4.2 *Planet gears bearings*

These bearings are the ones that allows the rotation of the planet gears on their pin shafts. The starting choice is to use needle cage roller bearings: they provide a good support of the planets with their bigger width while keeping a limited radial dimension. By the way, since the rolling elements are directly revolving on the pin surface, as said we need to have the calibrated pin shafts machined separately from the carrier.

As seen, the diameter of the pin shaft was set according to the results of the simulations on the carriers: it is d_p = 10 mm. For what concern its axial length (simply related to the stage facewidth), at beginning it is l = 10 mm, equal for both stages.

The definitive bearing selection is determined by the stage width differentiation:

- needle roller cage bearing on the first stage (SKF K 10x14x13 TN): even if the stage width is 15 mm, it has an axial length of 13 mm because the next available bigger size has a length of 16 mm, larger than the planet gears;
- simple ball bearing on the second stage (SKF 61800): this choice is forced by the reduced length of the pin, that being only 5 mm is not enough to accommodate any needle roller bearing.

For what concern the dimensioning, in this case we will take into account also the fatigue life, since the planet gears are subjected to rotational speeds higher than the input shaft.

We start with the bearing of the first stage: we want first of all to check the static strength when the maximum limit torque is applied as an impulsive load. If the limit torque T_{in} = 230 Nm is equally split among the planets, the resulting radial load on each needle bearing is F_r = 3407 N.

$$\begin{gathered}
\textit{first stage planet bearing}: \textit{static verification} \\
\begin{array}{ll}
\textit{equivalent static load} & P_0 = F_r = 3407\,N \\
\textit{bearing basic static load rating} & C_0 = 8{,}5\,KN
\end{array} \\
\textit{static safety factor} \quad s_0 = \frac{C_0}{P_0} = 2{,}5
\end{gathered} \qquad \textbf{Eq. 3.4}$$

On the other hand, the evaluation of the contact stress that is occurring on the pin shaft surface is also important: since this shaft has different material characteristics compared to a bearing ring raceway, it must have a proper surface finishing in term of hardness.

We will refer to the Hertz theory of contact between solid bodies (reference calculations taken from [22]), in particular it is a contact between the cylindrical surfaces of the needle rolling element and the shaft; the geometrical dimensions to compute the maximum contact stress are taken from the bearing 3D model.

$$\text{first stage planet bearing: Hertzian contact analysis}$$

$$\text{force on the most loaded roller element} \qquad P_0 = \frac{4 \cdot F_r}{z_{rollers}} = 1239\,N$$

$$\text{curvature} \qquad \rho = \frac{1}{1\,mm} + \frac{1}{5\,mm} = 1{,}2\,mm^{-1} \tag{Eq. 3.5}$$

$$\text{length of contact of cyclindrical surfaces} \qquad l = 10{,}54\,mm$$

$$\text{maximum contact pressure} \qquad \sigma_{max} = 0{,}418 \cdot \sqrt{\frac{P_0 \cdot E \cdot \rho}{l}} = 2275\,MPa$$

As we can see from the calculations, actually the maximum contact pressure on the pin shaft due to the Hertzian contact is higher that the endurance limit flank for pitting ($\sigma_{H\,lim}$ = 1500 MPa, material properties from KISSsoft database). Anyway this is not a critical issue because such loading conditions are not in the nominal operating range, and so this load will not be applied in a continuous way on the shaft surface.

After the static verification, we can evaluate in KISSsoft what is the bearing service life when it is subjected to the varying load represented by the ISO B road profile load spectrum. The results are reported in the following table: the bearing life is much bigger than the required service life of the system, while the static safety is related to the peak force value present in the load spectrum (about 150 Nm input torque).

Bearing life evaluation *Load spectrum input: ISO B road profile*		
Minimum service life	L_{nh}	210.302 h
Static safety factor	s_0	3,90

***Table 3.1**: planet bearing of first stage: fatigue life evaluation with load spectrum*

For what concern the planet bearing of the second stage, on the base of the previous results, clearly we will have no problems concerning the fatigue life or the maximum load. By the way, it is worth to check the speed values: with the maximum input speed (ω_{in} = 166 rpm), the planet gears of the second stage are rotating at 2039 rpm, a value that is much smaller than the bearing limiting speed (48.000 rpm).

3.4.3 *Electric machine rotor bearings*

The bearings that are supporting the rotor shaft of the electric motor have already been selected since the machine was used for a previous project: they are 2 single row ball bearings (SKF 61803).

The only modification in the design is concerning the bearing on the side of the planetary gearbox: since we want to keep the lubricant oil only in the planetary housing, this bearing must guarantee the sealing against oil leaks in order to avoid filling also the motor side (so reducing the amount of oil used with a benefit on the system mass). So the final choice is to use the same bearing type with an integral contact seal (SKF 61803 2RS1).

3.5 External housing

The external case that covers the rotative damper assembly is providing the support for all the internal components and on the other hand it is the interface with an external coupling (for example the mounting on a suspension subframe). In particular two main parts can be distinguished: the gearbox side and the motor side. We will focus on the design of the housing of the planetary gearbox (that is completely a new piece), while there will be only minor modifications on the case of the electric motor just to adapt it to the coupling between the two parts (anyway it need to be manufactured as a new one).

The material used for the housing is an aluminium alloy: it allows to reduce the weight but it guarantees also an easier manufacturability.

The first proposed model of housing is shown in ***Figure 3.28***: the planetary case is divided in two pieces (the front cover and the cylindrical element) to have simpler parts to be manufactured; moreover in this case the coupling with the motor is obtained with radial screws, that don’t affect the total external diameter. By the way, this solution presents some relevant issues: the cylindrical element requires to be fixed and sealed on both sides; the assembly with more pieces can have more problems concerning the tolerances and axis alignment; the use of radial screws is not suitable to have a good centering.

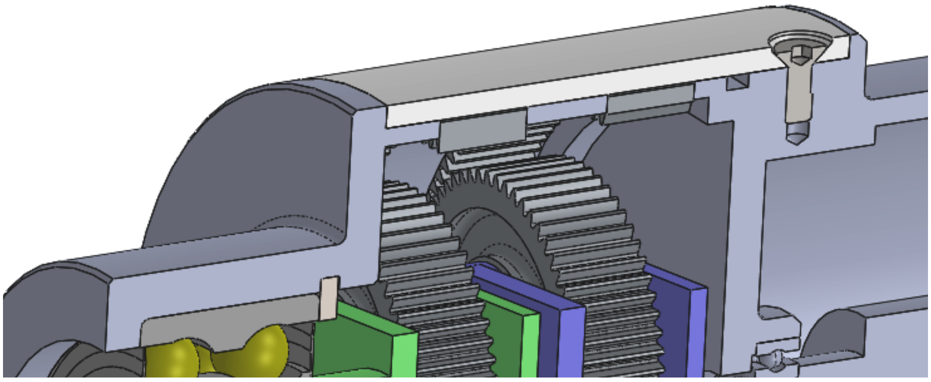

Figure 3.28*: first example of planetary housing, with two separated parts (front cover and cylindrical body) and radial screws*

For this reason, the improved version is a single piece planetary case, while the coupling with the motor case is obtained with a flanged connections with axial bolts. The use of bolts (instead of screws) is preferred in order to avoid to have the thread in the aluminium, more subjected to wear when using steel fasteners. This model is represented in the following figure.

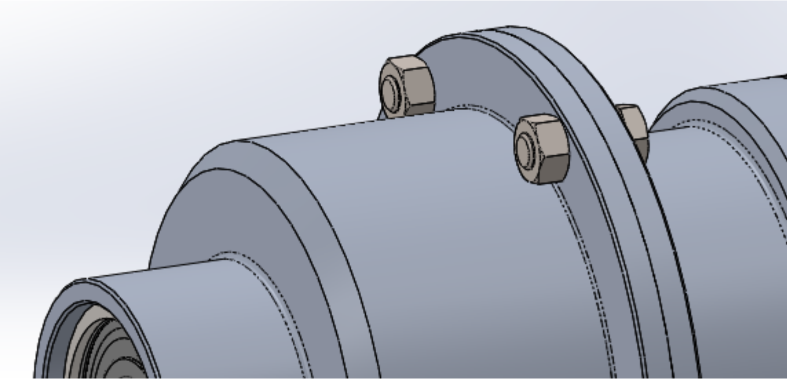

***Figure 3.29**: improved version of the case: single piece and flanged coupling with axial bolts*

Actually, if we consider that the damper system should be placed within the suspension assembly, the space constraints are very demanding. For this reason, this solution is not the optimal one because it has a relevant external diameter: the flange has a diameter $d = 116$ mm, against the 92 mm and 88 mm of the planetary and motor cylindrical housings respectively.

These considerations led to the final design shape of the overall case assembly: first of all, to reduce the dimensions of the flanged coupling we adopt a “squared” configuration with 4 axial screws. It is important to highlight the requirements for this coupling: once placed on a suspension assembly, if the device will be fixed only on the motor side, the overall system will be subjected to a bending moment determined by the input leverage, so the fastening of the flange must be verified with such type of external load. On the other hand, it is also true that this bending action will be compensated by the design of the support element that will fix the damper (its planetary-motor case) on the suspension subframe. Clearly, this connection should be optimized to be fit on the suspension architecture in a future development on the project.

At this moment, the project is devoted to the prototype phase so actually we have no issue concerning the coupling and the support: to have the possibility of installing the device on a bench test equipment, we simply introduce a flat surface that guarantees a complete constraint, without any bending action on the external case. The final version of the overall housing is shown in ***Figure 3.30***.

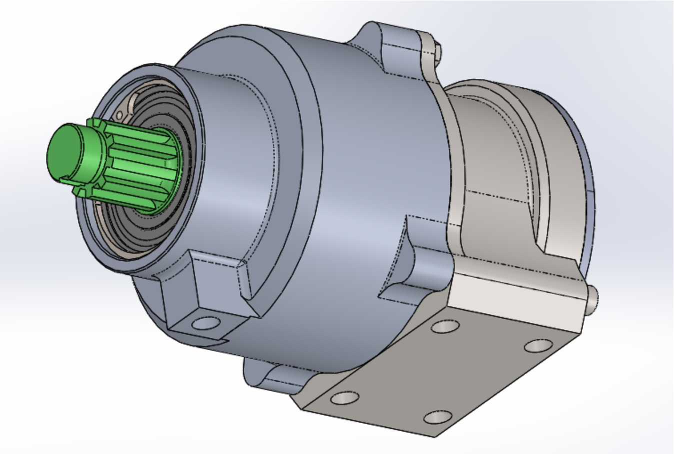

***Figure 3.30**: final version of the housing assembly: single piece planetary case, flat surface for fixing on test bench*

To conclude the overview of the external case, we summarize some of the other solutions adopted.

- To allow the filling of lubricant oil into the planetary gearbox, an oil plug is placed on the front cover. It is not necessary to place two caps because the filling and discharge operations will be performed when the system is not installed on the suspension.
- As said, on the motor case there is a toothing pattern that is engaging the ring gear side surface to fix its rotation.
- Possible oil leakages that can occur in the coupling between the gearbox and the motor are avoided thanks to an O-ring seal.
- The motor cover has not been modified: it accommodates all the components, the cables and the connections required to control the electric machine.
- To avoid problems with the wear of the thread in the aluminium, all the threaded holes on the housing include an helicoidal insert.

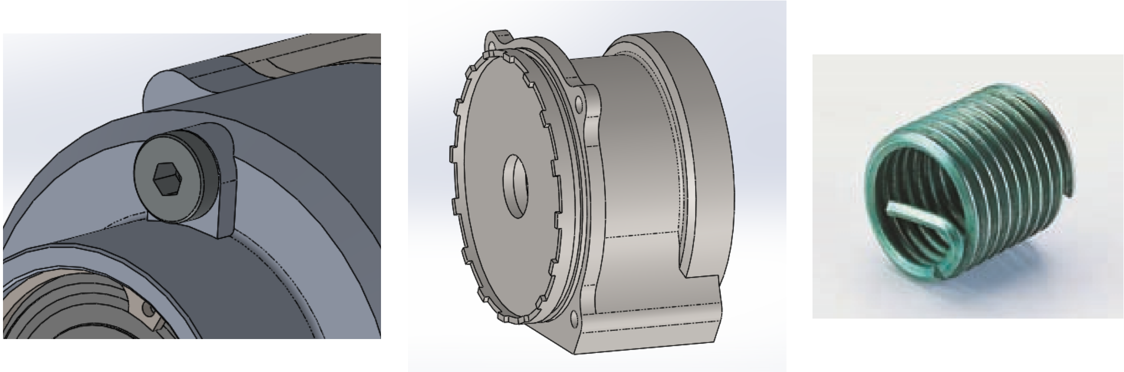

***Figure 3.31**: some details of the damper housing; from left to right: oil plug, toothing on motor case, helicoidal insert [Boellhoff]*

3.6 Assembly overview

Once having completely defined all the components of the rotative damper device, we can have a look to its characteristics as a whole assembly: in the following figures two section views (also showing the rotor and stator assembly of the electric machine) are represented, with the indication of the main dimensions.

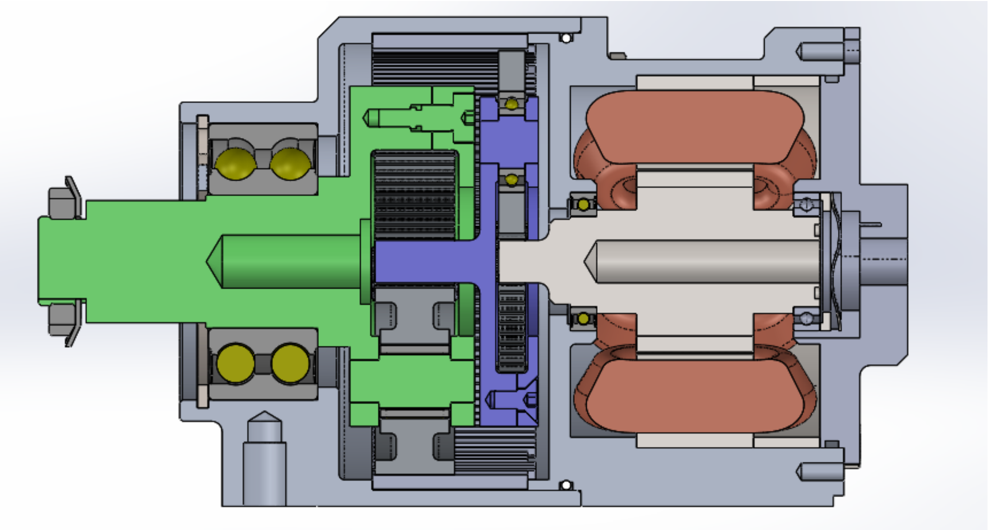

***Figure 3.32**: section view that shows the assembly with all the components*

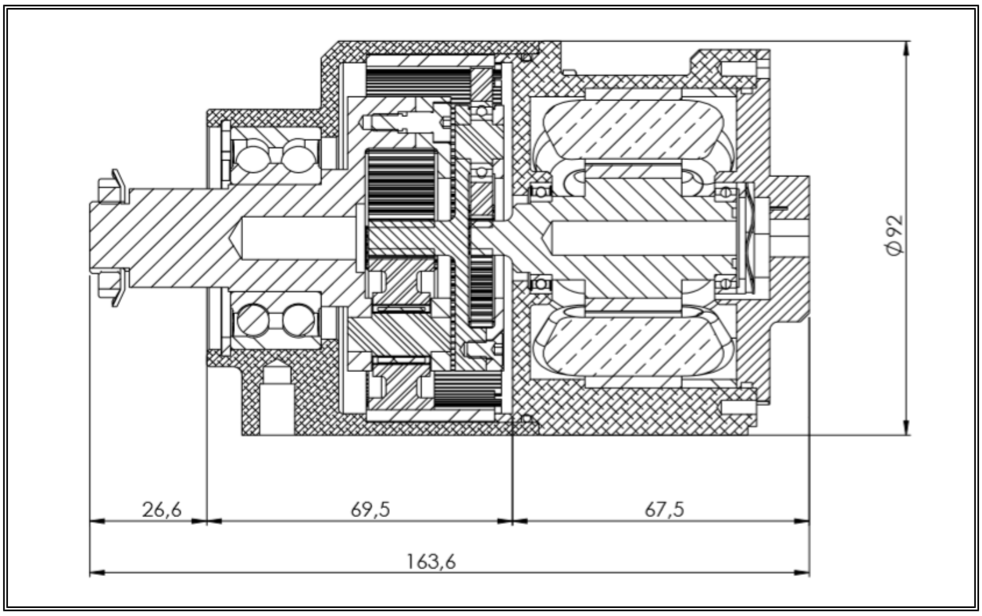

***Figure 3.33**: section view of the assembly, main dimensions*

It is important to remember that this final assembly is not a definitive version, because in order to perform some experimental bench tests, actually the prototype model will require further modifications. By the way, at this stage the information on the specific setup of the test bench was not available and so the design process just followed a general idea of having the case adapted to a generic flat bench.

Another fundamental feature to be considered is the mass of the system (***Table 3.2***): the evaluated values include all the components represented in the previous ***Figure 3.32***, but they do not take into account neither the lubricant oil that must be filled in the planetary gearbox, nor the cables and the plugs on the motor cover. Moreover, also the mass of the leverage system is not considered, because, as we will see, it will not be defined in this project.

Device masses		
Planetary gearbox assembly	1,47	kg
Motor assembly	1,69	kg
Total system mass m_{tot}	3,16	kg

Table 3.2*: total mass of the final 3D model of the damper actuator*

From the point of view of performances, the system weight is totally added to the vehicle sprung mass, since the rotative damper will be directly placed on the suspension subframe. Anyway we need to remember that in case of use of this system, it completely replaces the conventional hydraulic damper and so that element will not be present any more, having a resulting increase of mass lower than the total mass computed.

3.7 Prototype development

As seen up to now, at the end of the design phase we defined a final version of the planetary gearbox and of the damper assembly as a virtual 3D model. The next step of our work is concerning the physical realization of the device: in order to move to the development of the prototype, we need to add some considerations and clarify the issues regarding the manufacturing of the components and the testing phase. Clearly, being the first version of such electromechanical rotary damper, the preliminary prototyping phase is then necessary in order to evaluate the feasibility of the device itself and then to perform a further experimental verification of its performances.

So starting from the model previously defined, some modifications are required in order to fit the rotary damper assembly on the test bench, which will be described later.

3.7.1 Modifications on the damper model

The introduced modifications (carried out by the project co-supervisors) are mainly regarding the external case, that is shaped to be fixed on the designed test bench: the new design of the assembly is shown in the figures below. The detailed damper assembly drawing and the related bill of materials are attached in *Appendix B*.

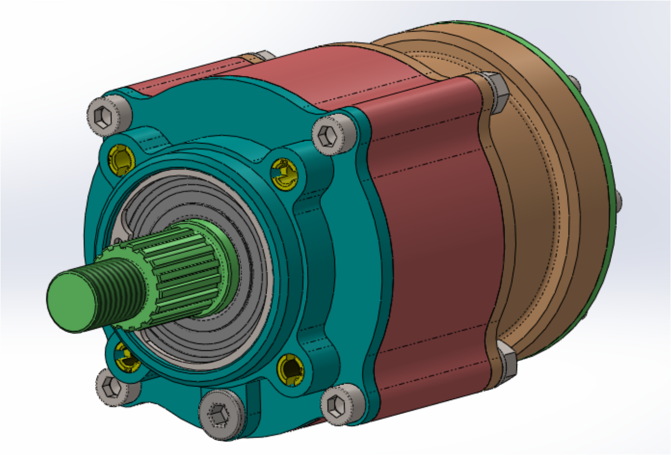

***Figure 3.34**: prototype model of the rotary damper assembly: external view*

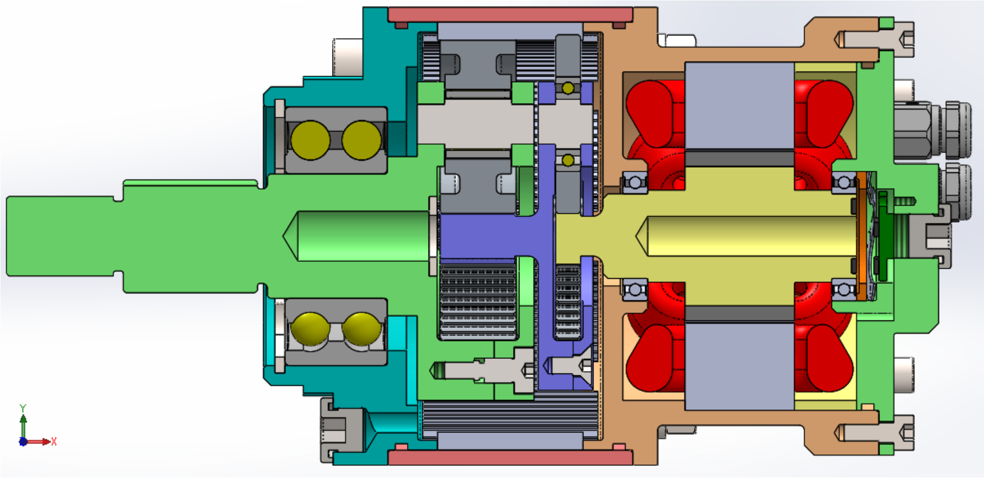

***Figure 3.35**: prototype model of the rotary damper assembly: section view*

As can be seen, the planetary housing is again divided into two pieces: a frontal cover and a main cylindrical body. The cover assures the fitting on the test bench thanks to a cylindrical surface (around the bearing) mating an hole on the bench, and the whole damper is fixed with screws and four threaded inserts (yellow parts in the previous ***Figure 3.34***). Since the resulting shape of the cover is more complicated, the cylindrical part of the case is machined separately for an easier manufacturing: an additional O-ring seal is required on the interface with the cover. The whole planetary case is assembled with four axial bolts, tightening the front cover with the motor housing.

The length of the input shaft is increased to guarantee the assembly of the pulley, while the hub-shaft coupling is performed with an involute spline shaft (as described in section *3.2.1*).

The gears remain practically unchanged; only the ring gear has an additional toothing pattern also on the planetary cover side to better constraint its rotation.

3.7.2 *Test bench setup*

The experimental test has the aim to reproduce real operating conditions but in order to simplify the design of the bench equipment actually we will not provide the input force through a leverage system: the input torque is directly applied on the input shaft with a belt pulley transmission system.

The dimensioning of such transmission is depending both on the driving power source (an electric motor) and on the nominal operating loads that we want to apply on our system (summarized in ***Table 3.3***).

Maximum limit load on damper (worst case)		
T_{max}	230	Nm
ω_{max}	166	rpm

Table 3.3*: maximum input load on the rotative damper*

The electric motor used as power source is a Danaher DBL5-1700: its characteristics are presented in the following table.

Driving motor characteristics			
Operating DC voltage		560	V
Stall torque	T_0	17	Nm
Nominal continuous torque	T_N	9,6	Nm
Maximum impulsive torque	T_{max}	68	Nm
Maximum speed	ω_{max}	5000	rpm

Table 3.4*: characteristics of the electric motor used as driving power source*

From the comparison of the previous data, we can see that the belt transmission must amplify the motor torque and reduce its speed in order to meet the working range of the damper: the driving pulley will have a diameter smaller than the one of the driven pulley (which is providing the input torque to the damper).

The final design of the customized bench test assembly is represented in ***Figure 3.36***: on the left there is the rotative damper, while the driving electric motor is on the right. For sake of completeness, the bench test assembly drawing is reported in *Appendix B*.

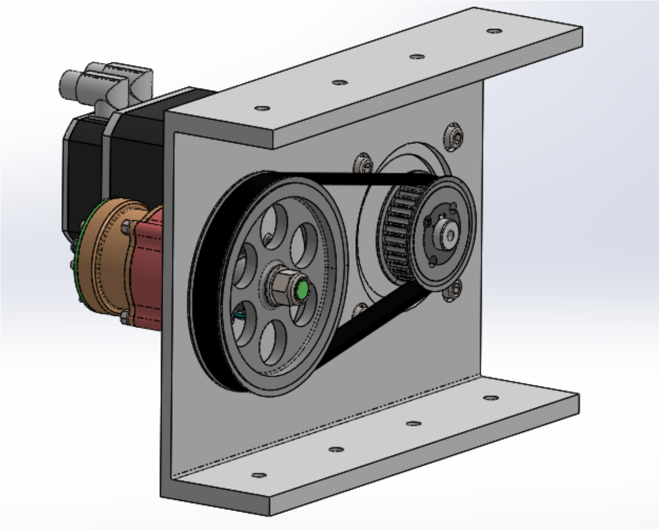

Figure 3.36*: customized test bench assembly: the rotative damper on the left is driven by an electric motor (black element) through a belt pulley*

4 Performances assessment

In the previous chapters we have focused mainly on the design of the model from a structural point of view (defining the gears and designing the actuator assembly), presenting just a few data of the results of the simulations only to better understand the optimization process (for example the gears safety factors, stresses on the different components).

At this point it is useful to analyze more in detail the performances of the device, in particular focusing on the gearbox efficiency (computed on the KISSsoft model), on the equivalent rotational inertia, and finally on the noise level that can be produced during the damper operation.

4.1 Evaluation of gearbox efficiency

In *Chapter 2* we defined the final version of the planetary gearbox: to complete the analysis of the gear stage, the efficiency is a fundamental aspect to be considered. Before to show the results, it is convenient to have a brief review on the gear efficiency calculation.

In power transmission systems, the power losses of a gearbox are classified according to the mechanical components that generates them: they are distinguished among losses generated by the gears (subscript Z), by the bearings (subscript B) and by the seals (subscript D). Moreover, in general we can distinguish the losses that are directly depending on the transmitted power and the losses that are independent from the applied load (subscript 0). In particular, for what concern the gears, these are respectively identified as the meshing losses (due to the sliding between the tooth flanks under load), and gear churning losses.

total gearbox power losses

$$P_V = P_{VZ} + P_{VZ0} + P_{VB} + P_{VB0} + P_{VD} \qquad \textbf{Eq. 4.1}$$

The different contributions are strongly depending on the specific gearbox configuration: in case of planetary gearboxes, the major contributions are given by the sliding between the teeth and by the churning losses of the planet carrier that is revolving inside the lubricant.

In the field of precision planetary gearboxes, the fundamental target of gear design is to maximize the efficiency: many researches (for example [17]) show that an improvement of the efficiency, in particular a reduction of the meshing losses due to sliding, can be obtained by reducing the module of the gears, together with other modifications of the tooth form (pressure angle, profile shift).

In the design of our planetary gearbox, the main parameters that affected the efficiency were the normal module and the profile shift, while the pressure angle was not changed. As said, the profile shift was set to minimize the specific sliding, and the normal module (m_n = 0,6 mm is already a small value) cannot be further reduced due to the limitation on minimum acceptable safety factors.

To compute the efficiency in KISSsoft, the model requires a constant input torque; in order to obtain an efficiency map covering a wide range of the possible operating points, the calculation is carried out by changing time by time the values of input torque and speed in such range. In the calculation setup we considered a constant operating temperature of the lubricating oil equal to 20 °C (oil ISO VG 220 set by default), and the input values of speed and torque ranging in the intervals ω_{in} = [1; 55,4] rpm and T_{in} = [20; 180] Nm. The computed efficiency map is represented in ***Figure 4.1***: on the right the axis are rescaled respect to the input force and vertical speed at the wheel, so we have the possibility to identify also the minimum and maximum damping characteristics.

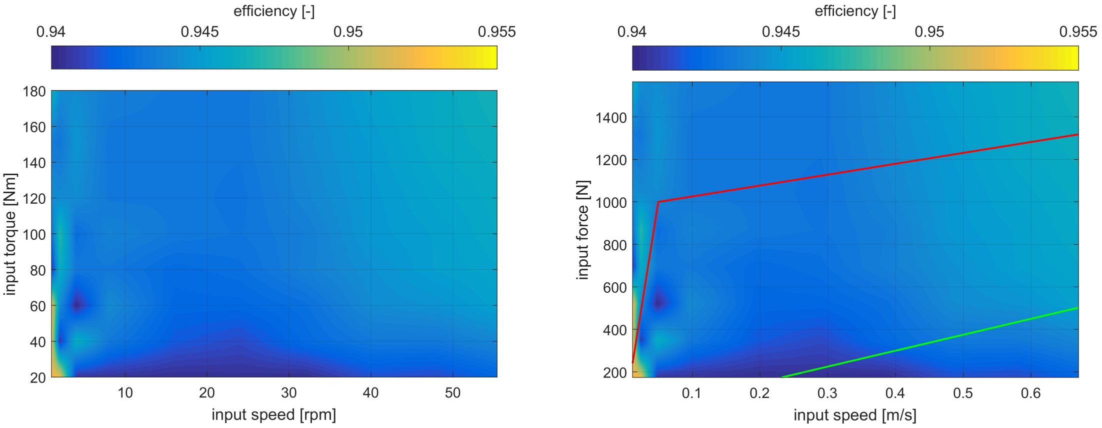

***Figure 4.1**: planetary gearbox efficiency map at constant temperature (obtained by KISSsoft model calculation): T - ω and F - v axis*

As can be seen, in the investigated range the total efficiency varies from a minimum 94,02 % (60 Nm @ 4 rpm) to a maximum 95,24 % (at minimum speed and torque). The computed efficiency accounts both for gear meshing losses and bearing losses: the seal losses are not considered, while the gear churning losses are negligible in this speed range. These values are comparable to the other efficiency evaluations that can be found in literature: the efficiency ranges from the 80 % of some gearbox catalogues to the 97 % of high precision gear sets.

In the efficiency map, a characteristic behaviour can be identified: the efficiency is lower with smaller torque values because the bearing viscous losses are bigger compared to the input power; at lowest speed the total efficiency is higher because the bearing viscous losses are negligible.

By the way, we are not only interested in the efficiency of the gearbox alone: we need to consider that in the system we have also the electric machine and it will contribute in a relevant way to the total efficiency of the rotative damper. Since the efficiency of the motor reaches very low values (from a minimum about 0 % to 80 %), in comparison the planetary gearbox can be considered to have almost a constant efficiency (with a total variation of 1,2 %). The resulting total efficiency map is represented in the following figure.

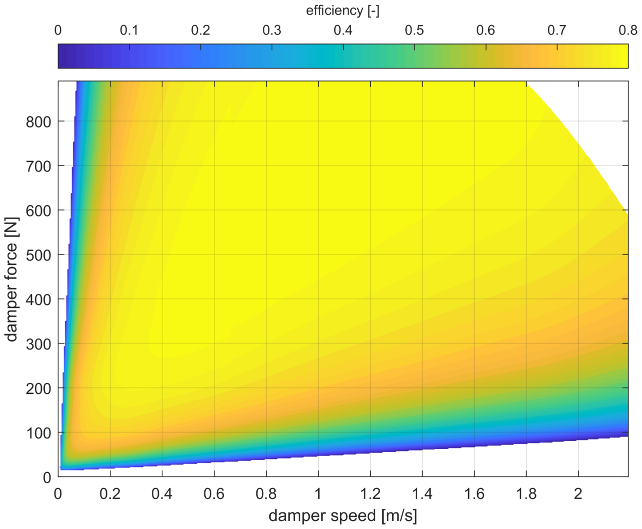

***Figure 4.2**: map of the total efficiency of damper device: gearbox + electric motor*

Just to conclude the efficiency analysis of the planetary gearbox model, it is interesting to point out a curiosity on the efficiency calculation; in our case the efficiency is clearly computed in the gearbox configuration of speed multiplier as required for the damping action, while typically those gearboxes are used as reducers for torque multiplication.

In order to have a comparison, we will compute the efficiency as reducer, so with the input on the sun gear of the second stage. To have a reference point, we consider the efficiency computed in the point nearest to the knee of the maximum damping characteristic: it corresponds to an input T_{in} = 120 Nm @ ω_{in} = 4 rpm. To keep the same input power, the corresponding values at the output shaft are obtained by the overall transmission ratio *i*.

As we can see in ***Table 4.1***, the computed efficiency is equal in both cases, so actually there is no difference in the software calculation between the multiplier and reducer configuration, also because we have not considered the same input of torque and speed but the same input power.

Multiplier *(input on carrier stage 1)*			***Reducer*** *(input on sun gear stage 2)*	
T_{in} **[Nm]**	120	i = 87,89	T_{out} **[Nm]**	1,365
ω_{in} **[rpm]**	4		ω_{out} **[rpm]**	351,6
Total efficiency	94,43 %		***Total efficiency***	94,43 %

Table 4.1*: efficiency comparison between the multiplier and reducer gearbox configurations*

4.2 Evaluation of the equivalent rotational inertia

In *Chapter 3* we have analyzed the different components of the actuator assembly, so we have presented some data concerning the masses and the inertia involved in the rotation of the damper; clearly in the optimization of the different parts we have tried to minimize the dimensions, with beneficial effect also on the total system mass, but always considering the design limits concerning strength and safety values.

Beside the total system mass that sums up to the one of the vehicle, actually from the functional point of view we need to consider the inertial contribution that is added to the suspension motion. In fact, being the rotative damper connected to the suspension through the leverage system, the rotational inertia of the planetary gearbox and the electric machine is transferred as linear inertia on the wheel unsprung mass. So actually the evaluation of the equivalent mass is fundamental because it will affect the suspension vertical comfort dynamics.

As seen in the previous chapter, we have already presented the moment of inertia of some components (planet gears and carriers): just to summarize them, the values of inertia of such parts are presented in the following ***Table 4.2***.

Planet gear stage 1	J_{p1}	123,6 g*cm^2
Planet gear stage 2	J_{p2}	50,6 g*cm^2
Carrier stage 1 (without planets)	J_{c1}	1,50 kg*cm^2
Carrier stage 2 (without planets)	J_{c2}	0,72 kg*cm^2

Table 4.2*: moments of inertia of planet gears and carrier shafts*

In addition to these data, we need a more detailed analysis on the gearbox kinematics to compute the equivalent rotational inertia.

- The carrier of the first stage is rotating at the input speed ω_{in}, but it is not composed only by the carrier shaft shown in ***Figure 3.20***: in its motion it includes also the needle bearings and the planet gears of the first stage. It is easy to understand that in such planetary stages, a relevant contribution to the inertia is represented by the planet gears that have not a fixed axis of rotation: in this case, the rotational inertia is doubled with respect to the simple carrier (***Figure 4.3***).

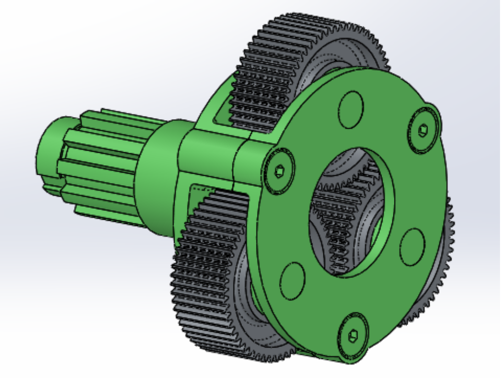

Mass m_{c1}	636	g
Moment of inertia J_{c1}	3,02	kg*cm^2
Speed ratio ω / ω_{in}	1	-

***Figure 4.3**: rotational inertia of the input shaft*

- The planet gears (of both stages) contribute in two ways to the rotational inertia: they rotate with the carrier (as a unique rigid body, as said before) but they also rotate on their own axis. We have already evaluated the moment of inertia of the planet gears, but now we need to compute their absolute angular speed: we need to remember that they are revolving respect to the carrier shaft which is already rotating. To compute the angular speed of gears in a planetary gearbox, we will use the Willis formula: it allows to rewrite the transmission ratios as a conventional gear stage with fixed gears axis by referring all the rotational speeds to the carrier rotation. The resulting minus sign indicates that the planet gear and the carrier shaft rotate in opposite directions.

$\omega_p = planet\ gear\ absolute\ speed$
$\omega_c = planetary\ carrier\ angular\ speed$
$\omega_r = ring\ gear\ angular\ speed = 0\ rad/s$

Eq. 4.2

$$\frac{\omega_p - \omega_c}{\omega_r - \omega_c} = \frac{z_r}{z_p}$$

$$planet\ speed\ transmission\ ratio \qquad i_p = \frac{\omega_p}{\omega_c} = -\frac{z_r}{z_p} + 1 = -1{,}31$$

- The planets carrier of the second stage is actually the output sun shaft of the first stage: also in this case we will use the Willis formula to obtain the transmission ratio of the planetary stage. The minus sign indicates that the ring and the sun gears are revolving in opposite directions in the equivalent planetary stage (that has the carrier "fixed").

$\omega_{in} = \text{input speed on carrier shaft}$
$\omega_{out} = \text{output speed on sun shaft}$
$\omega_r = \text{ring gear angular speed} = 0\ rad/s$

Eq. 4.3

$$\frac{\omega_r - \omega_{in}}{\omega_{out} - \omega_{in}} = -\frac{z_s}{z_r}$$

$$\text{planetary stage transmission ratio} \qquad i = \frac{\omega_{out}}{\omega_{in}} = \frac{z_r}{z_s} + 1 = 9{,}375$$

The total rotational inertia of this second carrier (***Figure 4.4***) includes the ball bearings, the sun gear directly machined on it and the planet gears that also in this case almost double the inertia of the simple carrier shaft.

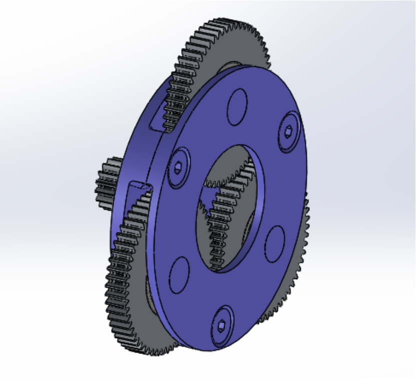

Mass $\boldsymbol{m_{c2}}$	242	g
Moment of inertia $\boldsymbol{J_{c2}}$	1,35	kg*cm^2
Speed ratio $\omega_{c2} / \omega_{in}$	9,375	-

Figure 4.4*: rotational inertia of the carrier of the second stage*

- The last rotating element in the device is the output shaft of the gearbox that coincides with the rotor of the electric machine (***Figure 4.5***). It includes the magnets and, as for the sun gear of the first stage, also the sun gear of the second stage is directly machined on the rotor shaft.

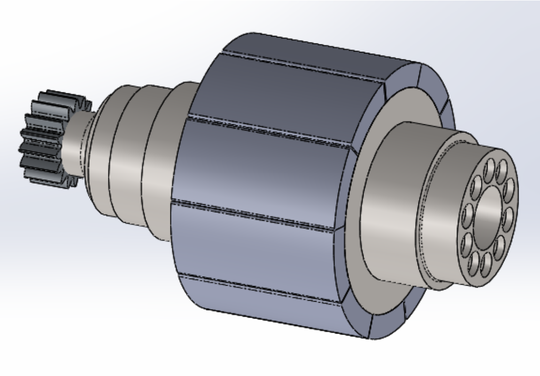

Mass $\boldsymbol{m}_{rot}$	202	g
Moment of inertia $\boldsymbol{J}_{rot}$	0,25	kg*cm^2
Speed ratio $\omega_{out} / \omega_{in}$	87,89	-

Figure 4.5: *rotational inertia of the rotor shaft*

Now that we have the complete data about the rotational moment of inertia of all the components, we can compute the equivalent rotational inertia of the system. This inertia will be referred to the input shaft: to obtain this, we simply consider all the different contributions to the total rotational kinetic energy, rewriting the rotational speeds by considering the transmission ratios previously evaluated.

$$\frac{1}{2} J_{eq}\, \omega_{in}^2 = \frac{1}{2} J_{c1}\, \omega_{in}^2 + 3 \cdot \frac{1}{2} J_{p1}\, \omega_{p1}^2 + \frac{1}{2} J_{c2}\, \omega_{c2}^2 + 3 \cdot \frac{1}{2} J_{p2}\, \omega_{p2}^2 + \frac{1}{2} J_{rot}\, \omega_{out}^2$$

$$J_{eq} = J_{c1} + 3 \cdot J_{p1} \cdot i_p^2 + J_{c2} \cdot i^2 + 3 \cdot J_{p2} \cdot i_p^2 \cdot i^2 + J_{rot} \cdot i^4 \qquad \textbf{Eq. 4.4}$$

$$\textit{equivalent rotational inertia at input shaft} \qquad J_{eq} = 0{,}205\ kg \cdot m^2$$

In order to have a more significant value, the rotational moment of inertia is converted into an equivalent mass related to the suspension stroke: this can be done by dividing the moment of inertia by the square of the leverage transmission ratio τ. Actually, this transmission ratio is varying with the suspension stroke, so we will consider two values: the nominal one corresponding to the equilibrium position of the suspension (τ *nominal* = 0,115 m/rad) and the mean value of the function τ (τ *mean* = 0,103 m/rad).

In addition to this, just to have a more complete view of the system, we will include the inertia of the input leverages represented as simple cylindrical bars. It was computed in [15], considering the reference leverage configuration (the solution 4 in ***Figure 5.2***), but actually their resulting contribution is minimal compared to the one of the damper. The data about the mass of the device are summarized in the following ***Table 4.3***.

	Damper total mass	$\boldsymbol{m_{tot}}$	3,16	kg
	Damper equivalent rotational inertia	$\boldsymbol{J_{eq}}$	0,205	kg*m^2
Damper equivalent mass	*τ nominal*	$\boldsymbol{m_{eq}}$	15,64	kg
	τ mean	$\boldsymbol{m_{eq}}$	19,55	kg
	Leverage equivalent linear inertia	$\boldsymbol{m_{eq\ lev}}$	0,255	kg
Damper and leverage equivalent mass	*τ nominal*	$\boldsymbol{m_{eq\ tot}}$	15,89	kg
	τ mean	$\boldsymbol{m_{eq\ tot}}$	19,81	kg

***Table 4.3**: summary of the inertial properties of the system*

As we can see, in the end the total equivalent mass remains slightly below 20 kg: this is a good value if compared with the previous results. In fact the electro-hydraulic rotative damper had an equivalent mass equal to 35 kg, while the improvement obtained respect to the preliminary model is even more remarkable: the equivalent mass of the system was 55 kg without taking into account the inertia moments of the shafts [15].

Equivalent linear inertia		
Electro-hydraulic solution	35	kg
Electro-mechanical preliminary model	55	kg
Electro-mechanical final model	20	kg

***Table 4.4**: comparison of the equivalent linear inertia among the different rotative damper versions*

4.3 Acoustic analysis

Nowadays, among the key performances of a vehicle, the noise has become a fundamental aspect that the customer will take into account, besides cost and driving performances. The car manufacturers are focusing more and more in the reduction of the overall noise generated by a vehicle: they are not only improving the insulation of the passenger compartment, but they are also acting in minimizing the noise produced toward the road environment, with beneficial effects for all the users. To reach this objective, clearly it is also necessary to act on the noise sources (as engine or tyres), by taking into account such noise issues during the components design phase.

Once stated the relevance of such aspect, it is important to carry out a preliminary analysis on our rotary damper model in order to evaluate the noise level in realistic operating conditions. By the way, we need to remember that, as first approach in the design, we did not consider the target of minimizing the noise.

In the following sections we will present the results about the acoustic performances of the damper, in particular focusing on the planetary gearbox: starting from the preliminary study performed in [15], we will develop a more detailed analysis trying to integrate different methodologies.

4.3.1 *Preliminary analysis on the gearbox noise level*

In the previous thesis work [15], the evaluation of the noise level was one of the factors that was considered in the comparison of the different gearbox configurations. The calculation of the sound level generated by the gearbox has been performed in analytical way by using the empirical formula proposed by Masuda (***Eq. 4.5***), directly implemented in the KISSsoft gear calculation module:

$$L = \frac{20 \cdot (1 - \tan(\beta/2)) \cdot \sqrt[8]{i}}{\sqrt[4]{\epsilon_\alpha}} \cdot \sqrt{\frac{5{,}56 + \sqrt{v}}{5{,}56}} + 20 \cdot \log(P) + 20 \cdot \log(X) \qquad \textit{Eq. 4.5}$$

In the equation, the different quantities are:

- *L*: sound pressure level generated by the gearbox at 1 meter of distance [dBA];
- *β*: gear helix angle [deg];
- *i*: gear transmission ratio;
- ε_α: gear transverse contact ratio;
- *v*: speed on the pitch line [m/s];
- *P*: power transmitted by the gear pair [kW];
- *X*: teeth vibration displacement amplitude normalized by static deflection.

As we can see, the major influencing parameters are related to the gear geometry, to the rotational speed and to the total power transmitted.

In the following ***Figure 4.6***, the results of this preliminary analysis are presented (as calculated in [15]): the sound pressure level is evaluated in a limited region of the gearbox operating range, and it only takes into account the sun - planets and planets - ring gear meshings of the first stage. It is evident that the peak of the noise level (75 dBA) is reached in correspondence of the highest considered input load (140 Nm @ 166 rpm), that is not corresponding to the limit working point of the damper.

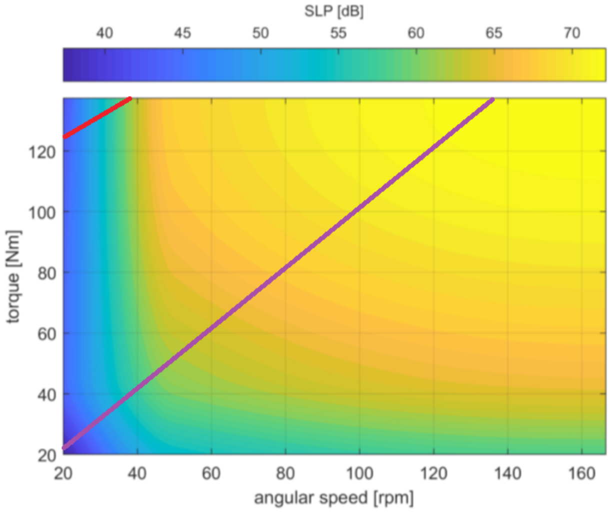

Figure 4.6*: sound pressure level generated by the gearbox, computed in [15] with the KISSsoft model (SPL given by the Masuda formula); in the plot also the maximum (red line) and minimum (purple line) damping characteristics are represented (rescaled according to the F-v characteristic)*

Actually these results are presented just to have a reference starting point, but we need to remember that, following the first preliminary version, the gearbox has been optimized and redesigned. Moreover, such empirical formula only takes into account the noise produced by the gear meshing, without considering the vibrational effects of the whole housing and assembly.

For these reasons, a more detailed study is necessary: even if this analytical evaluation is implemented in the KISSsoft model calculation and it is much faster, we decide to develop a finite elements model simulation in order to obtain more realistic results.

4.3.2 *COMSOL model and simulation setup*

The software used to perform the acoustic numerical simulations is COMSOL Multiphysics® (***Figure 4.7***): “it is a simulation platform that encompasses all the steps in the modelling workflow: from defining geometries, material properties and the physics that describe the phenomena up to the solving and post-processing models for producing accurate and trustworthy results. These models are used for understanding, designing, and optimizing processes and devices for realistic operating conditions”. The benefits on the engineering activity are relevant since “the modelling, compared to running experimental methods or testing prototypes, allows for quicker and often more efficient and accurate optimization of processes and devices”. The major feature of this software is the possibility “to couple any number of physics phenomena of different nature together in a single model” [25].

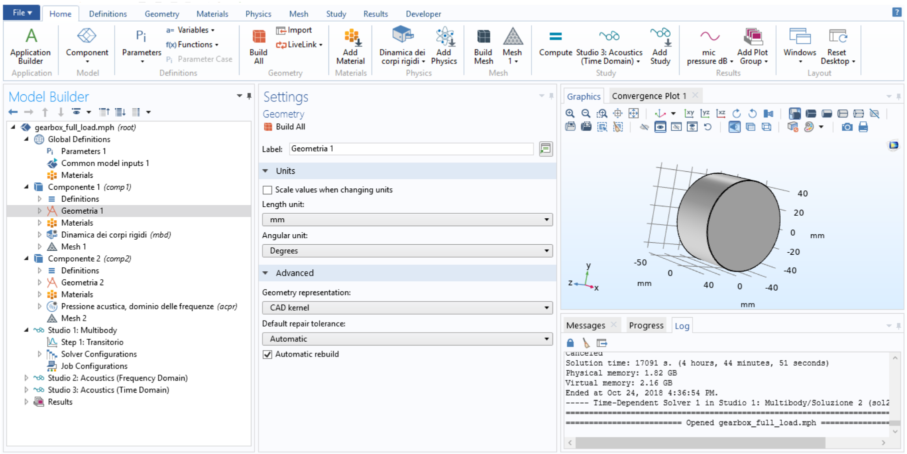

Settings

Geometry

Build All

Label: Geometria 1

Units

☐ Scale values when changing units

Length unit: mm

Angular unit: Degrees

Advanced

Geometry representation: CAD kernel

Default repair tolerance: Automatic

☑ Automatic rebuild

```
Canceled
Solution time: 17091 s. (4 hours, 44 minutes, 51 seconds)
Physical memory: 1.82 GB
Virtual memory: 2.16 GB
Ended at Oct 24, 2018 4:36:54 PM.
----- Time-Dependent Solver 1 in Studio 1: Multibody/Soluzione 2 (sol2
======================================================================
======================== Opened gearbox_full_load.mph ================
```

***Figure 4.7**: COMSOL Multiphysics user interface: here we can distinguish the elements tree on the left, the parameters setting in the center and the results graphic window on the right*

In particular we want to analyze the noise level produced by the planetary gearbox, including the effect determined by the whole housing: the model will include the multibody structural analysis (to evaluate the vibrations on the assembly due to the gear pairs) and then the acoustic study on the air surrounding the gearbox. The functional scheme that is summarizing the steps of the simulation is represented in ***Figure 4.8***.

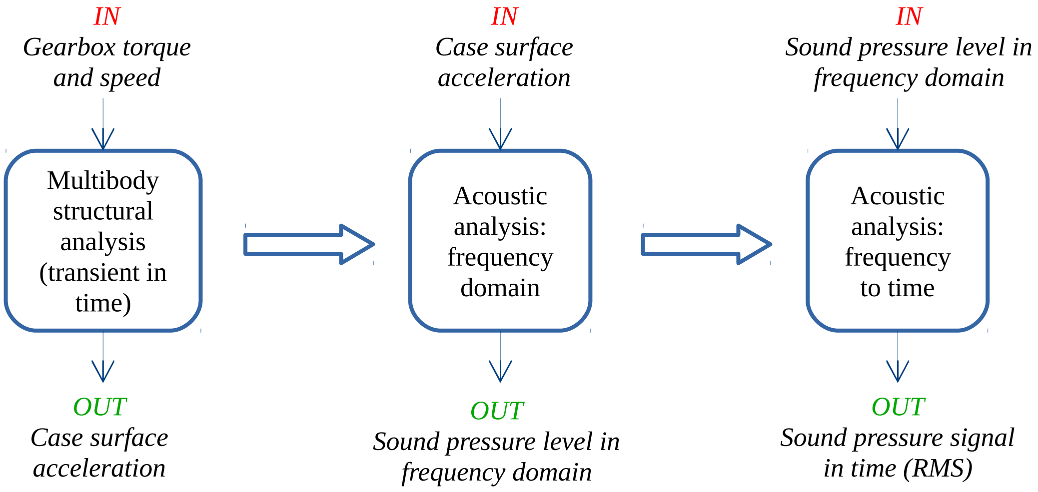

***Figure 4.8**: functional scheme describing the steps of the COMSOL acoustic analysis*

After this short introduction we will describe more in detail how the model was built to highlight its main features and some faced issues.

As said, the model includes two physics domains: the multibody structural domain and the acoustic domain, then the first step is to build the 3D model of the gearbox assembly. Actually the geometry is much simplified respect to the prototype model described in *Chapter 3* in order to reduce the time required for the simulations; moreover we will consider only the planetary gearbox stage, excluding from the model the whole motor side. Here below we describe how we modelled the main components of the gearbox.

- *Carriers shafts*: the shafts of the final prototype model have some complicate features (as the splined coupling and the holes for the screws) but since we want to focus on the noise propagation outside the gearbox, it is worth to simplify the geometry of the carriers to reduce the computation time. In addition to this, the shafts are all considered as rigid bodies, so such level of detail is not necessary, also because we will not perform a stress and deformation FEM analysis on them.
- *Gears*: these are the most important components since their meshing is defining the vibrations in the assembly. By the way, the spur gear component included in the COMSOL library is defined as a rigid body and it is identified by a few parameters (number of teeth, pitch diameter and pressure angle). In fact the numerical simulation does not take into account the tooth contact directly from the 3D geometry, but the actual gear operation is described by some lumped parameters that are set in the gear pair connection. For this reason we can simply model the spur gears as plain cylindrical bodies (as also suggested by the COMSOL user guide).
- *Gearbox housing*: as for the shafts, the geometry of the external housing is simplified respect to the prototype model: it is reduced to a simpler cylinder including only the planetary gearbox. It has a relevant function in the model because it represents the interface with the surrounding air: in order to evaluate the vibrations on its surface, the case is the only element in the assembly to be considered with elastic material properties.

Some details of the modified geometry of the model are presented in the following ***Figure 4.9***: we can see the simplified shaft with the plain cylindrical gears and the gearbox housing.

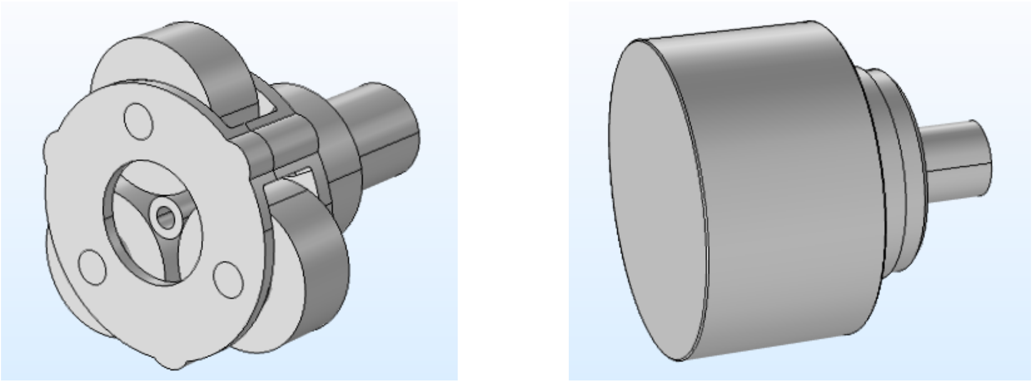

Figure 4.9*: simplified geometry of the 3D model: carrier shaft of the first stage and gearbox case*

Once the 3D model is built, we need to set up the multibody structural study: here we define the constraints and the couplings among the different components. The most important feature is the gear pair connection: it defines the meshing between two gears through some characteristic parameters like friction, meshing stiffness and transmission error. In particular we include only the tooth meshing stiffness: this parameters describes the bending of the tooth when it is engaged, so contributing to the gear transmission error. Another factor that is increasing the irregularity of the gear rotation is the contact ratio *ε* that in our case is not an integer number: this means that during the rotation, the number of teeth pairs in contact is varying. In general these are the major sources of vibration during gears operation.

In particular in the COMSOL model we set up the two parameters explained below:

- *singular tooth stiffness c'*: it is defined as the load which is necessary to deform one meshing gear teeth having 1 mm facewidth by an amount of 1 μm (in the plane of contact). The *c'* value is taken from the KISSsoft gear calculation (detailed data are available in *Appendix A*).

$$\textit{tooth stiffness}$$

$$sun-planet\ \ gear\ \ pair \qquad c' = 9{,}914\ \frac{N}{mm\cdot\mu m}$$

$$planet-ring\ \ gear\ \ pair \qquad c' = 11{,}324\ \frac{N}{mm\cdot\mu m}$$

  Clearly, to obtain the tooth stiffness (expressed in [N/m]) we need to multiply *c'* by the gears facewidth *b*, that is different for the two stages (15 mm and 5 mm).

- *Contact ratio ε*: as said, this ratio not an integer number and so this means that the number of mating teeth pairs is varying during the meshing cycle (*ε* sun-planet = 1,45 and *ε* planet-ring = 1,93). The figure below is useful to better understand this concept: *ε* can be seen as the average number of teeth pairs in contact over a mesh cycle.

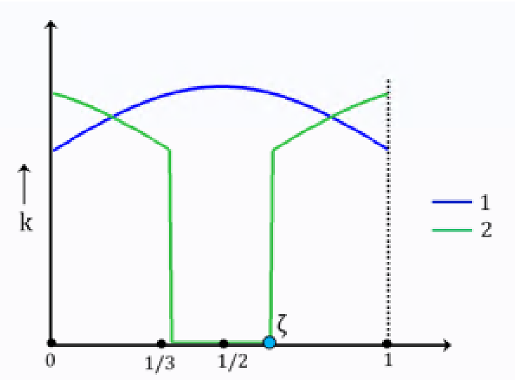

***Figure 4.10**: diagram showing the different teeth pairs engaged during a meshing cycle: in the central part of the contact line, only one teeth pair is mating*

- In the COMSOL model, this is described by the factor ζ “next tooth engagement position in the mesh cycle”: it can be computed by the length of the contact line and the base pitch (evaluated by gear calculation in KISSsoft model, the detailed data are available in the report in *Appendix A*).

$$next\ tooth\ engagement\ \ position$$

$$\zeta = \frac{base\ \ pitch}{length\ of\ \ path\ of\ \ contact}$$

$$\begin{aligned} &base\ \ pitch = 1{,}77\ \ mm \\ &length\ of\ \ contact\ \ path\ \ sun-planet = 2{,}58\ \ mm \\ &length\ of\ \ contact\ \ path\ \ planet-ring = 3{,}42\ \ mm \end{aligned} \qquad \textbf{Eq. 4.6}$$

$$\begin{aligned} &\zeta\ \ sun-planet = 0{,}69 \\ &\zeta\ \ planet-ring = 0{,}52 \end{aligned}$$

In addition to these parameters, actually in a real operating gearbox the friction is another relevant factor to be considered. By the way, the introduction of the friction in our model determines additional degrees of freedom and the need to evaluate the teeth contact forces: this increases exponentially the computation time and introduces some problems in the convergence of the numerical simulation. For this reason, we decide to neglect the friction. This choice is acceptable from the point of view of the simulation meaningfulness: first of all because the presence of lubricating oil reduces the friction to a minimum (the friction coefficient can be lower than 0,1); second, neglecting the friction, we stay in a worse condition since there is no damping effect due to the friction itself and so the vibrations are bigger.

For what concern the constraints among the components, generally the bearings in the assembly (the one on the input shaft and on the ones on the planet gears) are modelled as rigid hinge joints. The ring gear is rigidly fixed on the gearbox case: even if this is not representing the real situation (the ring has some radial clearance respect to the case), it is the only solution that allows the convergence of the numerical simulation without issues. Finally, only the cylindrical surface around the input shaft is constrained to a fixed point, as to reproduce the fitting of the whole damper prototype on the test bench.

This concludes the presentation of the model prepared for the simulations: in the following section we will provide further details about the input and the simulation set up, together with the presentation of the results of the analysis.

4.3.3 *Results of the COMSOL acoustic simulations*

In the presentation of the results we will follow the logical steps of the simulation already described in ***Figure 4.8***.

The first analysis to be carried out is the multibody structural study, as a transient in the time domain: here we will simulate the rotation of the gearbox to evaluate the vibrations due to the gears engaged. So we need to define the values of rotational speed and torque: these input are constant, then we can only simulate a limited number of operating points in the damper working range. The considered loading conditions are:

- **Full load**: input T_{in} = 230 Nm @ ω_{in} = 166 rpm, corresponding to the maximum limit load of the damping characteristic.
- **Half load**: we will consider half of the maximum value of speed and torque, so with input T_{in} = 115 Nm @ ω_{in} = 83 rpm.

Actually, the speed is prescribed on the input shaft, while the torque is applied as resisting action on the output sun gear of the second stage, clearly reduced by the gearbox transmission ratio. Moreover, they are applied as ramp signals in order to favour the solution of the numerical simulation, but then, as we will see, we will neglect this initial transient phase in the acoustic study.

The simulation time is selected according to the number of teeth engaged: in fact, a few number of teeth contacts is enough to reach the steady state condition of the vibratory phenomenon. In our case we decided to consider the rotation corresponding to 7 teeth engaged between the planet and the ring gears.

The relevant output result of this first simulation step is the normal acceleration on the gearbox case surface: just to have an idea of its order of magnitude, the plot in ***Figure 4.11*** is showing the normal acceleration on a point on the edge of the housing as function of time (we have cut the first half of the simulation time).

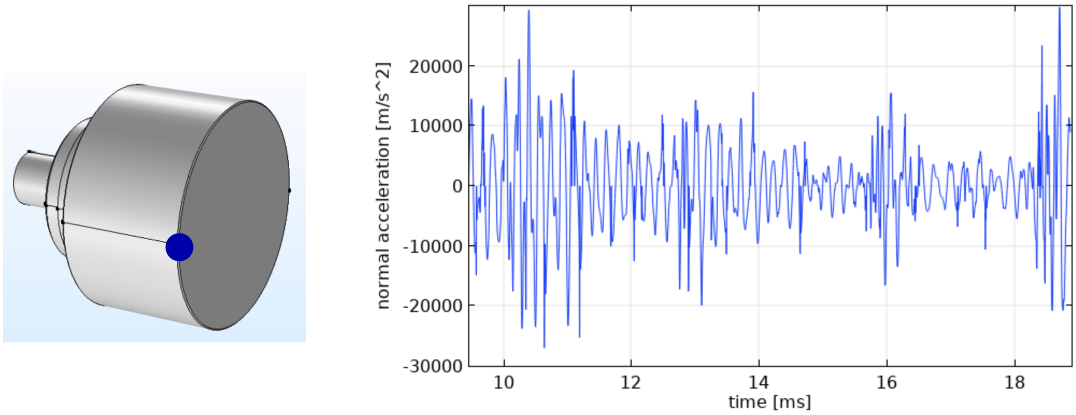

Figure 4.11: *normal acceleration as function of time (plot on the right), measured on a point on the case surface (represented on the left), with full load input*

This case vibration is the source for the propagation of air pressure waves that are determining a certain perceived noise outside the gearbox: the case surface acceleration is then the input of the acoustic analysis in frequency domain. In order to study such pressure levels, we need to define an air domain around the gearbox: it is represented by a sphere with a radius equal to 1 m, since also in the Masuda formula the noise level is evaluated at 1 m reference distance. By the way, in order to simplify the analysis of the results, we will consider only 3 points were to evaluate the noise levels, as corresponding to the positioning of 3 microphones. This set up of the acoustic study is shown in ***Figure 4.12***.

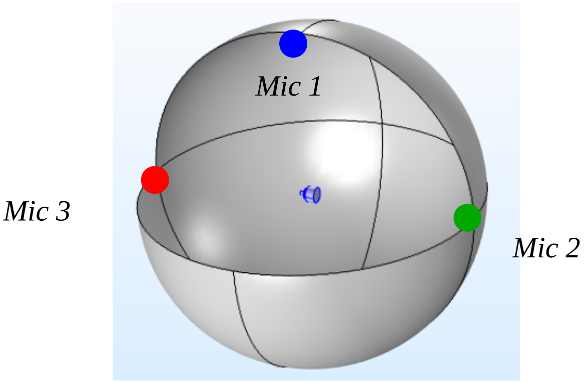

Figure 4.12: *air domain for the acoustic analysis (sphere with 1 m radius) and positions of the three points where the noise levels are evaluated*

Before to see the results concerning the three microphones, it is also interesting to see how the acceleration is transformed into air pressure: the case surface is the boundary interface with the air domain and so the surface acceleration is directly determining a certain air pressure, as shown in ***Figure 4.13***. Clearly this maximum value (about 90 dB) will result higher than the sound pressure level (*SPL*) measured at a distance of 1 m. By the way, the time to frequency domain transformation only allows to obtain the sound pressure level at a given frequency.

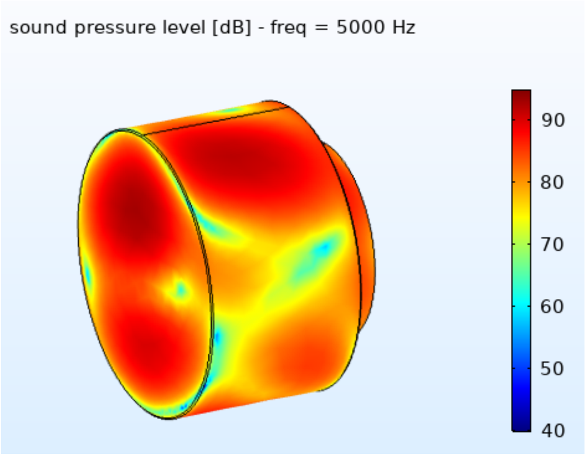

***Figure 4.13**: sound pressure level on the case surface boundary, at f = 5 kHz (full load)*

To have a more complete overview of the results, we need to consider the noise level variations over the frequency range. As said, the time to frequency domain transformation only considers the second half of the multibody simulation, while the investigated frequency range goes from 100 Hz to 8000 Hz, since we have noticed that the pressure level is practically negligible outside this interval; this can be seen in the following plot, which is showing the air pressure on the three microphones as function of the frequency.

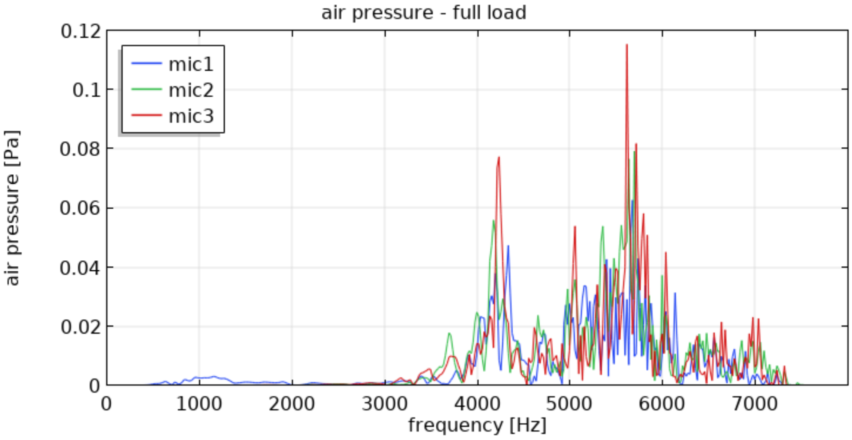

***Figure 4.14**: air pressure evaluated on the 3 microphones (full load)*

Actually, when talking about noise, the air pressure is not directly representative of the perceived noise, so it is better to transform the pressure value into a sound pressure level expressed in decibel [dB] (the reference pressure is 20 μPa, corresponding to the minimum auditory threshold). It is important to point out that all the results concerning the sound pressure level in this COMSOL acoustic analysis are expressed as “absolute” decibel: this means that the *SPL* spectra in frequency domain have not been filtered with any weighting function (needed for example to evaluate the dBA, weighted according to human sensitivity).

The *SPL* measured on the three microphones in both loading conditions is represented in the two plots in ***Figure 4.15***: here the relevant frequency range is much more evident (frequency in logarithmic scale). As we can see, the peaks are concentrated in the same region (related to the natural frequencies of the system), but, as expected, the *SPL* in the full load condition is higher and shifted to higher frequencies due to the bigger rotational speed.

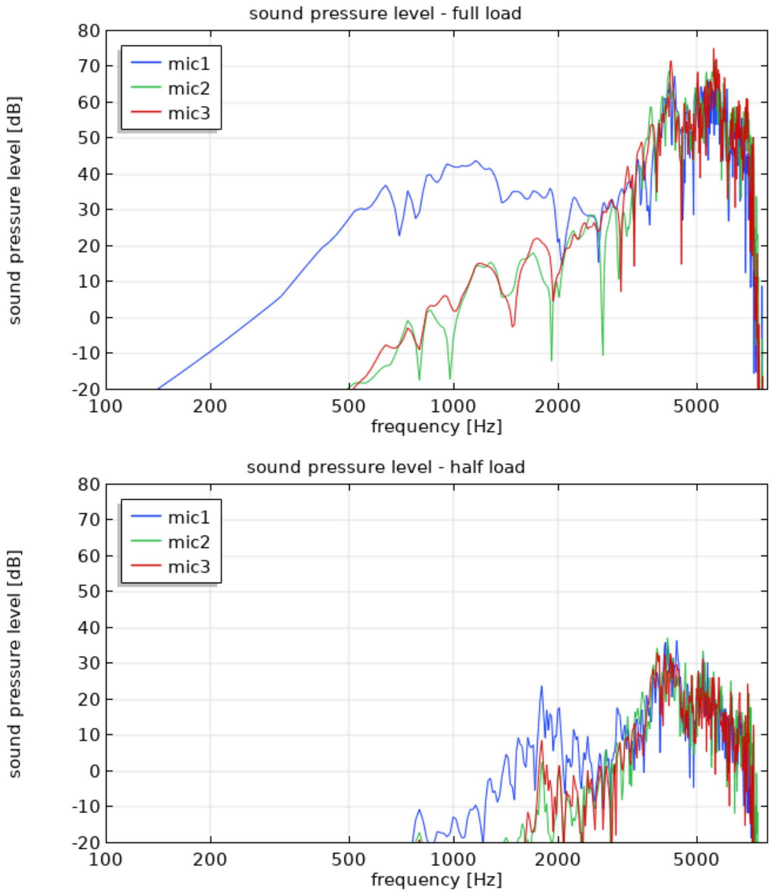

Figure 4.15*: sound pressure level [dB] as function of frequency evaluated on the 3 microphones: full load (upper plot) and half load (lower plot)*

To have a quantitative comparison, in the following ***Table 4.5*** we summarize the SPL peak values and the frequencies at which they are occurring.

	Full load			*Half load*		
	Mic 1	*Mic 2*	*Mic 3*	*Mic 1*	*Mic 2*	*Mic 3*
SPL max [dB]	69,9	72,0	75,2	36,6	37,3	33,2
@ f [Hz]	5680	5700	5620	4400	4140	3860

***Table 4.5**: maximum values of the sound pressure level on the frequency range, and the corresponding frequencies at which they are occurring*

At this point it is necessary to briefly discuss the selection of the positions of the microphones around the gearbox: since we calculated the noise level only in three points, we don't have a general overview of the real sound propagation in the surrounding space. In order to do this, we evaluate the *SPL* on the whole circumference of the sphere: these polar plots (***Figure 4.16***) are showing the noise level at 1 meter distance on three orthogonal planes; the considered frequencies are different and corresponding to the average of the three microphones peaks. As we can clearly see, there is not a preferred direction of sound propagation, so the considered points are equivalent and representative of the noise level generated all around the gearbox.

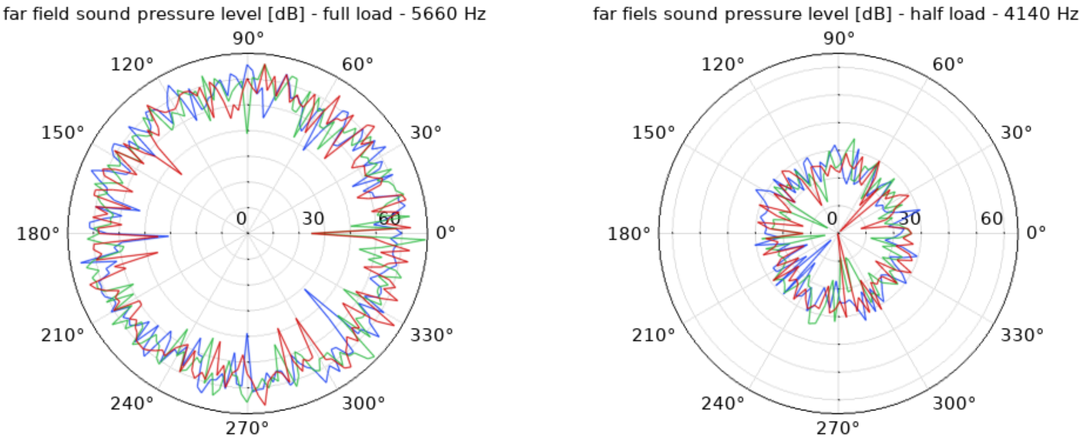

***Figure 4.16**: SPL evaluated at 1 m distance on three orthogonal planes: full load (on the left) and half load (on the right)*

Up to now we have considered the acoustic analysis in frequency domain, that actually separates the contributions (to the total noise level) of the different frequencies. For this reason, in order to obtain a more representative value of *SPL*, we need to proceed with the last step of the study that consists in the back transformation from frequency to time domain: in fact, the actual perceived noise is composed by the whole frequency spectrum shown in ***Figure 4.15***.

As result of the transformation in time domain, we obtain the air pressure variation as function of the time, clearly including all the different frequencies: the reconstructed pressure signal in time is represented in the ***Figure 4.17*** below (the considered time is 1/10 of the total simulation time).

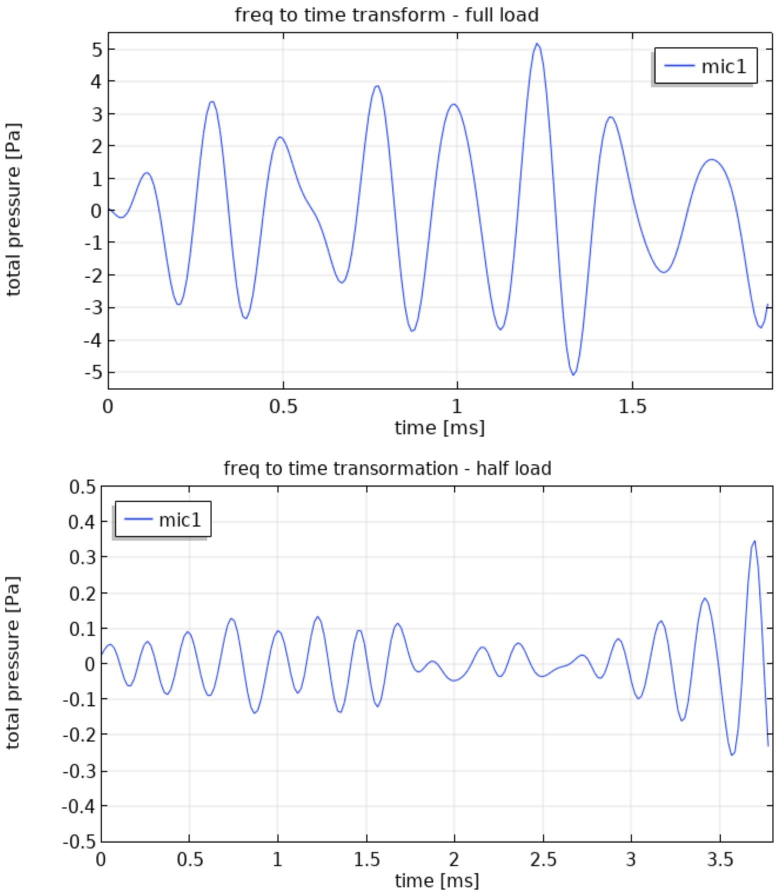

Figure 4.17*: pressure variations in time: full load (upper plot) and half load (lower plot); the signals are reconstructed by the frequency to time domain transformation*

As we can see in the previous plots, in half load condition the pressure level is generally an order of magnitude smaller than the full load case. Anyway, as already remarked, it is better to compute the *SPL* to have a quantitative indication of the perceived noise. In this case, since we have a signal that is varying in time, we will not simply consider the peak values: we evaluate the root mean square of the air pressure in time and then we transform such value into decibel. The results are summarized in ***Table 4.6***: the RMS values of the sound pressure level in time are bigger than the corresponding maximum values in frequency domain (***Table 4.5***) because, as said, these time signals contains all the frequencies contributions.

	SPL RMS [dB]	
	Full load	*Half load*
Mic 1	81,0	52,7
Mic 2	84,0	52,0
Mic 3	82,3	48,7

Table 4.6*: root mean square value of the sound pressure level (evaluated by the reconstructed pressure signals in time)*

To conclude the presentation of the results of the COMSOL model, we can briefly compare the obtained results with the preliminary acoustic study described in section *4.3.1*. Even if the two acoustic analysis have two completely different approaches, actually we obtained consistent results between the two cases:

- preliminary noise evaluation with Masuda empirical formula (accounting only for the gears meshing): the maximum noise level is 75 dBA (input load T_{in} = 140 Nm @ ω_{in} = 166 rpm);
- COMSOL numerical simulation (the model includes the whole gearbox housing assembly): the maximum RMS noise level is 84 dB (at full load T_{in} = 230 Nm @ ω_{in} = 166 rpm).

Anyway we need to remember that a direct comparison is not possible, since the considered gearbox models are different: the COMSOL simulation has been performed on the final model of the gearbox, that is smaller than the preliminary planetary configuration.

As seen, the acoustic numerical simulation with the finite element method requires a lot of time for the model setup, for running the simulation and then for processing the results. By the way we managed to evaluate the performances with two loading conditions: the study of points at lower speed was also limited by problems in the convergence of the simulation. These two working points give an indication of the worst case noise level, since we have considered the damper running at constant maximum limit load, that clearly is not a nominal operating point. Actually the damper is working in a wider operating region and most of all at very low speeds: we should evaluate the noise level on the whole working range to have an idea of the noise produced in more realistic conditions.

4.3.4 *New evaluation of sound pressure level in KISSsoft*

As seen in the previous section, the COMSOL numerical simulations have two major limitations: the long computational time required and the impossibility to investigate very low rotational speeds.

On the other hand, the obtained results are consistent with the noise level obtained by the preliminary analysis with the Masuda empirical formula: so if we want to study the gearbox noise in a wider operating range, the use of such analytical formula is for sure a faster and straightforward approach.

As did in the previous thesis work, the *SPL* is computed in the KISSsoft gear calculation module: here we set the constant input torque and rotational speed (separately for the first and second stage) and among the report results we automatically obtain the gear meshing noise level evaluated with the Masuda formula (***Eq. 4.5***). Actually, these values are referred to a single engaged gear pair (sun-planet and planet-ring pairs), so the total generated noise must account for all the meshing gears in the planetary gear set.

Since the noise level is a logarithmic quantity, the direct algebraic summation of *SPL* is not possible, so we need to consider the following logarithmic sum: here we take into account the contributions of 3 sun-planet gear meshing pairs and of 3 planet-ring gear pairs (of both stages) to the total gearbox noise level.

$$SPL\,sp = sun - planet\ \ gear\ \ meshing\ \ noise\ \ level$$
$$SPL\,pr = planet - ring\ \ gear\ \ meshing\ \ noise\ \ level$$

$$planetary\ \ gearbox\ \ total\ \ noise\ \ level \qquad \textbf{Eq. 4.7}$$

$$SPL_{tot} = 10 \cdot \log\left(3 \cdot 10^{\frac{SPL\,sp\,1}{10}} + 3 \cdot 10^{\frac{SPL\,pr\,1}{10}} + 3 \cdot 10^{\frac{SPL\,sp\,2}{10}} + 3 \cdot 10^{\frac{SPL\,pr\,2}{10}}\right)$$

The so computed total gearbox noise level is represented in the plot of ***Figure 4.18***; in the map we also highlighted the maximum (red line) and minimum (green line) damping characteristics.

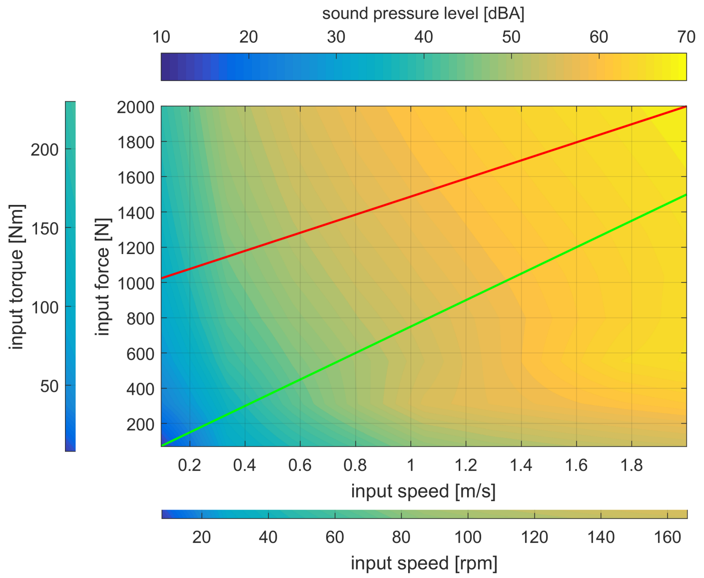

***Figure 4.18**: gearbox sound pressure level (computed in KISSsoft with the Masuda formula) as function of the input torque and speed; the axis are not starting from zero*

As we can see, the investigated operating range does not include the first part of the linear characteristic, that actually represents the normal working conditions of the damper: the minimum torque and speed (8 Nm @ 8 rpm) are limited by the calculation that requires a minimum input power to evaluate the *SPL*.

At this point it is interesting to compare these results with the noise level evaluated in the previous COMSOL simulations: in the following ***Table 4.7***, we summarize the noise level obtained in the two analyzed loading conditions (the noise level related to the COMSOL model is the mean value of the *SPL* of the three microphones).

	Sound pressure level	
	Full load	*Half load*
COMSOL simulation *[RMS dB]*	82,4	51,1
KISSsoft model *[dBA]*	68,4	55,9

***Table 4.7**: comparison between the sound pressure levels evaluated with the two different approaches (COMSOL and KISSsoft models)*

The *SPL* values are clearly not equal: there is a difference of 14 dB (full load) and of 4,8 dB (half load) between the COMSOL model and the KISSsoft analytical evaluation. Anyway, these differences are acceptable and the results are consistent since, as already explained, the two approaches are completely different.

4.3.5 *Noise level evaluation with road profile excitation*

The noise level map evaluated in the previous section actually gives limited information about the noise generated in normal operating conditions: in fact, up to now, the *SPL* was evaluated by considering a constant input (both in COMSOL and KISSsoft analysis). For this reason, the next step of the acoustic study consists in trying to evaluate the noise level produced by the damper when a realistic load is applied to it: this means to have the input provided by a random road profile excitation.

Such type of input cannot be used with the previous methods: as seen, in COMSOL we simulated just a few milliseconds of gears rotation, so it is not feasible to run the FEM analysis for several seconds. On the other hand, even if in KISSsoft calculations we have the possibility to use a load spectrum input to reproduce the road profile, the constant input is intrinsic in the definition of the load spectrum itself (this issue was already analyzed in section *2.3.2* when introducing the load spectrum definition).

The idea is to integrate the “static” *SPL* map obtained by KISSsoft in the Simulink model used to perform the road profile simulations (described in section *2.3.2*). In this way we have the instantaneous values of input torque and speed provided by the quarter car suspension dynamics, which are used to evaluate the corresponding *SPL* on the map as in a look-up table, obtaining the variation of noise level in time.

In order to do this, we need to evaluate the noise level along the maximum damping characteristic that represents the actual damper working points. By the way, as already highlighted, the *SPL* data are not available below ω_{in} = 8 rpm, where most of the device operating points are concentrated during normal loading conditions. So the solution is to extrapolate the noise level trend in the low speed region from the available data; obviously, in order to obtain a more realistic estimation, it is not possible to simply consider the noise level constant in such range.

In the following plot (***Figure 4.19***), the trend of the noise level along the maximum damping characteristic is represented: as we can see it is clearly non linear, so we decide to interpolate such data with cubic polynomial and logarithmic curves.

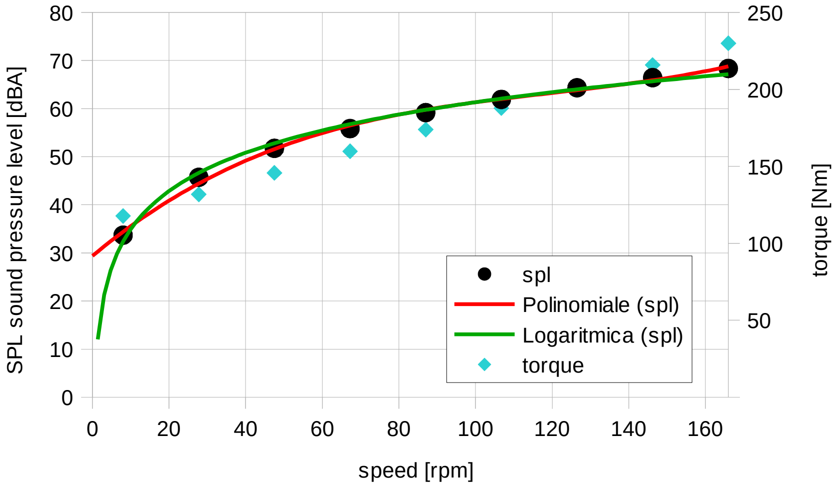

Figure 4.19: SPL trend on the maximum damping characteristic (black circles) and two data interpolations: cubic polynomial (red curve) and logarithmic (green curve)

These two interpolation curves are both introduced into the Simulink model (***Figure 2.4***): we considered as input an ISO B class road, travelled at 70 km/h. By running the random road profile simulations (an example of the output was shown in ***Figure 2.6***), we obtain the corresponding sound pressure level time histories, which are represented in the plots in ***Figure 4.20***.

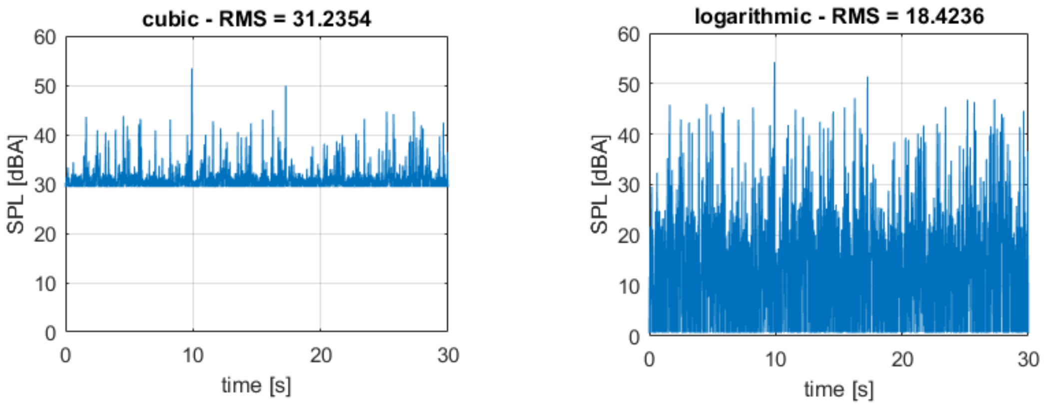

Figure 4.20: Simulink model road profile simulations: SPL with cubic (on the left) and logarithmic (on the right) interpolations; only 30 s of simulation are shown

In order to have a more representative evaluation, we compute the root mean square value of the previous *SPL* signals over time (***Table 4.8***).

	SPL RMS
Cubic interpolation	31,2 dB
Logarithmic interpolation	18,4 dB

***Table 4.8**: RMS values of the noise level signals obtained by the Simulink road profile simulations*

Actually, the results are quite different: with the cubic interpolation the *SPL* remains always greater than zero because the extrapolation gives a positive noise level also at zero speed (about 30 dB). Clearly, this is not a realistic condition since we reasonably assume that at zero speed the noise produced is also zero: for this reason we also considered a logarithmic interpolation that gives the *SPL* decreasing almost to zero in the lowest speed range.

Anyway, these results must be taken only as limit reference values of the real operating noise, that actually can be intermediate between the two values: in fact, on one side the cubic interpolation is a worst case condition, where the minimum *SPL* is 30 dB; on the other side we should consider that at low speeds the damper is continuously oscillating and reversing the rotation, so this is an additional contribution to the total noise level that we will not investigate.

4.3.6 *Acoustic analysis: conclusions*

To conclude the study of the noise level generated by the rotary damper, we will briefly summarize the obtained results: the noise levels computed with the different approaches are presented in ***Table 4.9***.

	Loading condition	***Noise level***
COMSOL simulation	Max limit load	82,4 dB
KISSsoft model	Max limit load	68,4 dBA
Simulink model	ISO B road profile @ 70 km/h	18,4 - 31,2 dB

***Table 4.9**: comparison of damper noise levels evaluated with different approaches*

By the way these values are only indicative and are not estimating the noise level in real operating conditions, since each method of analysis has is own limitations, that are summarized here below.

- *COMSOL model*: the numerical acoustic analysis with finite element method includes the vibrations of the whole damper housing, but the simulations are performed with constant input load.

- *KISSsoft model*: the sound level is computed with the Masuda empirical formula and, being a fast calculation, it allows to investigate a larger operating range, but anyway the input load is constant.
- *Simulink model*: it integrates the road profile simulation (providing a realistic input load) with the *SPL* map, but still we are not able to estimate the real noise generated by the continuous small oscillations of the damper.

The preliminary study to evaluate the noise level of such automotive component has the aim to obtain a first rough evaluation of its contribution to the total noise produced by a car on the road. In fact, nowadays, institutions and car manufacturers are pushing toward the reduction of the noise level produced by vehicles to improve the overall quality of life. This objective is clearly stated in the provisional agreement of the European Union concerning the vehicles noise limits [26]: "the regulation is aimed at improving environmental protection and public safety and at ensuring a better quality of life and health, by reducing major sources of noise caused by motor vehicles".

This agreement was successively enforced by a law [27]: it introduced a new testing method for measuring noise emissions and defined lower limits for vehicle noise emissions. These limit values are defined for the different vehicle categories: just to have an idea, in the following table we will consider the lowest class of passenger car.

	Limit values [dBA]		
	from 2016 (new type)	*from 2020 (new type) and from 2022 (first registration)*	*from 2024 (new type) and from 2026 (first registration)*
M1 - Passengers vehicles with power to mass ratio ≤ 120 kW/1000 kg	72	70	68

Table 4.10*: noise level limit values for a passenger cars category set by European regulation [27]*

Actually, the normatives are all referring to the whole vehicle noise emissions, with no reference to the noise produced by the single components (as engine or tyres): for this reason the comparison between the results of the acoustic analysis performed on the damper model (***Table 4.9***) and the vehicle noise limits (***Table 4.10***) is only qualitative. Moreover there are no data available regarding the noise level generated by other similar rotative damper devices.

In the future development of the project, when the prototype model will be ready, the only way to confirm such preliminary analysis results will be to run some bench tests to experimentally evaluate the noise level.

5 Future development: assembly on suspension

The designed rotative damper is intended for automotive applications, so the final objective of the project would be to install the device on a real vehicle suspension, but only after having performed some tests to verify its good operation and its structural strength. Actually this phase will not be included in this thesis work, anyway some preliminary analysis have been carried out in order to evaluate the feasibility of installation on an existing suspension architecture, studying different solutions to fit such damper on the car.

In particular the work was focused on the leverage system (analysis performed in the previous thesis project [15]), and then we pointed out possible arrangements of the input arm and the position of the device inside the suspension assembly.

5.1 Preliminary analysis on the leverage system

As mentioned in *Chapter 2*, one of the fundamental parts of the whole rotary damper assembly is represented by the leverage system that transmits the suspension motion as rotational input to the planetary gearbox. Its main requirement, coupled with the gearbox stage, is to assure the proper motor rotation, since the damping force provided by the electric machine is proportional to the speed. The target in leverage analysis is then to maximize the leverage transmission ratio τ to reduce the requirements on the gearbox transmission ratio i.

A detailed study of the leverages has been performed in [15]: here we will summarize the results to have a first idea of the possible positioning of the device inside the suspension architecture. The starting point to define the leverages is to consider the characteristic of the electric motor (speed and torque) and from this we can set what is the total transmission ratio k required in order to obtain the desired value of damping force.

$$\textit{overall transmission ratio} \qquad k = \frac{v}{\omega_{out}} = \tau \cdot \left(\frac{1}{i}\right) = 1{,}5\, mm/rad$$

Clearly the transmission ratio τ depends on the leverage configuration, and once defined it we can compute the required gearbox ratio i; for this reason, also the ratio τ must be as low as possible in order to reduce i and so the gearbox dimensions. The other important limitation is represented by the suspension: in fact, during the analysis of the leverages configurations, it was considered to minimize the modifications on the suspension components and obviously to avoid interferences among the moving parts.

The reference suspension architecture is shown in ***Figure 5.1***: it is a front suspension of the Alfa Romeo Stelvio. In particular it is a high double wishbone suspension, in which the damper tube has not the major structural function (differently from a McPherson suspension), and so it can be substituted by the rotative damper.

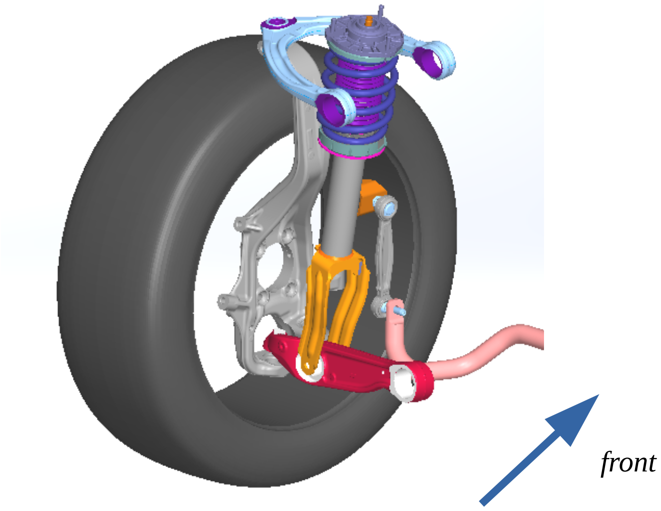

Figure 5.1: *3D model of the reference suspension architecture [15]*

At this point we will show the results regarding the different leverage configurations [15]: to simplify, the suspension kinematics is reduced on a 2D plane, and the linkages are studied with the mechanism synthesis approach to obtain the desired motion. The four alternative configurations are shown in ***Figure 5.2***. The input action is represented by the vertical motion of the wheel, applied to the external point of the lower arm; the additional leverages are represented by green lines and the position of the rotative damper axis is identified by the red circle.

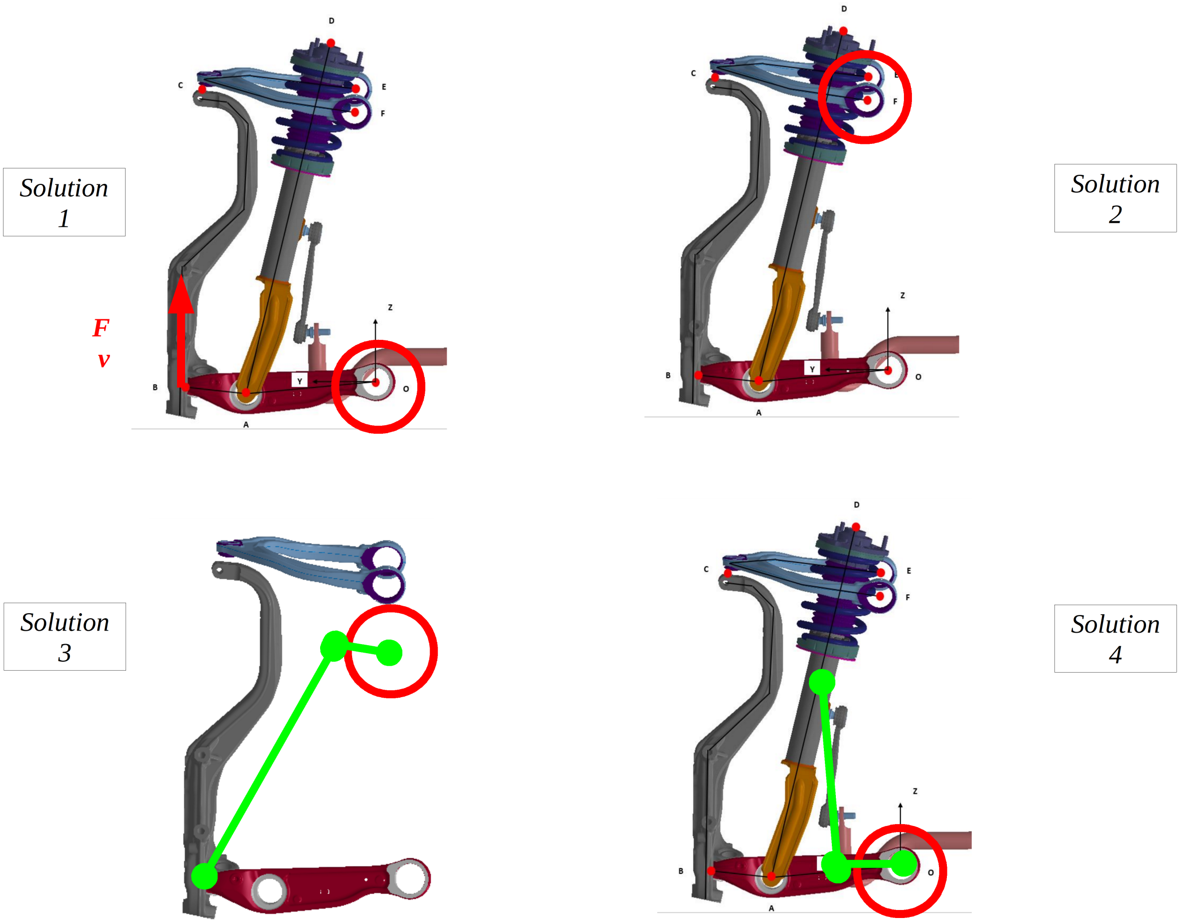

Figure 5.2: preliminary analysis of the leverage system: the four proposed configurations [15]

The differences among them are mainly related to the transmission ratio *τ*, but also the complexity of the linkages and eventual modifications required on the suspension are important factors to be taken into account.

- *Solution 1:* it is the simplest one because it does not modify the suspension architecture, but it has the worst transmission ratio *τ* = 346 mm/rad (constant).
- *Solution 2:* it is similar to the solution 1, but the damper is placed in the pivot point of the upper suspension arm; the transmission ratio is not constant (nominal *τ* = 251 mm/rad).
- *Solution 3:* this system requires to eliminate completely the damper strut assembly to accommodate the two additional leverages; it has a resulting nominal transmission ratio *τ* = 100 mm/rad.
- *Solution 4:* also in this case two additional leverages are required; the longer input arm is hinged on the damper tube while the rotary damper axis is coincident with the pivot point of the lower arm (nominal *τ* = 115 mm/rad).

On the base of these results, among the analyzed configurations the solution 4 represents a good trade off between a lower transmission ratio and the leverage complexity. For this reason its kinematics has been taken as reference set up since from the beginning of the design phase (for example τ = 115 mm/rad was used for the conversion of wheel vertical force into gearbox input torque). By the way, the transmission ratio is only obtained in an analytical way, and at this point we need to analyze more in detail the real suspension assembly to investigate what are the actual configurations that could be developed.

5.2 Suspension assembly 3D model

After having defined the final version of the damper model, a more detailed 3D model of the Stelvio front suspension has been obtained: as we can see in ***Figure 5.3***, the suspension assembly now includes also the subframe (green and grey components); on the right of the same figure, a representation of the real model is taken from the Alfa Romeo website [23].

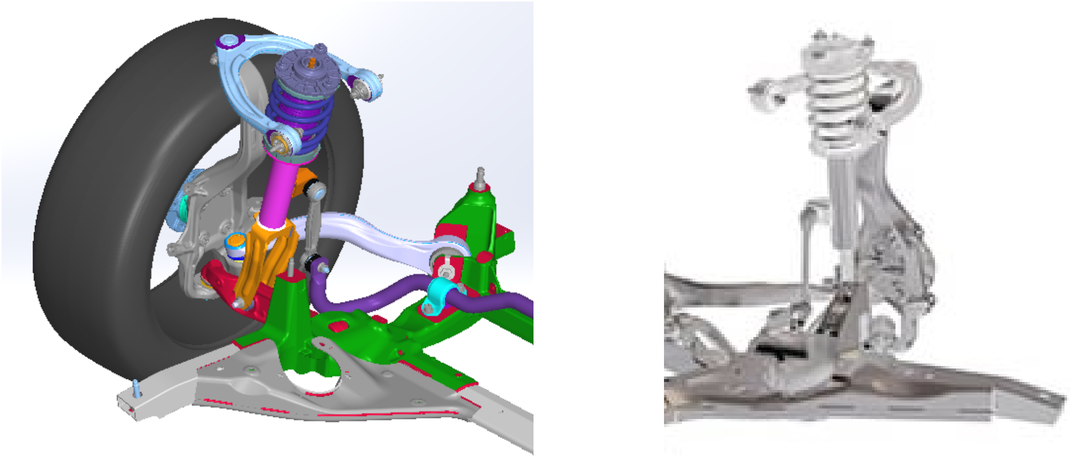

Figure 5.3: *more detailed 3D model of the suspension (on the left) and a realistic picture of the same model (on the right, Alfa Romeo Stelvio front suspension [23])*

It is immediately evident that most of the proposed leverage configurations are non practically feasible: in fact the presence of the subframe, of the anti-roll bar (the purple bar in the previous figure) and moreover all other components that are not shown (the wheel arch, the vehicle front frame, the engine bay components, the steering mechanism and the drive shaft) surely reduce to a minimum the available space. Clearly, such space is already optimized to extreme levels and for this reason, as said, the reduction of the dimensions of the damper assembly is a critical aspect to be considered.

In particular the solutions 1, 2 and 4 are not applicable since the damper must be placed in correspondence of the subframe attachment points; the solution 3 is even more complex because the whole damper tube assembly should be removed and substituted by the new leverage and the rotary damper.

So actually the leverage system that should drive the electromechanical damper must be redesigned taking into account additional constraints.

Only to have a first idea of the relative dimensions of the damper actuator in the suspension assembly, we try to identify a possible positioning inside in the 3D model, obviously avoiding interferences at least with the visible components. In the following ***Figure 5.4***, two possible solutions are presented, but we need to take into account that the final position will strongly depend also on the new leverage configuration.

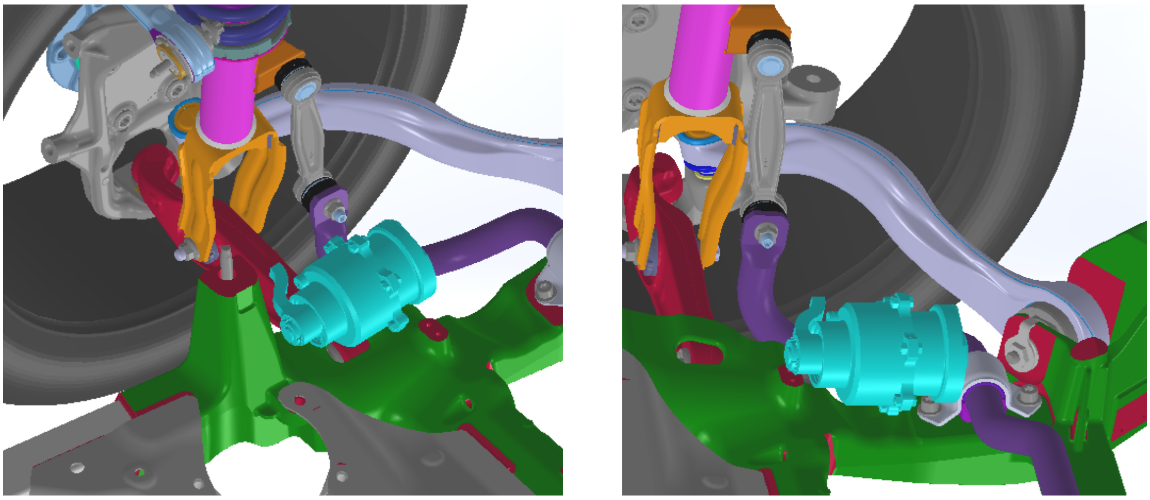

***Figure 5.4**: possible positionings of the rotative damper (light blue component, including a simple input arm) inside the suspension assembly*

The investigated positions exploit the “available” space on the suspension subframe:

- in the figure on the left, the damper is placed just onto the lower arm attachment point: in so doing the eventual connection arm is also aligned with the damper tube where it should be hinged. By the way the drive shaft of a 4 wheel drive vehicle would pass exactly through this position, as we can easily understand by the fork shape of the orange strut;
- on the right, the damper is positioned on the fixing point of the anti-roll bar, so in this case we could exploit an integration between the hinge of the bar and the support of the damper.

Obviously any position in the free space between the subframe and the wheel is not acceptable: that zone allows the motion of the suspension arms and the steering of the wheel itself inside the wheel arch.

In this model of the damper we also included an input arm, whose length is related to the leverage of solution 4 (l = 72 mm). On the other hand, another relevant issue concerning this configuration is the resulting excessive length of the vertical arm connecting the damper to the hydraulic tube: it should be l = 383 mm, much bigger than the swing arm of the anti-roll bar (about 190 mm).

5.3 Damper model modifications

After having analyzed more in general the suspension architecture, now we will briefly describe what are the major modifications to be introduced on the damper assembly to allow its fitting on the suspension in a future development of the project.

The first important modification is regarding the external case and how to fix it on the vehicle: such support must be designed in order to minimize the bending action on the whole assembly caused by the input force from the leverage. Clearly it is not enough to fix the damper only on the motor side, but ideally it requires a support on the entire case length, similar to the solution proposed for the test bench (***Figure 3.30***).

The other aspect is concerning the input arm: we have already analyzed its main features when talking about the design of the input shaft and its bearing, where we justified its bent shape. At this point we will show the results of a preliminary simulation that was performed to check the arm strength. We considered an arm length l = 70 mm (as in solution 4 leverage) and the arm was loaded on the tip by a tangential force F = 3286 N (corresponding to the force value that generates the maximum input torque T_{max} = 230 Nm). The result of the simulation concerning the equivalent stress on the shaped arm is shown in ***Figure 5.5***.

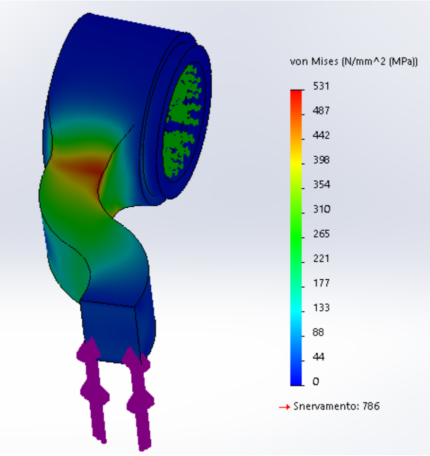

Figure 5.5*: stress on the input arm with maximum input static load*

The dimensions of the arm profile are optimized to reduce the stress: the resulting maximum stress is $\sigma = 531$ MPa. This value is below the yield limit of the material, but we need to take into account that the real loading on the arm is an oscillating load that is causing fatigue stress. By the way, on the other hand this maximum load is not a continuous normal operating condition and so we can consider such maximum stress a safe value.

To conclude this chapter, we need to remember that these modifications are not further developed within this thesis work because the model design was oriented to the prototype for bench testing. For this reason, for a future development of the device also additional insights regarding the arrangement of the damper in the suspension architecture will be required.

110

6 Conclusions

To end this thesis work, it is worth to summarize the results obtained in the different phases of the project, even if the conclusions concerning each aspect of the design process have already been presented at the end of each chapter.

The most important component of the new electromechanical rotative damper is the planetary gearbox: it has been designed thanks to the KISSsoft software, and we finally arrived to the definition of a final optimized model. The ideal efficiency of the gearbox itself results very high (more than 94 %) but, as we have seen, the one of the electric machine is reaching much lower values: for this reason, any further gears optimization will have not a significant effect on the operating efficiency of the total system, that is dominated by the one of the electric motor. By the way, the computer modelling alone is not enough to design a component with the best trade off between ideal performances and physical feasibility issues. This is even more true for what concern such precision gearbox: the gears design requires a certain level of expertise, and some more feedbacks from the gear manufacturer would have given better hints on the gear set optimization.

The following phase consists in the design of a prototype model of the damper actuator with the aim of manufacturing it: in our work we defined the detailed drawings of all the components, and at this moment we are waiting for their physical realization. The final prototype actuator has a resulting mass slightly higher than 3 kg: this is a significant improvement compared to the electro-hydraulic solution (implemented in a previous project) which had a total system mass bigger than 5 kg. Also the equivalent inertia is lower: the designed damper has an equivalent linear inertia that is about 20 kg. This value is smaller than the equivalent mass of the electro-hydraulic solution (35 kg), but the real improvement has been obtained thanks to the optimization of the planetary gearbox, since the preliminary model had an equivalent inertia equal to 55 kg. Clearly, in the evaluation of masses and inertia we did not consider the contribution of the leverage system, that requires a further detailed design stage according to the activity development.

In a future development of the project, once the prototype model will be ready, the experimental testing phase will be carried out. These tests will verify the results obtained during the computer modelling phase, as for example by checking the components strength, the device efficiency and the level of noise in operating conditions. In particular, the most realistic noise level that we have obtained with simulations is about 30 dB: it seems an acceptable value, but actually we don't have any reference noise limit for such component (experimental or legislative limits).

Finally, after having verified the feasibility of the device, the damper should be installed on a real vehicle suspensions: all the issues concerning this topic have already been analyzed in *Chapter 5*. Clearly, this next step will require a complete revision of the model and a closer cooperation among the entities involved in the project.

A Appendix

Here we present the KISSsoft report for the gear calculation only of the first planetary stage, since it is more critical from the point of view of loading conditions.

Start of Report

KISSsoft Release 03/2017 F

File Name: v4 stage 1

CALCULATION OF A SPUR PLANETARY GEAR STAGE

Load spectrum: Planet carrier

road profile ISO B 70kmh max damp

Number of bins in the load spectrum: 31

Reference gear: Planet carrier

Bin No.	Frequency [%]	Power [W]	Speed [1/min]	Torque [Nm]
1	0.00200	839.3236	-53.4	-150.0000
2	0.13900	576.9451	-39.4	-140.0000
3	2.15100	344.0421	-25.3	-130.0000
4	5.55900	140.6428	-11.2	-120.0000
5	1.59900	45.7426	-4.0	-110.0000
6	2.08900	37.8038	-3.6	-100.0000
7	2.57700	30.6211	-3.2	-90.0000
8	3.13800	24.1945	-2.9	-80.0000

9	3.57500	18.523	-2.5	-70.0000
10	3.95900	13.6094	-2.2	-60.0000
11	4.39300	9.4510	-1.8	-50.0000
12	4.77300	6.0486	-1.4	-40.0000
13	5.14000	3.4023	-1.1	-30.0000
14	5.35900	1.5122	-0.7	-20.0000
15	5.41100	0.3780	-0.4	-10.0000
16	5.28100	0.3780	0.4	10.0000
17	5.28000	1.5122	0.7	20.0000
18	5.12700	3.4023	1.1	30.0000
19	4.83500	6.0486	1.4	40.0000
20	4.41200	9.4510	1.8	50.0000
21	4.12800	13.6094	2.2	60.0000
22	3.66000	18.5239	2.5	70.0000
23	3.14100	24.1945	2.9	80.0000
24	2.58900	30.6211	3.2	90.0000
25	2.18800	37.8038	3.6	100.0000
26	1.65000	45.7426	4.0	110.0000
27	5.69000	140.6428	11.2	120.0000
28	2.00900	344.0421	25.3	130.0000
29	0.13300	576.9451	39.4	140.0000
30	0.01200	839.3236	53.4	150.0000
31	0.00100	1131.1912	67.5	160.0000

Bin	Coefficients									Temperature
No.	KV	KHβ1	KHβ2	KHα1	KHα2	Kγ	YM1	YM2	YM3	Oiltemp
1	1.0073	2.5146	1.1293	1.0000	1.2128	1.0000	1.0000	0.7000	1.0000	70.0000
2	1.0057	2.4948	1.1362	1.0000	1.2295	1.0000	1.0000	0.7000	1.0000	70.0000
3	1.0038	2.4743	1.1441	1.0000	1.2482	1.0000	1.0000	0.7000	1.0000	70.0000
4	1.0018	2.4531	1.1531	1.0000	1.2693	1.0000	1.0000	0.7000	1.0000	70.0000
5	1.0007	2.4310	1.1634	1.0000	1.2930	1.0000	1.0000	0.7000	1.0000	70.0000
6	1.0007	2.4080	1.1755	1.0000	1.3197	1.0000	1.0000	0.7000	1.0000	70.0000
7	1.0006	2.3842	1.1900	1.0000	1.3509	1.0000	1.0000	0.7000	1.0000	70.0000
8	1.0006	2.3596	1.2075	1.0000	1.3878	1.0000	1.0000	0.7000	1.0000	70.0000
9	1.0006	2.3342	1.2294	1.0000	1.4322	1.0000	1.0000	0.7000	1.0000	70.0000
10	1.0006	2.3085	1.2575	1.0000	1.4499	1.0000	1.0000	0.7000	1.0000	70.0000
11	1.0006	2.2873	1.2961	1.0000	1.4499	1.0000	1.0000	0.7000	1.0000	70.0000
12	1.0006	2.3371	1.3702	1.0000	1.4499	1.0000	1.0000	0.7000	1.0000	70.0000

13	1.0005	2.4201	1.4936	1.0000	1.4499	1.0000	1.0000	0.7000	1.0000	70.0000
14	1.0005	2.5839	1.7403	1.0785	1.4499	1.0000	1.0000	0.7000	1.0000	70.0000
15	1.0005	2.9875	2.4284	1.1781	1.4499	1.0000	1.0000	0.7000	1.0000	70.0000
16	1.0005	1.4359	2.4284	1.1781	1.4499	1.0000	1.0000	0.7000	1.0000	70.0000
17	1.0005	1.5900	1.7403	1.1781	1.4499	1.0000	1.0000	0.7000	1.0000	70.0000
18	1.0005	1.7560	1.4936	1.0704	1.4499	1.0000	1.0000	0.7000	1.0000	70.0000
19	1.0006	1.8391	1.3702	1.0000	1.4499	1.0000	1.0000	0.7000	1.0000	70.0000
20	1.0006	1.8889	1.2961	1.0000	1.4499	1.0000	1.0000	0.7000	1.0000	70.0000
21	1.0006	1.9621	1.2575	1.0000	1.4499	1.0000	1.0000	0.7000	1.0000	70.0000
22	1.0006	2.0256	1.2294	1.0000	1.4322	1.0000	1.0000	0.7000	1.0000	70.0000
23	1.0006	2.0804	1.2075	1.0000	1.3878	1.0000	1.0000	0.7000	1.0000	70.0000
24	1.0006	2.1286	1.1900	1.0000	1.3509	1.0000	1.0000	0.7000	1.0000	70.0000
25	1.0007	2.1719	1.1755	1.0000	1.3197	1.0000	1.0000	0.7000	1.0000	70.0000
26	1.0007	2.2111	1.1634	1.0000	1.2930	1.0000	1.0000	0.7000	1.0000	70.0000
27	1.0018	2.2471	1.1531	1.0000	1.2693	1.0000	1.0000	0.7000	1.0000	70.0000
28	1.0038	2.2805	1.1441	1.0000	1.2482	1.0000	1.0000	0.7000	1.0000	70.0000
29	1.0057	2.3115	1.1362	1.0000	1.2295	1.0000	1.0000	0.7000	1.0000	70.0000
30	1.0073	2.3406	1.1293	1.0000	1.2128	1.0000	1.0000	0.7000	1.0000	70.0000
31	1.0088	2.3679	1.1232	1.0000	1.1979	1.0000	1.0000	0.7000	1.0000	70.0000

Notice:

- Tooth flank with load spectrum: Check both cases and document the unfavourable case
- Tooth root with load spectrum: Check both cases and document the more realistic case (DIN3990-6, Method C)

Is only applied on load spectrum bins, where the alternating bending factor (mean stress influence factor) YM=1.0.

S-N curve (Woehler line) in the endurance domain according: according to standard

Notice:

Calculation with methods ISO6336 and AGMA 2001 results in a reduction of resistance in the domain of fatigue resistance (from circa 10^7 to 10^10 cycles).

The lifetime calculation takes this into account (also with the S-N curve (Woehler Curve) of the Miner type).

Results

Safeties, calculated with load spectrum:

Root safety	1.029	1.041 / 2.230	1.986

Flank safety	1.027	1.346 / 5.024	4.908
Wear safety factor	122.383	2911.578	13431.155

Safeties against scuffing/micropitting/EHT/TFF are indicated for the most critical element of the load spectrum:

Scuffing safety (integral temperature)	3.266	5.069
Scuffing safety (flash temperature)	9.507	224.891

ONLY AS INFORMATION: CALCULATION WITH REFERENCE POWER

Calculation method ISO 6336:2006 Method B

		--------- Sun -----------	Planets ----------	Internal gear ---
Number of planets	[p]	(1)	3	(1)
Power (W)	[P]		0.105	
Speed (1/min)	[n]	9.4		0.0
Speed difference for planet bearing calculation (1/min)	[n2]		2.3	
Speed planet carrier (1/min)	[nSteg]		1.0	
Torque (Nm)	[T]	0.107	0.000	0.893
Torque Pl.-Carrier (Nm)	[TSteg]		1.000	
Application factor	[KA]	1.00		
Distribution factor	[Kgam]	1.00		
Required service life (h)	[H]	3600.00		
Gear driving (+) / driven (-)		-	+/-	+

Working flank gear 1: Left flank

Sense of rotation gear 1 clockwise

1. TOOTH GEOMETRY AND MATERIAL

(geometry calculation according to ISO 21771:2007, DIN ISO 21771)

		------- GEAR 1 ----------	GEAR 2 ---------	GEAR 3 ---
Center distance (mm)	[a]		22.500	

Centre distance tolerance ISO 286:2010 Measure js7

Normal module (mm)	[mn]		0.6000	
Pressure angle at normal section (°)	[alfn]		20.0000	

```
Helix angle at reference circle (°)             [beta]                 0.0000
Number of teeth                                 [z]       16               58                -134
Facewidth (mm)                                  [b]       15.00            15.00             15.00
Hand of gear:                 Spur gear

Planetary axles can be placed in regular pitch:        120°

Accuracy grade                [Q-ISO1328:1995]            6                6                 6
Inner diameter (mm)                             [di]      4.31             28.95
External diameter (mm)                          [di]                                         85.50
Inner diameter of gear rim (mm)                 [dbi]     0.00             0.00
Outer diameter of gear rim (mm)                 [dbi]                                        0.00

Material
Gear 1: Steel, Grade 3, HRC58-64(AGMA), Case-carburized steel, case-hardened AGMA 2001-C95
Gear 2: Steel, Grade 3, HRC58-64(AGMA), Case-carburized steel, case-hardened AGMA 2001-C95
Gear 3: Steel, Grade 3, HRC58-64(AGMA), Case-carburized steel, case-hardened AGMA 2001-C95

                                                --------- GEAR 1 -------------- GEAR 2 ------------ GEAR 3 ---
Surface hardness                                HRC 60  HRC 60  HRC 60
          Material quality according to ISO 6336:2006 Normal (Life factors ZNT and YNT >=0.85)

Fatigue strength. tooth root stress (N/mm²)     [σFlim]   515.00           515.00            515.00
Fatigue strength for Hertzian pressure (N/mm²) [σHlim] 1895.00           1895.00           1895.00
Tensile strength (N/mm²)                        [σB]      1035.00          1035.00           1035.00
Yield point (N/mm²)                             [σS]      887.00           887.00            887.00
Young's modulus (N/mm²)                         [E]       206843           206843            206843
Poisson's ratio                                 [v]       0.300            0.300             0.300

Roughness average value DS, flank (µm)          [RAH]     0.63             0.63              0.63
Roughness average value DS, root (µm)           [RAF]     2.40             2.40              2.40
Mean roughness height, Rz, flank (µm)           [RZH]     5.00             5.00              5.00
Mean roughness height, Rz, root (µm)            [RZF]     16.00            16.00             16.00

Summary of reference profile gears:             1.25 / 0.38 / 1.0 ISO 53:1998 Profil A
Dedendum coefficient                            [hfP*]              1.250            1.250             1.250
Tooth root radius Refer. profile                [rhofP*]            0.380            0.380             0.380
          (rhofPmax*=0.472)
```

```
Addendum coefficient                    [haP*]          1.000           1.000           1.000
Tip radius factor                       [rhoaP*]        0.000           0.000           0.000
Protuberance height coefficient         [hprP*]         0.000           0.000           0.000
Protuberance angle (°)                  [alfprP]        0.000           0.000           0.000
Tip form height coefficient             [hFaP*]         0.000           0.000           0.000
Ramp angle (°)                          [alfKP]         0.000           0.000           0.000
        not topping
Type of profile modification: for uniform mesh
Tip relief (µm)                         [Ca]            0.00            0.00            0.00

Lubrication type                Oil bath lubrication
Type of oil                     Oil: ISO-VG 220
Lubricant base: Mineral-oil base
Kinem. Viscosity oil at 40 °C (mm²/s)   [nu40]          220.00
Kinem. Viscosity oil at 100 °C (mm²/s)  [nu100]         17.50
Specific density at 15 °C (kg/dm³)      [roOil]         0.895
Oil temperature (°C)                    [TS]            70.000

                                                ------- GEAR 1 ---------- GEAR 2 --------- GEAR 3 ---
Overall transmission ratio              [itot]  0.107
Gear ratio                              [u]                     3.625           -2.310
Transverse module (mm)                  [mt]    0.600
Pressure angle at pitch circle (°)      [alft]  20.000
Working transverse pressure angle (°)   [alfwt]                 22.003          17.783
                                        [alfwt.e/i]     22.069 / 21.937         17.699 / 17.866
Working pressure angle at normal section (°)
                                        [alfwn]                 22.003          17.783
Helix angle at operating pitch circle (°) [betaw]               0.000           0.000
Base helix angle (°)                    [betab] 0.000
Reference center distance (mm)          [ad]                    22.200          2.800
Sum of profile shift coefficients       [Summexi]               0.5244          0.4739
Profile shift coefficient               [x]             0.4593          0.0651          0.4088
Tooth thickness (Arc) (module) (module) [sn*]           1.9051          1.6182          1.8684

Tip alteration (mm)             [k*mn]          -0.015          -0.015          0.000
Reference diameter (mm)         [d]             9.600           34.800          80.400
Base diameter (mm)              [db]            9.021           32.701          75.551
Tip diameter (mm)               [da]            11.321          36.048          78.709
```

```
                (mm)                  [da.e/i]   11.321 / 11.311   36.048 / 36.038          78.709 / 78.719

Tip diameter allowances
            (mm) [Ada.e/i]            0.000 / -0.010               0.000 / -0.010           -0.000 / 0.010
Tip form diameter
            (mm) [dFa]                11.321                       36.048                   78.709
            (mm) [dFa.e/i]            11.321 / 11.311              36.048 / 36.038          78.709 / 78.719
Active tip diameter
            (mm) [dNa.e/i]            11.321 / 11.311              36.048 / 36.038          78.709 / 78.719

Operating pitch diameter (mm)         [dw]       9.730             35.270 / 34.342          79.342
                         (mm)         [dw.e]     9.734             35.287 / 34.326          79.305
                         (mm)         [dw.i]     9.725             35.254 / 34.358          79.379
Root diameter (mm)                    [df]       8.651                   33.378             81.409
Generating Profile shift coefficient
                          [xE.e/i]    0.3837 / 0.3379              -0.0585 / -0.1272        0.2486 / 0.1570

Manufactured root diameter with xE (mm)   [df.e]     8.560         33.230                   81.602
                                   (mm)   [df.i]     8.506         33.147                   81.712
Theoretical tip clearance (mm)            [c]        0.150         0.150 / 0.181            0.166
Tip clearance upper allowance (mm)        [c.e]      0.281         0.239 / 0.347            0.297
Tip clearance lower allowance (mm)        [c.i]      0.214         0.185 / 0.266            0.229
Active root diameter (mm)                 [dNf]      9.178         34.202 / 33.745          80.894
                      (mm)                [dNf.e]    9.193         34.223 / 33.771          80.861
                      (mm)                [dNf.i]    9.168         34.185 / 33.728          80.919
Root form diameter (mm)                   [dFf]      9.127         33.819                   80.983
                      (mm) [dFf.e/i]      9.090 / 9.072   33.711 / 33.653          81.214 / 81.341

Internal toothing: Calculation dFf with pinion type cutter ( z0 = 44, x0 = 0.000 ) Reserve (dNf-dFf)/2
                   (mm) [cF.e/i]          0.061 / 0.039   0.059 / 0.009            0.240 / 0.147

Addendum (mm)  [ha = mn * (haP*+x)]       0.861           0.624           0.845
           (mm) [ha.e/i]                  0.861 / 0.856   0.624 / 0.619   0.845 / 0.840

Dedendum (mm)  [hf = mn * (hfP*-x)]       0.474           0.711           0.505
           (mm) [hf.e/i]                  0.520 /   0.547 0.785 / 0.826   0.601 / 0.656

Roll angle at dFa (°) [xsi_dFa.e/i]   43.445 / 43.340              26.577 / 26.535          16.739 / 16.766
```

Roll angle to dNf (°)	[xsi_dNf.e/i]	11.246 / 10.383	17.682 / 17.457	
	[xsi_dNf.e/i]	14.776 / 14.473	21.856 / 21.978	
Roll angle at dFf (°)	[xsi_dFf.e/i]	7.122 / 6.102	14.347 / 13.925	22.595 / 22.857
Tooth height (mm)	[h]	1.335	1.335	1.350
Virtual gear no. of teeth	[zn]	16	58	-134
Normal tooth thickness at tip circle				
(mm)	[san]	0.277	0.478	0.547
(mm)	[san.e/i]	0.246 / 0.215	0.427 / 0.391	0.481 / 0.439
Normal space width at root circle				
(mm)	[efn]	0.000	0.472	0.385
(mm)	[efn.e/i]	0.000 / 0.000	0.493 / 0.506	0.379 / 0.375
Max. sliding velocity at tip (m/s)	[vga]	0.001	0.002 / 0.000	0.000
Specific sliding at the tip	[zetaa]	0.596	0.596 / 0.175	0.128
Specific sliding at the root	[zetaf]	1.475	-1.475 / -0.147	-0.212
Sliding factor on tip	[Kga]	0.419	0.256 / 0.077	0.036
Sliding factor on root	[Kgf]	-0.256	-0.419 / -0.036	-0.077
Pitch on reference circle (mm)	[pt]	1.885		
Base pitch (mm)	[pbt]	1.771		
Transverse pitch on contact-path (mm)	[pet]	1.771		
Length of path of contact (mm)	[ga]	2.575	3.420	
(mm)	[ga.e/i]	2.603 / 2.527	3.454 / 3.356	
Length T1-A (mm)	[T1A]	3.420	5.010 / 7.584	14.456
Length T1-B (mm)	[T1B]	2.617	5.813 / 5.936	12.807
Length T1-C (mm)	[T1C]	1.823	6.607 / 5.244	12.116
Length T1-D (mm)	[T1D]	1.649	6.781 / 5.813	12.685
Length T1-E (mm)	[T1E]	0.845	7.584 / 4.164	11.036
Diameter of single contact point B (mm)	[d-B]	10.429	34.707 / 4.789	79.775
(mm)	[d-B.e]	9.605	35.381 / 34.707	79.719
(mm)	[d-B.i]	9.599	35.430 / 34.699	79.668
Diameter of single contact point D (mm)	[d-D]	9.605	35.402 / 34.707	79.697
(mm)	[d-D.e]	10.401	34.707 / 34.766	79.775

```
                                    (mm)   [d-D.i]  10.469          34.699 / 34.825               79.787

Transverse contact ratio                   [eps_a]        1.454                         1.931
Transverse contact ratio with allowances   [eps_a.e/i]    1.469 / 1.426                 1.950 / 1.895
Overlap ratio                              [eps_b]        0.000                         0.000
Total contact ratio                        [eps_g]        1.454                         1.931
Total contact ratio with allowances        [eps_g.e/i]    1.469 / 1.426                 1.950 / 1.895
```

2. FACTORS OF GENERAL INFLUENCE

```
                                           ------------------- GEAR 1 ----------- GEAR 2 ----------- GEAR 3 --
Nominal circum. force at pitch circle (N)  [Ft]                     7.407               7.407
Axial force (N)                            [Fa]           0.0                 0.0                 0.0
Axial force (total) (N)                    [Fatot=Fa*3]             0.0                 0.0
Radial force (N)                           [Fr]                     2.696               2.696
Normal force (N)                           [Fnorm]        7.9                 7.9                 7.9
Nominal circumferential force per mm (N/mm) [w]                     0.49                0.49
Only as information: Forces at operating pitch circle:
Nominal circumferential force (N)          [Ftw]                    7.309               7.506
Axial force (N)                            [Fa]           0.0                 0.0 / 0.0           0.0
Axial force (total) (N)                    [Fatot=Fa*3]             0.0                 0.0
Radial force (N)                           [Fr]                     2.953               2.407
Circumferential speed reference circle (m/s) [v]                              0.00 (Planet)
Running-in value (µm)                      [yp]                     0.495               0.525
Running-in value (µm)                      [yf]                     0.412               0.487
Gear body coefficient                      [CR]                     1.000               1.000
Correction coefficient                     [CM]                     0.800               0.800
Basic rack factor                          [CBS]                    0.975               0.975
Material coefficient                       [E/Est]                  1.004               1.004
Singular tooth stiffness (N/mm/µm)         [c']                     9.914               11.324
Meshing stiffness (N/mm/µm)                [cgalf]                  13.287              19.230
Meshing stiffness (N/mm/µm)                [cgbet]                  11.294              16.345
       The formula for c' and cg at w*KA < 25 N/mm is imprecise!
       c', cg is calculated with w*KA = 25 N/mm.
Reduced mass (kg/mm)                       [mRed]                   0.0001              0.0022
Resonance speed (min-1)                    [nE1]                    203309              15548
Resonance ratio (-)                        [N]                      0.000               0.000
```

```
Running-in value (μm)                   [ya]                    0.495           0.525
        KHb calculated according to ISO 6336-1: 2006, Annex E (takes into account KA*KV)
Axis alignment, pair 1 (μm)             [fΣβ / fΣδ]                     0.0 / 0.0
Axis alignment, pair 2 (μm)             [fΣβ / fΣδ]                     0.0 / 0.0
Torque (0: -, 1: <I, 2: <II, 3: <from shaft calculation)        2       0               0

Dynamic factor          [KV = max(KV12,KV23)]           1.01
                        [KV12,KV23]                             1.00            1.01

Face load factor        - flank         [KHb]                   5.00            5.00
                        - Tooth root    [KFb]                   4.30            4.28
                        - Scuffing      [KBb]                   5.00            5.00

Transverse load factor  - flank         [KHa]                   1.18            1.45
                        - Tooth root    [KFa]                   1.31            1.57
                        - Scuffing      [KBa]                   1.31            1.57

Helical load factor scuffing            [Kbg]                   1.00            1.00
Number of load cycles (in mio.)         [NL]            5.4             0.5             0.6


3. TOOTH ROOT STRENGTH

Calculation of Tooth form coefficients according method: B
Internal toothing: Calculation of roF and sFn according to ISO 6336-3:2007-04-01
Internal toothing: Calculation of YF, YS        with pinion type cutter ( z0 = 44, x0 = 0.000, rofP* = 0.380 )

                                        ------------ GEAR 1 ------------- GEAR 2 ------------ GEAR 3 ---
Calculated with manufacturing profile shift [xE.e]      0.3837          -0.0585         0.2486
Tooth form factor                       [YF]            1.48            1.74 / 1.08     1.08
Stress correction factor                [YS]            2.02            1.85 / 2.18     2.39
Bending moment arm (mm)                 [hF]            0.68            0.84 / 0.51     0.77
Working angle (°)                       [alfFen]        25.76           21.40 / 18.44   19.13
Tooth thickness at root (mm)            [sFn]           1.26            1.31 / 1.31     1.61
Tooth root radius (mm)                  [roF]           0.27            0.31 / 0.31     0.26
        ( hF* = 1.134 / 1.393 / 0.850 / 1.285   sFn* = 2.103 / 2.179 / 2.179 / 2.685 )
        ( roF* = 0.457 / 0.518 / 0.518 / 0.439  dsFn = 8.747 / 33.476 / 33.476 / -81.528
                                                alfsFn = 30.0 / 30.0 / 30.0 / 60.0)
```

```
Helix angle factor                      [Ybet]                  1.00            1.00
Deep tooth factor                       [YDT]                   1.00            1.00
Gear rim thickness (mm)                 [sr]            2.10            2.10            1.89
Gear rim factor                         [YB]            1.00            1.00            1.1
Effective facewidth (mm)                [beff]          15.00           15.00 / 15.00   15.00
Nominal stress at tooth root (N/mm²)    [sigF0]         2.46            2.66 / 1.95     2.36
Tooth root stress (N/mm²)               [sigF]          13.98           15.12 / 13.22   16.00

Permissible bending stress at root of Test-gear
Notch sensitivity factor                [YdrelT]        0.998           0.982 / 1.014   1.035
Surface factor                          [YRrelT]        0.972           0.978           0.977
size factor (Tooth root)                [YX]            1.000           1.000           1.000
Finite life factor                      [YNT]           0.988           1.228           1.192

Alternating bending factor (mean stress influence coefficient)
                                        [YM]            1.000           0.700           1.000
Stress correction factor                [Yst]           2.00
Yst*sigFlim (N/mm²)                     [sigFE]         1030.00         1030.00         1030.00
Permissible tooth root stress (N/mm²)
                   [sigFP=sigFG/SFmin]          987.18          850.23 / 878.20         1241.09
Limit strength tooth root (N/mm²)       [sigFG]         987.18          850.23 / 878.20         1241.09
Required safety                 [SFmin]         1.00            1.00                    1.00
```

4. SAFETY AGAINST PITTING (TOOTH FLANK)

```
                                        --------- GEAR 1 ------------------ GEAR 2 -------------- GEAR 3 ---
Zone factor                     [ZH]                            2.37            2.66
Elasticity factor (√N/mm²)      [ZE]                            190.20          190.20
Contact ratio factor            [Zeps]                          0.921           0.830
Helix angle factor              [Zbet]                          1.000           1.000
Effective facewidth (mm)        [beff]                          15.00           15.00
Nominal contact stress (N/mm²)  [sigH0]                         106.28          37.66
Contact stress at operating pitch circle (N/mm²) [sigHw]        259.76          102.10

Single tooth contact factor     [ZB,ZD]         1.04            1.00 / 1.00             1.00
Contact stress (N/mm²)          [sigHB, sigHD]  269.58          259.76 / 102.10         102.10
```

Lubrication coefficient at NL	[ZL]	1.013	1.005 / 1.005	1.006
Speed coefficient at NL	[ZV]	0.955	0.982 / 0.982	0.979
Roughness coefficient at NL	[ZR]	0.942	0.976 / 0.989	0.987
Material pairing coefficient at NL	[ZW]	1.000	1.000 / 1.000	1.000
Finite life factor	[ZNT]	1.183	1.417	1.389
Limited pitting is permitted: No				
Size factor (flank)	[ZX]	1.000	1.000	1.000
Permissible contact stress (N/mm²)	[sigHP=sigHG/SHmin]	2043.66	2586.87 / 2620.41	2559.02
Pitting stress limit (N/mm²)	[sigHG]	2043.66	2586.87 / 2620.41	2559.02
Required safety	[SHmin]	1.00	1.00	1.00

4a. WEAR

Line load at reference diameter (N/mm)	[w]	0.49	0.49
Line load at reference diameter (N/mm)	[KA*Kγ*KV*KHβ*KHα*w]	2.95	3.63
Loss factor	[HV]	0.17	0.04

Length of active flank (mm)	[lFl]	1.21	0.98 / 1.22	1.14
Wear factor (mm3/Nm/106)	[kw]	0.00071	0.00060	0.00035
Normal tooth thickness in pitch circle (mm)	[sn]	1.14	0.97	1.12
Wear removal (mm)	[δWn]	0.00001	0.00000	0.00000
Maximum permissible wear (%)	[Wlimit]	15.00		
Permissible wear on flank (mm)	[δWlimn]	0.17	0.15	0.17
Required safety	[SWmin]	1.10		

Calculation of local wear with speeds and load distribution according to method A:
Calculation was not carried out. (Contact analysis under load is required.)

4b. MICROPITTING ACCORDING TO ISO/TR 15144-1:2014

Pairing Gear 1 - 2: Calculation did not run. (Lubricant: Load stage micropitting test is unknown.)
Pairing Gear 2 - 3: Calculation did not run. (Lubricant: Load stage micropitting test is unknown.)

5. SCUFFING LOAD CAPACITY

Calculation method according to ISO TR 13989:2000

Lubrication coefficient (for lubrication type) [XS]		1.000				
Scuffing test and load stage [FZGtest]						
FZG - Test A / 8.3 / 90 (ISO 14635 - 1) 12						
Multiple meshing factor	[Xmp]		2.0		2.0	
Relative structure coefficient (Scuffing)	[XWrelT]	1.000		1.000		
Thermal contact factor (N/mm/s^.5/K)	[BM]	13.780		13.780		13.780
Relevant tip relief (µm)	[Ca]	0.00		0.00		0.00
Optimal tip relief (µm)	[Ceff]		0.05		0.04	
Ca taken as optimal in the calculation						
(0=no, 1=yes)		0		0 / 0		0
Effective facewidth (mm)	[beff]		15.000		15.000	
Applicable circumferential force/facewidth (N/mm) [wBt]			3.269		3.922	
(1) Kbg = 1.000	wBt*Kbg = 3.269					
(2) Kbg = 1.000	wBt*Kbg = 3.922					
Angle factor	[Xalfbet]		1.007		0.944	
Flash temperature-criteria						
Lubricant factor	[XL]		0.830		0.830	
Tooth mass temperature (°C)	[theMi]		70.06		70.01	
(theMi = theoil + XS*0.47*Xmp*theflm)						
Average flash temperature (°C)	[theflm]		0.07		0.01	
Scuffing temperature (°C)	[theS]		348.80		348.80	
Coordinate gamma (point of highest temp.)	[Gamma]		0.434		0.426	
(1) [Gamma.A] = 0.876	[Gamma.E] = -0.536					
(2) [Gamma.A] = 0.446	[Gamma.E] = -0.206					
Highest contact temp. (°C)	[theB]		70.17		70.01	
Flash factor (°K*N^-.75*s^.5*m^-.5*mm)	[XM]		50.109		50.109	
Approach factor	[XJ]		1.000		1.000	
Load sharing factor	[XGam]		1.000		0.354	
Dynamic viscosity (mPa*s) (70.0 °C)	[etaM]		41.90		41.90	
Coefficient of friction	[mym]		0.146		0.108	

Integral temperature-criteria				
Lubricant factor	[XL]	1.000		
Tooth mass temperature (°C)	[theMC]		70.12	70.01
(theMC = theoil + XS*0.70*theflaint)				
Mean flash temperature (°C)	[theflaint]		0.08	0.00
Integral scuffing temperature (°C)	[theSint]		360.78	360.78
Flash factor (°K*N^-.75*s^.5*m^-.5*mm)	[XM]		50.109	50.109
Running-in factor (well run in)	[XE]		1.000	1.000
Contact ratio factor	[Xeps]		0.261	0.215
Dynamic viscosity (mPa*s)	[etaOil]		41.90	41.90
Mean coefficient of friction	[mym]		0.249	0.117
Geometry factor	[XBE]		0.363	0.046
Meshing factor	[XQ]		0.964	0.822
Tip relief factor	[XCa]		1.070	1.114
Integral tooth flank temperature (°C)	[theint]		70.24	70.01

6. MEASUREMENTS FOR TOOTH THICKNESS

		------- GEAR 1	------------------ GEAR 2	----------------------- GEAR 3 ---
Tooth thickness deviation		DIN 3967 d25	DIN 3967 cd25	DIN 3967 cd25
Tooth thickness allowance (normal section) (mm)				
	[As.e/i]	-0.033 / -0.053	-0.054 / -0.084	-0.070/ -0.110
Number of teeth spanned				
	[k]	3.000	7.000	15.000
	(Internal toothing: k = (Measurement gap number))			
Base tangent length (no backlash) (mm)				
	[Wk]	4.751	12.027	26.642
Actual base tangent length ('span') (mm)				
	[Wk.e/i]	4.720 / 4.701	11.977 / 11.948	26.708 / 26.745
Diameter of measuring circle (mm)				
	[dMWk.m]	10.177	34.821	80.139
Theoretical diameter of ball/pin (mm)				
	[DM]	1.234	1.018	0.982
Effective diameter of ball/pin (mm)				

	[DMeff]	1.250	1.100	1.000
Radial single-ball measurement backlash free (mm)				
	[MrK]	6.026	18.280	39.269
Radial single-ball measurement (mm)				
	[MrK.e/i]	5.997 / 5.980	18.214 / 18.176	39.373 / 39.432
Diameter of measuring circle (mm)				
	[dMMr.m]	10.106	34.892	80.133
Diametral measurement over two balls without clearance (mm)				
	[MdK]	12.052	36.560	78.539
Diametral two ball measure (mm)				
	[MdK.e/i]	11.995 / 11.960	36.428 / 36.353	78.747 / 78.863
Measurement over pins according to DIN 3960 (mm)				
	[MdR.e/i]	11.995 / 11.960	36.428 / 36.353	78.747 / 78.863
Measurement over 3 pins (axial) according to AGMA 2002 (mm)				
	[dk3A.e/i]	11.995 / 11.960	36.428 / 36.353	78.747 / 78.863
Effective dimensions over 3 pins (mm)				
	[Md3R.e/i]	0.000 / 0.000	0.000 / 0.000	-0.000 / -0.000
Tooth thickness (chordal) in pitch diameter				
	(mm) [sc]	1.140	0.971	1.121
	(mm) [sc.e/i]	1.107 / 1.087	0.917 / 0.887	1.051 / 1.011
Reference chordal height from da.m				
	(mm) [ha]	0.892	0.628	0.839
Tooth thickness (Arc)				
	(mm) [sn]	1.143	0.971	1.121
	(mm) [sn.e/i]	1.110 / 1.090	0.917 / 0.887	1.051 / 1.011
Backlash free center distance (mm)				
	[aControl.e/i]		22.389 / 22.324	22.684 / 22.782
Backlash free center distance, allowances (mm)				
	[jta]		-0.111 / -0.176	0.184 / 0.282
dNf.i with aControl (mm)	[dNf0.i]	9.050	33.357	81.535
Reserve (dNf0.i-dFf.e)/2 (mm)	[cF0.i]	-0.020	-0.177	-0.161
Tip clearance (mm)	[c0.i(aControl)]	0.048	0.020	-0.042
Center distance allowances (mm)	[Aa.e/i]		0.011 / -0.011	-0.011 / 0.011
Circumferential backlash from Aa (mm)	[jtw_Aa.e/i]		0.008 / -0.008	0.007 / -0.007

Radial clearance (mm)	[jrw]	0.187 / 0.100	0.293 / 0.173
Circumferential backlash (transverse section) (mm)	[jtw]	0.147 / 0.080	0.198 / 0.116
Normal backlash (mm)	[jnw]	0.138 / 0.075	0.186 / 0.109

Torsional angle at entry with fixed output:

Entire torsional angle (°)	[j.tSys]	0.4214 / 0.2687

7. GEAR ACCURACY

------- GEAR 1 ------------ GEAR 2 ------------ GEAR 3 ---

According to ISO 1328-1:1995, ISO 1328-2:1997

		GEAR 1	GEAR 2	GEAR 3
Accuracy grade	[Q]	6	6	6
Single pitch deviation (μm)	[fptT]	6.50	7.00	7.50
Base circle pitch deviation (μm)	[fpbT]	6.10	6.60	7.00
Sector pitch deviation over k/8 pitches (μm)	[Fpk/8T]	9.00	13.00	16.00
Profile form deviation (μm)	[ffaT]	5.00	5.50	6.50
Profile slope deviation (μm)	[fHaT]	4.20	4.60	5.50
Total profile deviation (μm)	[FaT]	6.50	7.50	8.50
Helix form deviation (μm)	[ffbT]	7.00	7.00	7.50
Helix slope deviation (μm)	[fHbT]	7.00	7.00	7.50
Total helix deviation (μm)	[FbT]	9.50	10.00	11.00
Total cumulative pitch deviation (μm)	[FpT]	16.00	20.00	26.00
Runout (μm)	[FrT]	13.00	16.00	21.00
Single flank composite, total (μm)	[FisT]	30.00	33.00	43.00
Single flank composite, tooth-to-tooth (μm)	[fisT]	14.00	13.00	16.00
Radial composite, total (μm)	[FidT]	16.00	20.00	25.00
Radial composite, tooth-to-tooth (μm)	[fidT]	3.80	3.90	3.90

8. ADDITIONAL DATA

Mass (g)	[m]	7.49	33.86	83.09
Total mass (g)	[m]	192.16		

Moment of inertia (system with reference to the drive):

calculation without consideration of the exact tooth shape

single gears ((da+df)/2...di) (kg*m²)	[TraeghMom]	1.107e-007	8.647e-006	0.0001425

System ((da+df)/2...di) (kg*m²) [TraeghMom] 0.000245

Torsional stiffness on input for stopped output:

Torsional stiffness (MNm/rad)	[cr]		0.691	
Torsion when subjected to nominal torque (°)	[delcr]		0.000	
Mean coeff. of friction (acc. Niemann)	[mum]	0.193		0.100
Wear sliding coef. by Niemann	[zetw]	0.866		0.276

Meshpower (W)	0.094		0.094
Gear power loss (W)	0.001		0.000
Total power loss (W)		0.003	
Total efficiency		0.968	

Classification according to F.E.M. (Edition 1.001, 1998)

Spectrum factor	[km]	0.125
Spectrum class	[L]	2
Application class (predefined service life)	[T]	5
Machine class (predefined service life)	[M]	5
Application class (achievable service life)	[T]	4
Machine class (achievable service life)	[M]	4

9. MODIFICATIONS AND TOOTH FORM DEFINITION

Data for the tooth form calculation :

Calculation of Sun gear Tooth form, Sun gear, Step 1: Automatic (final machining)

haP* = 1.069, hfP* = 1.250, rofP* = 0.380

Calculation of Planets Tooth form, Planets, Step 1: Automatic (final machining)

haP* = 1.129, hfP* = 1.250, rofP* = 0.380

Calculation of Internal gear Tooth form, Internal gear, Step 1: Automatic (final machining)

z0 = 44, x0 = 0.0000, da0 = 27.904 mm, a0 = -26.876 mm

haP0* = 1.254, roaP0* = 0.380, hfP0* = 1.198, rofP0* = 0.000

10. SERVICE LIFE, DAMAGE

Calculation with load spectrum

Required safety for tooth root	[SFmin]	1.00
Required safety for tooth flank	[SHmin]	1.00

In accordance with user-specific instructions, the following criteria only taken into account:

Tooth root: Taken into account

Tooth flank: Taken into account

Wear: Not taken into account

Service life (calculated with required safeties):

System service life (h)	[Hatt]	2915

Tooth root service life (h)	[HFatt]	1e+006	5529	1e+006
Tooth flank service life (h)	[HHatt]	2915	4.661e+004	1e+006

Wear: Not taken into account

(Note: The entry 1e+006 h means that the Service life > 1,000,000 h)

Damage calculated on the basis of the required service life (3600 h)

(Wear: Not taken into account)

No.	F1%	F2%	F3%	H1%	H2%	H3%	W1%	W2%	W3%
1	0.00	0.23	0.00	0.17	0.01	0.00	0.00	0.00	0.00
2	0.00	5.85	0.00	5.80	0.36	0.00	0.00	0.00	0.00
3	0.00	27.27	0.00	37.96	2.39	0.00	0.00	0.00	0.00
4	0.00	13.79	0.00	27.94	1.76	0.00	0.00	0.00	0.00
5	0.00	0.04	0.00	1.77	0.11	0.00	0.00	0.00	0.00
6	0.00	0.00	0.00	1.24	0.08	0.00	0.00	0.00	0.00
7	0.00	0.00	0.00	0.53	0.01	0.00	0.00	0.00	0.00
8	0.00	0.00	0.00	0.07	0.00	0.00	0.00	0.00	0.00
9	0.00	0.00	0.00	0.01	0.00	0.00	0.00	0.00	0.00
10	0.00	0.00	0.00	0.00	0.00	0.00	0.00	0.00	0.00
11	0.00	0.00	0.00	0.00	0.00	0.00	0.00	0.00	0.00
12	0.00	0.00	0.00	0.00	0.00	0.00	0.00	0.00	0.00
13	0.00	0.00	0.00	0.00	0.00	0.00	0.00	0.00	0.00
14	0.00	0.00	0.00	0.00	0.00	0.00	0.00	0.00	0.00
15	0.00	0.00	0.00	0.00	0.00	0.00	0.00	0.00	0.00

```
16      0.00    0.00    0.00    0.00    0.00    0.00    0.00    0.00    0.00
17      0.00    0.00    0.00    0.00    0.00    0.00    0.00    0.00    0.00
18      0.00    0.00    0.00    0.00    0.00    0.00    0.00    0.00    0.00
19      0.00    0.00    0.00    0.00    0.00    0.00    0.00    0.00    0.00
20      0.00    0.00    0.00    0.00    0.00    0.00    0.00    0.00    0.00
21      0.00    0.00    0.00    0.00    0.00    0.00    0.00    0.00    0.00
22      0.00    0.00    0.00    0.00    0.00    0.00    0.00    0.00    0.00
23      0.00    0.00    0.00    0.01    0.00    0.00    0.00    0.00    0.00
24      0.00    0.00    0.00    0.08    0.00    0.00    0.00    0.00    0.00
25      0.00    0.00    0.00    0.60    0.02    0.00    0.00    0.00    0.00
26      0.00    0.00    0.00    1.13    0.07    0.00    0.00    0.00    0.00
27      0.00    0.98    0.00    18.29   1.15    0.00    0.00    0.00    0.00
28      0.00    13.02   0.00    23.35   1.47    0.00    0.00    0.00    0.00
29      0.00     2.99   0.00    3.75    0.24    0.00    0.00    0.00    0.00
30      0.00     0.77   0.00    0.70    0.04    0.00    0.00    0.00    0.00
31      0.00     0.16   0.00    0.11    0.01    0.00    0.00    0.00    0.00
--------------------------------------------------------------------------------
Σ       0.00    65.11   0.00    123.51  7.72    0.00    0.00    0.00    0.00


Damage calculated on basis of system service life       [Hatt] ( 2914.8 h)
(Wear: Not taken into account)
No.     F1%     F2%     F3%     H1%     H2%     H3%     W1%     W2%     W3%
1       0.00    0.19    0.00    0.14    0.01    0.00    0.00    0.00    0.00
2       0.00    4.74    0.00    4.69    0.29    0.00    0.00    0.00    0.00
3       0.00    22.08   0.00    30.74   1.93    0.00    0.00    0.00    0.00
4       0.00    11.17   0.00    22.62   1.42    0.00    0.00    0.00    0.00
5       0.00    0.03    0.00    1.44    0.09    0.00    0.00    0.00    0.00
6       0.00    0.00    0.00    1.00    0.06    0.00    0.00    0.00    0.00
7       0.00    0.00    0.00    0.43    0.01    0.00    0.00    0.00    0.00
8       0.00    0.00    0.00    0.06    0.00    0.00    0.00    0.00    0.00
9       0.00    0.00    0.00    0.01    0.00    0.00    0.00    0.00    0.00
10      0.00    0.00    0.00    0.00    0.00    0.00    0.00    0.00    0.00
11      0.00    0.00    0.00    0.00    0.00    0.00    0.00    0.00    0.00
12      0.00    0.00    0.00    0.00    0.00    0.00    0.00    0.00    0.00
13      0.00    0.00    0.00    0.00    0.00    0.00    0.00    0.00    0.00
14      0.00    0.00    0.00    0.00    0.00    0.00    0.00    0.00    0.00
15      0.00    0.00    0.00    0.00    0.00    0.00    0.00    0.00    0.00
```

```
16      0.00    0.00    0.00    0.00    0.00    0.00    0.00    0.00    0.00
17      0.00    0.00    0.00    0.00    0.00    0.00    0.00    0.00    0.00
18      0.00    0.00    0.00    0.00    0.00    0.00    0.00    0.00    0.00
19      0.00    0.00    0.00    0.00    0.00    0.00    0.00    0.00    0.00
20      0.00    0.00    0.00    0.00    0.00    0.00    0.00    0.00    0.00
21      0.00    0.00    0.00    0.00    0.00    0.00    0.00    0.00    0.00
22      0.00    0.00    0.00    0.00    0.00    0.00    0.00    0.00    0.00
23      0.00    0.00    0.00    0.01    0.00    0.00    0.00    0.00    0.00
24      0.00    0.00    0.00    0.07    0.00    0.00    0.00    0.00    0.00
25      0.00    0.00    0.00    0.49    0.01    0.00    0.00    0.00    0.00
26      0.00    0.00    0.00    0.92    0.06    0.00    0.00    0.00    0.00
27      0.00    0.79    0.00    4.81    0.93    0.00    0.00    0.00    0.00
28      0.00    10.54   0.00    18.91   1.19    0.00    0.00    0.00    0.00
29      0.00    2.42    0.00    3.03    0.19    0.00    0.00    0.00    0.00
30      0.00    0.62    0.00    0.56    0.04    0.00    0.00    0.00    0.00
31      0.00    0.13    0.00    0.09    0.01    0.00    0.00    0.00    0.00
-----------------------------------------------------------------------------------------------------------------
Σ       0.00    52.72   0.00    100.00  6.25    0.00    0.00    0.00    0.00


Damage calculated on basis of individual service life HFatt & HHatt & HWatt
        HFatt1          HFatt2          HFatt3          HHatt1          HHatt2          HHatt3
(h)     1e+006          5529            1e+006          2915            4.661e+004      1e+006

No.     F1%     F2%     F3%     H1%     H2%     H3%
1       46.9    0.36    0.00    0.14    0.14    0.00
2       0.00    8.99    0.00    4.69    4.71    0.00
3       0.00    41.89   0.00    30.74   30.90   0.00
4       0.00    21.19   0.00    22.62   22.78   0.00
5       0.00    0.06    0.00    1.44    1.45    0.00
6       0.00    0.00    0.00    1.00    1.01    0.00
7       0.00    0.00    0.00    0.43    0.19    0.00
8       0.00    0.00    0.00    0.06    0.03    0.00
9       0.00    0.00    0.00    0.01    0.00    0.00
10      0.00    0.00    0.00    0.00    0.00    0.00
11      0.00    0.00    0.00    0.00    0.00    0.00
12      0.00    0.00    0.00    0.00    0.00    0.00
13      0.00    0.00    0.00    0.00    0.00    0.00
```

```
14      0.00    0.00    0.00    0.00    0.00    0.00
15      0.00    0.00    0.00    0.00    0.00    0.00
16      0.00    0.00    0.00    0.00    0.00    0.00
17      0.00    0.00    0.00    0.00    0.00    0.00
18      0.00    0.00    0.00    0.00    0.00    0.00
19      0.00    0.00    0.00    0.00    0.00    0.00
20      0.00    0.00    0.00    0.00    0.00    0.00
21      0.00    0.00    0.00    0.00    0.00    0.00
22      0.00    0.00    0.00    0.00    0.00    0.00
23      0.00    0.00    0.00    0.01    0.00    0.00
24      0.00    0.00    0.00    0.07    0.03    0.00
25      0.00    0.00    0.00    0.49    0.21    0.00
26      0.00    0.00    0.00    0.92    0.92    0.00
27      0.00    1.50    0.00    14.81   14.92   0.00
28      0.00    19.99   0.00    18.91   19.01   0.00
29      0.00    4.59    0.00    3.03    3.05    0.00
30      0.00    1.18    0.00    0.56    0.57    0.00
31      53.03   0.25    0.00    0.09    0.09    0.00
-------------------------------------------------------------------------------
Σ       100.00  100.00  0.00    100.00  100.00  0.00
```

Most critical duty cycle elements for Scoring (SB, Sint), Tooth Flank Fracture (SFF), hardened layer (SEHT) and Micropitting (Slam)

Calculation of the factors required to define reliability R(t) according to B. Bertsche with Weibull distribution; t in (h):

R(t) = 100 * [Exp (- ((t*fac - t0) / (T - t0))^b)]^p %

Gear		p	fac	b	t0	T	R(H)%
1	Tooth root	1	5940	1.7	1.11e+013	1.705e+013	100.00
1	Tooth flank	1	5940	1.3	1.561e+007	7.436e+007	95.21
2	Tooth root	3	546	1.7	2.916e+006	4.481e+006	100.00
2	Tooth flank	3	546	1.3	2.295e+007	1.093e+008	100.00
3	Tooth root	1	709	1.7	3.804e+030	5.846e+030	100.00
3	Tooth flank	1	709	1.3	3.552e+030	1.692e+031	100.00

Reliability of the configuration for required service life (%) 95.21 (Bertsche)

REMARKS:

- Specifications with [.e/i] imply: Maximum [e] and Minimal value [i] with consideration of all tolerances
- Specifications with [.m] imply: Mean value within tolerance
- For the backlash tolerance, the center distance tolerances and the tooth thickness deviation are taken into account. Shown is the maximal and the minimal backlash corresponding the largest resp. the smallest allowances. The calculation is done for the operating pitch circle.
- Details of calculation method:
  cg according to method B
  KV according to method B
- The logarithmically interpolated value taken from the values for the fatigue strength and the static strength, based on the number of load cycles, is used for coefficients ZL, ZV, ZR, ZW, ZX, YdrelT, YRrelT and YX.

End of Report

B Appendix

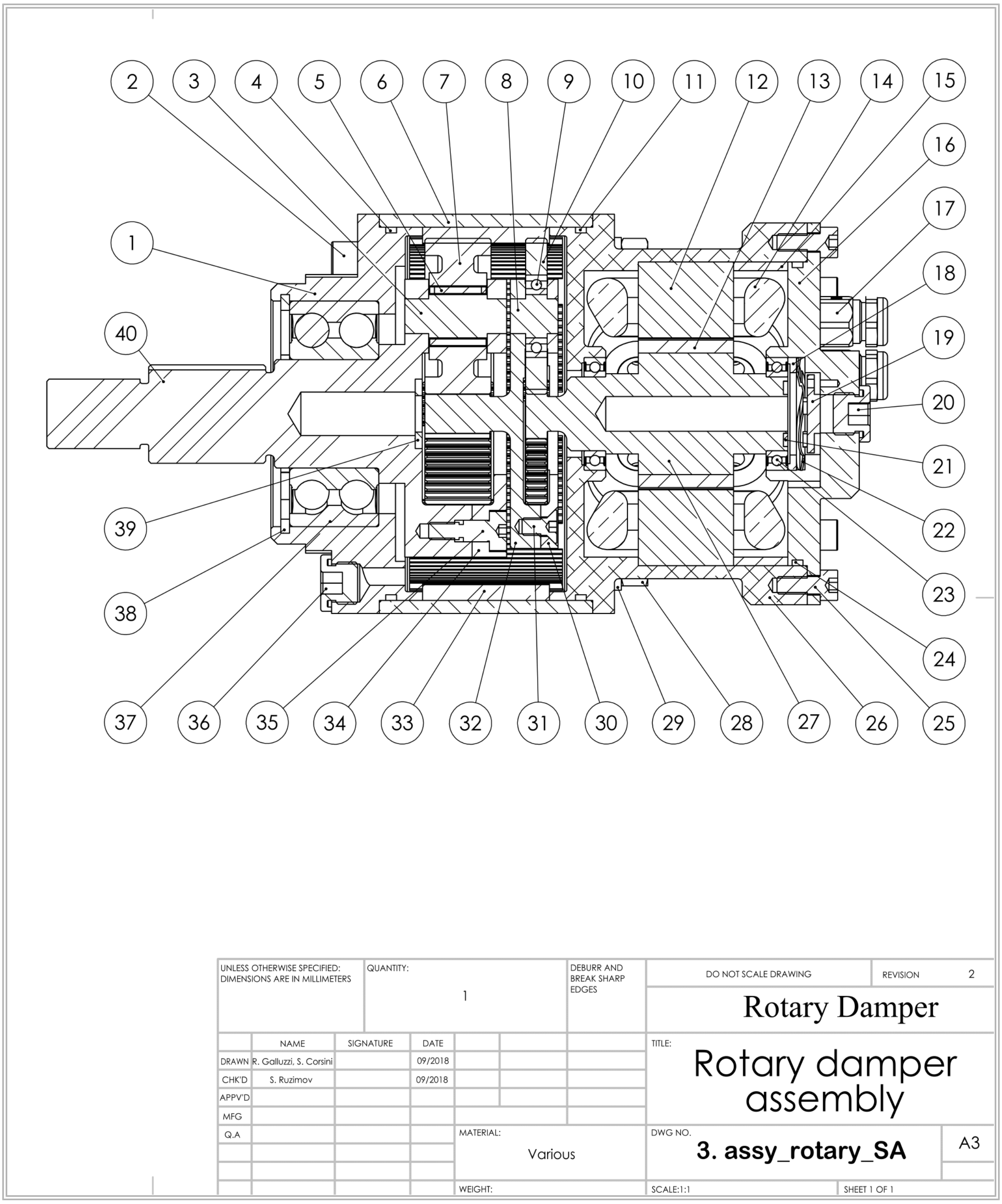

UNLESS OTHERWISE SPECIFIED:
DIMENSIONS ARE IN MILLIMETERS

QUANTITY: 1

DEBURR AND BREAK SHARP EDGES

DO NOT SCALE DRAWING

REVISION 2

Rotary Damper

	NAME	SIGNATURE	DATE
DRAWN	R. Galluzzi, S. Corsini		09/2018
CHK'D	S. Ruzimov		09/2018
APPV'D			
MFG			
Q.A			

TITLE: Rotary damper assembly

MATERIAL: Various

DWG NO. 3. assy_rotary_SA

A3

WEIGHT:

SCALE:1:1

SHEET 1 OF 1

Figure B.1: Prototype model: section view of the damper actuator assembly

BILL OF MATERIALS				
No.	*Part Name*	*Q.ty*	*Dwg No.*	*Notes**
1	Gearbox cover	1	**4**	**gb_cover**
2	Gearbox screw	4	-	ISO 4762 M6x70
3	Stage 1 planet pin	3	**5**	**gb_pin_shaft1**
4	Gearbox cover OR	2	-	OR 2325
5	Stage 1 planet bearing	3	-	SKF K 10x14x13 TN
6	Gearbox casing	1	**6**	**gb_tube**
7	Stage 1 planet gear	3	**7**	**gb_planet1**
8	Stage 2 planet pin	3	**8**	**gb_pin_shaft2**
9	Stage 2 planet bearing	3	-	SKF 61800, C3 int. clearance
10	Stage 2 planet gear	3	**9**	**gb_planet2**
11	Motor casing OR	2	-	OR 2325
12	Motor stator	1	-	*Available @ POLITO*
13	Rotor magnet	10	-	*Available @ POLITO*
14	Motor winding coil	6	-	*Available @ POLITO*
15	Motor spacer	1	**10**	**mot_spacer**
16	Motor cover	1	**11**	**mot_cover**
17	Motor cable gland	4	-	LAPP 52001880 (RS 458-3969)
18	Bearing preload ring	1	**12**	**bearing_preload**
19	Motor sensor	6	-	A1326LLHLT-T (RS 753-2018)
20	Drain cap	1	-	Festo 578406 (RS 125-9656)
21	Sensor magnets	10	-	*Available @ POLITO*
22	Wave spring	1	-	Smalley SSB-0102
23	Rotor bearings	2	-	SKF 61803-2RS1
24	Motor cover OR	2	-	OR 2262
25	Motor cover screw	8	-	ISO 4762 M4x10
26	Motor casing	1	**13**	**mot_casing**
27	Rotor & stage 2 sun	1	**14**	**rotor_sun2**
28	Gearbox nut	4	-	ISO 4034 M6
29	Gearbox washer	4	-	ISO 7089 6
30	Stage 2 plate	1	**15**	**gb_plate2**
31	Stage 2 calibrated screw	3	-	calibrated DIN 7991 M4x10
32	Stage 2 carrier & stage 1 sun	1	**16**	**gb_carrier2_sun1**
33	External ring	1	**17**	**gb_ext_ring**
34	Stage 1 plate	1	**18**	**gb_plate1**
35	Stage 1 calibrated screw	3	-	calibrated ISO 7379 M4x6
36	Lubricant cap	1	-	Festo 578406 (RS 125-9656)
37	Input shaft bearing	1	-	SKF 3205 A-2RS1
38	Input locking seeger	1	-	DIN 472 ∅52x2
39	Nylon washer	1	-	ISO 7089 8 (nylon)
40	Stage 1 carrier & input shaft	1	**19**	**gb_carrier1**
-	Gearbox cover inserts	4	-	Ensat M6 302 0061.16

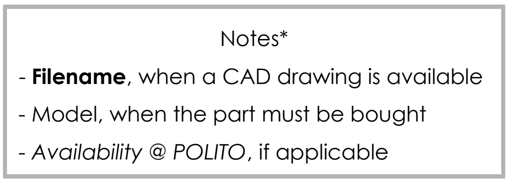

Notes*

- **Filename**, when a CAD drawing is available
- Model, when the part must be bought
- *Availability @ POLITO*, if applicable

***Table B.1**: Damper actuator assembly: bill of materials (related to the drawing of Figure B.1)*

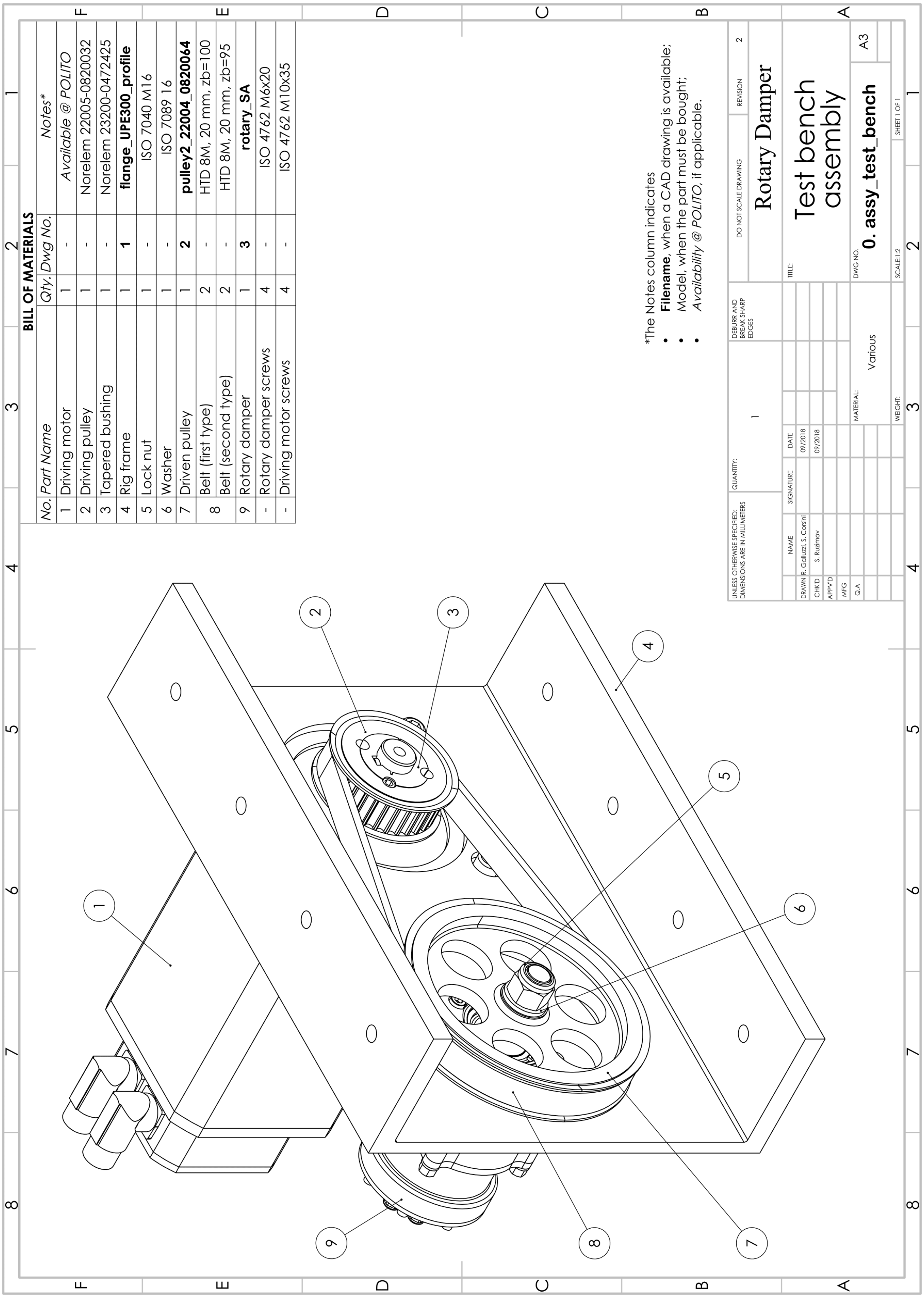

BILL OF MATERIALS

No.	*Part Name*	*Qty.*	*Dwg No.*	*Notes**
1	Driving motor	1	-	*Available @ POLITO*
2	Driving pulley	1	-	Norelem 22005-0820032
3	Tapered bushing	1	-	Norelem 23200-0472425
4	Rig frame	1	**1**	**flange_UPE300_profile**
5	Lock nut	1	-	ISO 7040 M16
6	Washer	1	-	ISO 7089 16
7	Driven pulley	1	**2**	**pulley2_22004_0820064**
8	Belt (first type)	2	-	HTD 8M, 20 mm, zb=100
	Belt (second type)	2	-	HTD 8M, 20 mm, zb=95
9	Rotary damper	1	**3**	**rotary_SA**
-	Rotary damper screws	4	-	ISO 4762 M6x20
-	Driving motor screws	4	-	ISO 4762 M10x35

*The Notes column indicates

- **Filename**, when a CAD drawing is available;
- Model, when the part must be bought;
- *Availability @ POLITO*, if applicable.

***Figure B.2**: Prototype model: customized test bench assembly*

References

[1] Genta G., Morello L., *The automotive chassis - components design*, 2009, Springer

[2] Genta G., Morello L., Cavallino F., Filtri L., *The motor car - past, present and future*, 2014, Springer

[3] *Energy-harvesting shock absorber that increases fuel efficiency wins R&D 100 award*, 14/07/2011, URL https://phys.org/news/2011-07-energy-harvesting-absorber-fuel-efficiency-award.html (verified October 2018)

[4] Matsuoka Y., *Vehicle suspension system using a rotary dampen*, Honda Motor Co Ltd, United States patent US5074581A, publication date 24/12/1991

[5] Willems M., *Electric shock absorber for a motor vehicle*, Audi AG, German application DE102010035087A1, application date 23/02/2012

[6] Willems M., *Rotary damper*, Audi AG, German application DE102011101701A1, application date 22/11/2012

[7] Merkes W., *Suspension with a rotary damper,* Audi AG, German grant DE102014011747B3, grant date 24/09/2015

[8] Willems M., *Rotation damper*, Audi AG, United States patent US 2017/0211658 A1, publication date 27/07/2017

[9] Willems M., Langhoff H., Idelevitch V., *Electromechanical rotary damper*, Audi AG, German application DE102014007846A1, application date 26/11/2015

[10] Willems M., *Electromechanical damper*, Audi AG, United States patent US 2014/0256501 A1, publication date 11/09/2014

[11] Willems M., *Damping device with a rotary damper*, Audi AG, German application DE102012009168A1, application date 14/11/2013

[12] *The electrification modular platform: new technologies with 12 and 48 volts*, 11/09/2015, URL https://www.audi-mediacenter.com/en/audi-future-performance-days-2015-5097/the-electrification-modular-platform-new-technologies-with-12-and-48-volts-5099 (verified October 2018)

[13] Wolf D., *Rotary damper for a vehicle*, ZF Friedrichshafen AG, German application DE102013203431A1, application date 28/08/2014

[14] *KISSsoft: Design software for mechanical engineering applications*, URL http://www.kisssoft.ch/english/home/index.php (verified September 2018)

[15] Cattabriga G., *Design of a Speed Multiplier for regenerative Shock Absorber*, Master degree thesis in mechanical engineering, Politecnico di Torino, 2018

[16] Múčka P., *Simulated Road Profiles According to ISO 8608 in Vibration Analysis*, Journal of Testing and Evaluation n. 46. 20160265, DOI: 10.1520/JTE20160265, 2018

[17] Concli F., Coenen J., *Low-loss gears for precision planetary gearboxes: Influence of the gear design on the meshing and the churning power losses*, International Conference on Gears, DOI: 10.13140/RG.2.1.1431.4725

[18] *Audi eROT – Analisi tecnica*, 21/08/2016, URL https://www.automobilissimo.com/audi-erot-analisi-tecnica/ (verified October 2018)

[19] Avalle M., Rossetto M., *Fundamentals of machine design and drawing - Shaft/hub coupling,* lecture slides, Politecnico di Torino

[20] *SKF Rolling bearings catalogue*, URL http://www.skf.com/it/index.html

[21] Viteritti M., *Drivetrain optimization of a Formula SAE racing prototype*, Master degree thesis in automotive engineering, Politecnico di Torino, 2017

[22] Belingardi G., *Fundamentals of machine design and drawing*, lecture slides, Politecnico di Torino

[23] *Alfa Romeo Stelvio*, URL https://www.alfaromeo.it/stelvio/business (verified October 2018)

[24] *Shock absorber*, URL https://en.wikipedia.org/wiki/Shock_absorber (verified October 2018)

[25] *COMSOL Multiphysics®*, URL https://www.comsol.com/comsol-multiphysics (verified October 2018)

[26] Council of the European Union, N*oise limits for motor vehicles*, 15/11/2013

[27] *Regulation (EU) No 540/2014 of the European Parliament and of the Council of 16 April 2014 on the sound level of motor vehicles and of replacement silencing systems, and amending Directive 2007/46/EC and repealing Directive 70/157/EEC*, Official Journal of the European Union, L 158/131, 27/05/2014